UNIVERSITY OF TWENTE.

Bridging Worlds in Wind

MASTER THESIS

The application of a functional approach for detecting wind turbine failures from SCADA-data

Author:
NIKITA ROEPLAL (S1484478)
MAINTENANCE ENGINEERING & OPERATIONS
FACULTY OF ENGINEERING TECHNOLOGY

Supervisors:
PROF. DR. IR. TIEDO TINGA (UNIVERSITY OF TWENTE)
DAMIAN ROMMEL (UNIVERSITY OF TWENTE)
ERIC KAMPHUES (INDEPENDENT EXPERTS)
ANDREA SANCHEZ (INDEPENDENT EXPERTS)

28TH OF AUGUST 2019

In memory of my grandmother, Ramdei

Summary

Unscheduled maintenance interventions on wind turbines (WTs) incurs significant downtime and thus loss of revenue. Therefore, it is important to perform maintenance just before it is needed. Due to the high costs of Condition Monitoring systems (CMs), data recorded by the Supervisory Control and Data Acquisition (SCADA) system of a WT is increasingly being used for detecting failures. Currently, the company Independent eXperts (IX) analyzes historical SCADA-data with a tool that, among others, presents deviations in SCADA-parameter behaviors. The company faces two main challenges when trying to relate this information for diagnosing turbine damage. Firstly, the relation between the behavior of the parameters and a (sub-)assembly damage is unclear as there is no one-to-one relation between the parameter deviations and (sub-)assembly damage and secondly, it is unclear whether the deviation of a parameter relates to the cause of a damage or its effect.

In order to tackle the above-mentioned challenges, IX has proposed to analyze SCADA-data through a functional approach. The goal of this work is to explore whether/to what extent knowledge of the functional relations between the WT (sub-)assemblies supports the detection of

To achieve this goal, a generic overview was created of the functional relations that generally exist in a Horizontal Axis Wind Turbine (HAWT). These relations were established based on the physical arrangement of the WT (sub-)assemblies and their functionalities. Hereafter, the fundamental physics governing the energy conversion process were studied in order to support analyzing the SCADA-data.

This research showed that the detection of (sub-)assembly failures based on the functional relations is not feasible as the failure effects of a certain (sub-)assembly failure cannot be fully captured based on the functional relations. To overcome this challenge, this work proposed to additionally consider the forces and moments, i.e. the load flow, seen by the WT (sub-)assemblies.

Application of the load flow showed that significantly more failure effects were identified. Additionally it was possible to provide a scientifically underpinned explanation of how SCADA-parameters are related and thus which parameters may be plotted against each other in order to detect failures. The latter is often lacking in literature. It was also possible to explain the deviations seen in the parameter behaviors.

Acknowledgments

This work would not have been possible without the support and help of many people, which I would like to extend my sincere thanks to.

First of all, I wish to express my gratitude to my daily supervisor Damian Rommel for his tireless personal and professional guidance. His patience and extensive knowledge and research skills have greatly contributed to the progress of this work. He has always brought great clarity to the context of this work and I can honestly say that this work would not have been completed without his support.

Secondly, I wish to express my gratitude to Prof.dr.ir. Tiedo Tinga for his unwavering support and guidance throughout this project.

I also wish to thank my company supervisors Eric Kampheus for having me intern at his company and Andrea Sanchez for her guidance and patience during this project.

Thank you to my aunt and uncle who welcomed me in their home in Amsterdam while completing a three month internship as part of my studies.

To my friends in Eschede, thank you for making this journey one worth remembering!

Finally, I wish to express my very profound gratitude to my parents and siblings for their unconditional love, constant motivation and truly inspiring view in life that has gotten me this far. Words cannot describe how grateful I am to have you in my life! The emotional support and unconditional love of my mother has gotten me through every challenge throughout this journey and in life. Thank you for being my role model in every way, Mom!

Contents

Chapter 1

Introduction

In this introductory chapter, the background of the thesis is discussed through a brief introduction to the topic. Based on this, the problem and research objective are described, followed by a presentation of the research questions that guide the study. Lastly, the chapter concludes with a description of the structure of the thesis.

1.1 Context

As the wind power energy industry has been growing significantly over the past decades, turbine capacities have shifted to the multi-megawatt (MW) category and Wind Farms (WFs) have moved offshore [1]. Generally, the Operation & Maintenance (O & M) costs of WFs increase when turbine failures occur - this is especially true for offshore Wind Turbines (WTs). Here, unexpected failures lead to excessive downtimes [3] due to i. harsh and unpredictable weather conditions, ii. large travel distances involved and iii. the modes of transportation [10] needed to access these WFs (i.e. vessels and helicopters [2]).

To reduce unscheduled downtime and thus O & M costs, increasing effort is being spent in the prediction of turbine faults [2][4]. Traditionally, Conditioned-Based Maintenance (CBM) was adopted as a maintenance regime for WF's in order to help reduce O & M costs [5][7][9] as it "promises to increase the efficiency of maintenance by optimising the point of intervention based on the condition of the system and the risks of imminent failures" [1]. To be more specific, Condition Monitoring (CM) is very effective in detecting any degradation or upcoming failures in an early stage [3][5] thereby preventing further fault escalation. Moreover, turbine outages are reduced since unnecessary scheduled maintenance operations are prevented [8]. In the past several Condition Monitoring Systems (CMS) have been developed and are normally installed additionally to the standard WT configuration [4]. They generally monitor drive train vibrations, oil quality and temperatures of some sub-assemblies. Despite the financial benefits of CMS, their adoption is seriously limited due to the high costs of the sensing devices they rely on to support fault detection [4][5].

In recent years, data recorded by the Supervisory Control and Data Acquisition (SCADA) system integrated in large utility scale WTs is increasingly being used for detecting developing failures [3][4][7]. These systems ensure the reliability of WTs by means of sensors that serve to protect, i.e. stop the turbine in case of an unsafe situations, and adapt the control of the various sub-assemblies of the turbine. SCADA systems typically measure multiple parameters, but "wind speed and direction, pitch and yaw angles, rotational speed, power output and ambient temperature are always monitored. Additionally, temperatures of parts in the drive train are often measured - although with different levels of detail, e.g. only a generator and a gearbox temperature in one setup or more than twenty temperatures at different locations at the shaft in a more detailed configuration." [1]. The measured data is stored every 10-minutes, where only a mean, maximum, minimum value and

standard deviation during the interval is calculated and recorded. Apart from the operational and environmental parameters, a record of alarms providing information about the WT sub-assemblies is also recorded by the SCADA-system. Given that SCADA-systems provide data with no requirements for additional sensor installations, they are a low cost solution for traditional condition monitoring systems [1][4][7].

1.2 Problem definition

Given the context, the company Independent eXperts (IX) - a consultancy bureau that supports clients with expertise in all wind power plant life stages (development, construction and operation, both on- and offshore) - has initiated a research project, called Wind turbine Maintenance & Operation decision Support (WiMOS), in collaboration with the University of Twente (UT) and the company Joulz.

The main objective of the WiMOS-project is to expand the functionalities of IX's maintenance decision support tool, SOMOS (Strategic Operation and Maintenance Optimization Simulation), such that it allows for the *short-term* (± 6-12 months) planning of maintenance activities and the required logistics of Horizontal Axis Wind Turbines (HAWTs - in the remainder of the report the abbreviation WTs is used interchangeably with HAWTs). The tool has been developed by IX and aids in the life-time, i.e. *long-term*, assessment of a WF's maintenance and logistics strategy through Monte-Carlo simulations of the WF's operations. These simulations are based on stochastic inputs related to reliability figures (i.e. Weibull distribution and MTBF) of main (sub-)assemblies failures, as well as weather patterns, procurement times of vessels and exchange parts, among others. In order to support short-term planning of maintenance activities and logistics, a more accurate assessment of the failure behavior of the WT main (sub-)assemblies is required.

Currently, IX analyzes *historical* SCADA-data of WFs with an additional tool, called MEcal SCada Analysis (MESCAL). This tool allows the assessment of WT and WF performance by i. comparing the monitored parameters of a predefined period with those of a reference period. The tool determines the deviations in the parameter values and classifies these according to the amount of deviation above the limit value. Also, ii. monthly information regarding among others the production, availability and losses of a WT for a predefined period can be determined in comparison with a reference WT. The tool additionally presents information on the triggered alarms for a given time period and the turbines of the complete WF. While the MESCAL tool presents deviations in the parameter behaviors for a selected time period, the company faces two main challenges when trying to relate this information for diagnosing turbine damage, namely:

1. *the relation between the behavior of the parameters and a (sub-)assembly damage is unclear as there is no one-to-one relation between the parameter deviations and (sub-)assembly damage. In other words, damage of a (sub-)assembly can effect many parameters and a specific parameter can relate to different damages;*

2. *it is unclear whether the deviation of a parameter relates to the cause of a damage or its effect. This means that the question arises whether the deviation of a parameter is an indicator that a certain (sub-)assembly has already failed or will fail.*

1.3 Research objective

Due to the above-mentioned challenges it is difficult to determine which WT (sub)-assemblies will fail. Given that the parameters provide information about the functionality of the (sub-)assemblies,

i.e. the extent to which they function properly, IX has proposed to tackle the above-mentioned challenges through a *functional approach*. This approach intends to describe a WT by means of the (sub-)assembly functions carried out (for transforming wind energy into electrical energy) and based on these functions, derive the functional relations/dependencies between the different (sub-)assemblies. The function-to-(sub-)assembly relations are intended to enable the analysis of the monitored parameters for the assessment of upcoming (sub-)assembly faults. Based on this, the goal of this work is:

To explore whether/to what extent knowledge of the functional relations between WT (sub-)assemblies supports the assessment of short-term failures from SCADA-data.

1.4 Research questions

In order to guide and support the research objective, it is translated into a main research question. The main research question is further divided into sub-questions in order to assist the research approach.

The **main** research question is:

Can a functional approach provide insight into failures of WT (sub-)assemblies from SCADA-data? If not, what information is additionally required?

The **sub**-questions in this regard are:

1. How are the (sub-)assemblies of a HAWT functionally linked to each other?
   a. What are the types of HAWT's that currently dominate the wind energy market?
   b. How are the WT (sub-)assemblies physically linked to each other?

2. How can the SCADA-parameters be related to the function disruption of a certain (sub-)assembly?
   a. Which methods currently exist for the detection of WT (sub-)assembly failures from SCADA-data?

3. If a functional approach does not support the detection of a certain (sub-)assembly failure, what information is additionally required to evaluate the functions (failure detection)?

Chapter 2

Research design & structure

In order to answer the earlier defined research questions, the research was divided into three phases with dedicated tasks that were based on the research questions. Recall that this work aims to explore, with gathered SCADA-data, whether/to what extent knowledge of the functional relations between WT (sub-)assemblies allows the detection of failures. In other words, the focus is to identify whether/to what extent knowledge of the functional relations can provide insight into the (sub-)assemblies that are failing based on the behavior of the SCADA-parameters. The research phases are described next.

Phase 1: Literature survey
In this phase the literature was surveyed in order to establish the functional relations that generally apply to a HAWT and how SCADA-parameters can be related to each other.

Phase 1a: Identify existing WT-configurations
In order to allow the functional approach/architecture to be applicable for the assessment of various WT's, first the HAWT types that have recently been installed in the wind energy market were identified.

Phase 1b: Establish general physical decomposition
Once the various configurations were identified, the (sub-)assemblies making up these turbines were studied. This physical decomposition of the WT's aided in identifying the common and differing (sub-)assemblies between the various WT types and supported establishing a general overview of the functional dependencies between the (sub-)assemblies of HAWT's. Namely, in Systems Engineering the design of a system generally starts with identifying the functions and functional requirements of the system, after which the physical architecture is established. With the various WT designs on the market, the physical architecture was thus already established. This means that in order to identify the manner in which the functionalities of a WT-system were connected, the opposite could be done of what is usually seen in Systems Engineering: based on the (sub-)assemblies present in a WT the functions could be derived and from the physical connection between the (sub-)assemblies it was possible to derive the connections between the different functions. Worth mentioning is that the level of detail of the physical decomposition was based on the SCADA-data available from the case study.

Phase 1c: Establish general functional decomposition
As mentioned previously, knowledge of the physical connections between the (sub-)assemblies allowed establishing how the WT (sub-)assemblies were connected and thus how the various functionalities were linked, i.e. how the WT works functionally. Therefore, this stage focused on building a general functional architecture that maps the functional relations between the WT (sub-)assemblies of HAWTs.

Phase 1d: Identify methods regarding the application of SCADA-parameters

As this research focuses on relating monitored SCADA-parameters to (sub-)assembly failures and each other (through a functional approach), the first step was to identify the methods which have been used in previous studies for the detection and of WT faults through SCADA-parameters.

Phase 1e: Study physics governing the energy conversion process
The fundamental physics governing the energy conversion process were studied as it aided the research in multiple ways, of which the two primary reasons were:

1. it supported understanding how the SCADA-parameters were related to each other;
2. it supported explaining deviations in the behavior of the SCADA-parameters;
3. it provided a scientifically underpinned explanation/reasoning of the effects of a (sub-)assembly failure on other (sub-)assembly functionalities. Namely, since the WT is an energy conversion system where the functionalities of the (sub-)assemblies are based on/support the conversion and transmission of energy, studying the physics gave insight into how this process, and thus the functionality of other (sub-)assemblies, is affected when one of the (sub-)assemblies no longer properly fulfills its function;

Additionally, the physics supported:

i. explaining the (normal) behaviors of the SCADA-parameters;
ii. help explaining and/or relating the deviations that appear in multiple parameters at the same time;

Phase 1f: Establish general load flow
With knowledge of the physics behind the transformation of kinetic energy in the wind into electrical energy it was possible to establish the various loads that the WT (sub-)assemblies experience. Therefore, in this phase a generic overview of the load flow along the (sub-)assemblies was produced.

Phase 2: Case study
In this phase the established physical decomposition (see phase 1b) and functional tree (see phase 1d) were applied to a case study in order to identify whether/to what extent knowlegde of the functional connections provided insight into failures.

Phase 2a: Establish specific physical and functional decomposition
For the case-specific turbine the applicable functional decomposition was established, since a certain turbine *type* functions differently compared to another turbine type. In order to establish the turbine-specific functional decomposition, first the physical decomposition that maps the physical arrangement of the (sub-)assemblies of this turbine was worked out. This implies that the general functional decomposition alone is not enough to establish the functional relations that apply to a specific WT.

Phase 2b: Derive failure modes, causes and effects
Generally, the system level function of the WT, i.e. power production, can be affected by the functional failure of any of the main (sub-)assemblies, e.g. blade failure, main bearing failure, gearbox failure, as they are all responsible for supporting the power production by the generator. Ideally, all possible root causes and effects of the (sub-)assembly failures are identified in order to present for each (sub-)assembly failure the set of SCADA-parameters that are the identifiers for the (sub-)assembly failure causes and effects. However, due to time constraints, this work focused on the functional failure of the blade pitch system as this had been identified as one of the failure cases of the WT of the case study. For this (sub-)assembly, the failure mode(s) and root causes of as well as the functionalities affected due to blade pitch failure were derived based on the functional relations (part 1) and additionally based on the load flow (part 2).

Phase 2c: Determine effects SCADA-parameters
Based on the description of the SCADA-parameters, the parameters were mapped to the (sub-)assemblies they monitor. Based on the failure mode(s) of pitch failure, the identified root causes of pitch failure and the failure effects of pitch failure it was possible to identify the SCADA-parameters that were affected and which parameters may be related. In order to understand how the SCADA-parameters were related, and thus which parameters could be plotted against each other, and how they were affected due to pitch failure, the physics were taken into account.

Phase 3: Assessment of the proposed method to detect failures
In this phase the applicability of the functional approach for the detection of upcoming failures was assessed.

Phase 3a: Data analysis
With knowledge of the expected parameters to be affected and how they were related to each other, the field data was analyzed based on the established parameter relations.

Phase 3b: Assess proposed method - conclusions and recommendations
The findings from the field data were compared with the theory in order to assess the applicability of the functional approach, load flow and physics to detect failures.

Figure 2.1 presents the previously described research phases. This research model presents the research steps and the chapters in which the research phases are treated.

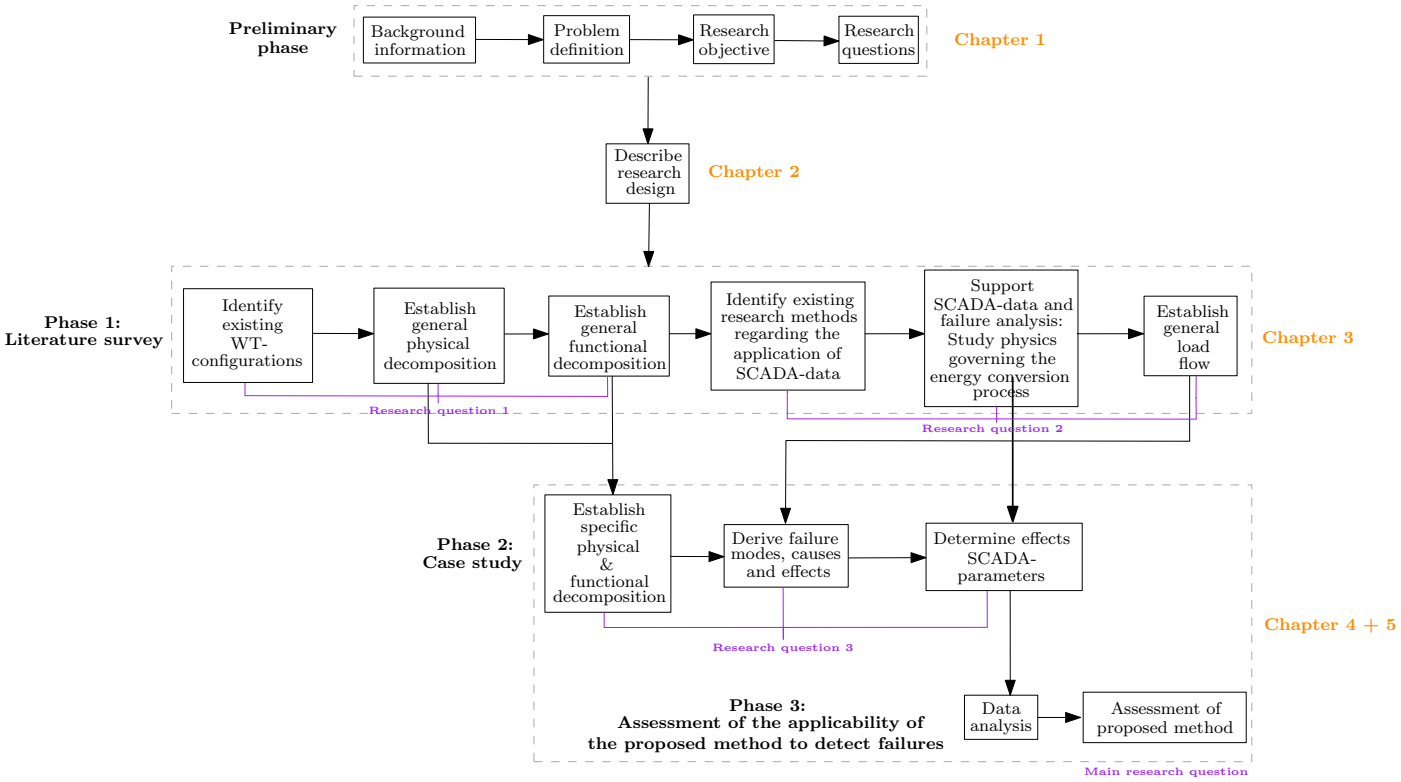

Figure 2.1: Research model

Chapter 3

Literature survey

In this chapter the literature is surveyed i. in order to gain an understanding on the fundamentals of wind turbine technology as well as the approaches and methods that currently exist regarding the analysis of SCADA-parameters and ii. to translate this knowledge into new insights that support failure detection based from SCADA-parameters.

3.1 Existing WT-configurations

In order to allow the functional tree, which will be developed later in this work, to be applicable to any type of HAWT, the various WT configurations that exist on the market must be identified. Worth mentioning is that the different HAWT concepts have been developed to maximize the energy that is harnessed from the wind, minimize the cost of energy and improve the power quality (= the quality of the electrical power fed into the grid assessed by the stability of frequency and voltage at the grid terminals [43]) during the past decades [68]. The identification of the different configurations will allow to establish a uniform taxonomy for analyzing the SCADA-data of the different WT's in a common way [13][14].

HAWT's are wind energy converters where the rotation axis of the blades lies in a horizontal position. They are commonly referred to as the propeller turbine and are the dominant design in the wind energy technology today [21]. The current techniques for converting wind energy into electrical energy in a HAWT can be categorized as *fixed speed* and *variable speed*. These are explained next.

Fixed speed vs variable speed WT's
As the name implies, fixed speed WT's operate at fixed speed, which means that regardless of the wind speed the turbine rotor speed is fixed. This is because for these configurations the generator is directly coupled to the grid and so the frequency of the power network determines the speed of the generator and thus the turbine rotor. For this reason it is said that the WT operates at fixed speed. These turbines thus achieve maximum power output at one certain wind speed. Variable speed WT's, on the other hand, can achieve maximum output over a wide range of wind speeds. This is because in this case the rotational speed of the turbine rotor is continuously accelerated or decelerated to the wind speed through power converters that control the generator speed [71]. Variable speed mode of operation, i.e. adjustment of the generator speed, occurs at wind speeds below the rated wind speed. This is the wind speed where the rated generator speed is reached.

Geared vs gearless WT's
Fixed speed and variable speed WT's can further be categorized based on their *transmission*, namely as geared or gearless. In the gearless, i.e. direct drive, mode of operation the generator rotor is directly connected to the hub and there is no gearbox between them. From the point of view of the energy yield, reliability and servicing, direct drive WT's are more superior compared to geared WT's [68][21]. However, a difficult condition to be satisfied for the direct drive mode of operation

is the necessity for the generator and the hub to be at the same speed [21]. Given that the speed of the WT rotor is generally low, the generator of a direct drive WT operates a low speed [69]. This means that a generator with a large number of poles, and thus a large diameter, is required for the generator to deliver the required frequency. This leads to a turbine weight that is higher compared to geared WT's.

Partially rated vs fully rated power converter WT's
As mentioned earlier, variable speed HAWT's can additionally be categorized according to the *power converter rating*. In this regard, three configurations exist, namely the *partial* variable speed WT with variable rotor resistance, the variable speed WT with *partial-rating* power converter and the variable speed WT with *full-rating* power converter. Worth mentioning is that the configuration of the partial variable speed WT is similar to the fixed speed concept [60][72], however, the rotor windings of the generator are connected in series with a variable resistance [73]. The size of this resistance defines the range of the variable speed. By altering the rotor resistance, through power electronics, the rotational speed of the WT can be partially adjusted [74]. With regard to the partially rated WT, only a part of the power production is fed through the converter, while in the case of the fully rated WT the total power production is fed through the power electronic system.

Fixed pitch vs variable pitch WT's
Lastly, fixed speed and variable speed WT's can each be classified as *fixed pitch* or *variable pitch* WT's, namely: *fixed-speed fixed-pitch*, *fixed-speed variable-pitch*, *variable-speed fixed-pitch* and *variable-speed variable-pitch* [43]. Pitch regulation adjusts the aerodynamic torque developed on the rotor and occurs above rated wind speed. As the name implies, fixed pitch means that the pitch angle of the turbine blades remain the same during operation. In the case of fixed speed - variable pitch WT's, the maximum power output is reached at a single wind speed and the pitch angle remains constant below rated wind speed. Once the rated wind speed is reached, the power is limited by continuously adjusting the blade pitch angle (note: fixed speed - fixed pitch WT's are stall regulated at high wind speeds). Further, variable speed - variable pitch mode of operation is more commonly applied in commercial WT's and in this scheme the turbine operates at variable speed - fixed pitch below rated wind speed and at variable pitch above rated wind speed.

With an overview of the existing HAWT-configurations, the following step is to establish a physical decomposition of HAWT's such that it covers the above mentioned concepts. This is done in ***section 3.2****.*

3.2 General physical decomposition for HAWT's

Apart from the gearbox, power converter and pitch system a HAWT is made up of other (sub-)assemblies, such as a main shaft, main bearings, mechanical brake, etc. to achieve kinetic-to-electric energy conversion. In order to be able to cover all possible (sub-)assemblies and how they are physically connected to each other, extensive literature review has been done on existing WT taxonomies. Several WT taxonomies have been developed in the past, with the ReliaWind taxonomy being the most extensive taxonomy available in literature [13][14]. However, according to [14], this taxonomy needs modernisation as most of the turbines used for the ReliaWind project were built earlier than 2008 and thus operate with older WT technologies. In [14] the ReliaWind taxonomy was carefully rearranged and extended by using detailed manufacturer information on current WT technologies and taking into account the functionality and physical location of components. It should be noted that the reviewed taxonomy is not an entirely new taxonomy, rather a modernization of the existing ReliaWind taxonomy and is aimed to allow its application to both older and modern WTs [14]. That is why this taxonomy (see **Figure 3.1**) is used as a basis for this work.

Next, the physical connections between the assemblies listed in **Figure 3.1** are discussed. These

connections are later used for identifying the functional dependencies between the assemblies (see **section 3.3**).

Subsystem	Assembly	Subsystem	Assembly	Subsystem	Assembly
Power Module		Control & Communications		Auxiliary System	
	Frequency Converter		Sensors		Cooling system
	Generator		Controller		Electrical Protection and Safety
	Switch Gear		Communication System		Human Safety
	Soft Starter		Emergency Control & Communication Series		Hydraulic Group
	MV/LV Transformer		Data Aquisition System		WTG Meteorological Station
	Power Feeder Cables	Nacelle			Lightning Protection
	Power Cabinet		Yaw System		Firefighting System
	Power Module Other		Nacelle Cover		Cabinets
	Power Protection Unit		Nacelle Bed plate		Service Crane
Rotor & Blades		Drive train			Lift
	Pitch System		Gearbox		Grounding
	Other Blade Brake		Main Bearing		Beacon/Lights
	Rotor		Bearings		Power Supply Auxiliary Systems
	Blades		Mechanical Brake		Electrical Auxiliary Cabling
	Hub		High Speed Shaft	Structure	
	Blade Bearing		Silent Blocks		Tower
			Low Speed (Main) Shaft		Foundations

Figure 3.1: Reviewed ReliaWind taxonomy [14].

Establishment of the physical connections between the assemblies

Rotor & blades
According to [21], the rotor of a WT is defined as all rotating parts outside the nacelle and consists of the blades, the hub and the pitch system. However, depending on the design, the pitch system and its control system are partly located in the rotor and partly in the nacelle [21]. In [22], [24] and [32], the rotor is specified as the assembly of the blades and hub only. With no agreed descriptor for WT (sub)assemblies [26], the current work defines the rotor as done by [21]. This means that the rotor shall not be considered seperate from the blades, hub and pitch system.

Regarding the physical connections of the above mentioned assemblies, the blades are attached to the hub by blade bearings. These bearings support the blades at their root in order to pitch, i.e. turn, the blades around their longitudinal axis. As the blade bearings are needed for pitching, they are generally considered part of the pitch system [21]. This is in contrast to the taxonomy presented by **Figure 3.1**, since they have listed the blade bearing and pitch system separately. Lastly, in the taxonomy two brakes are listed, namely "Other Blade Brake" and "Mechanical Brake". According to [27], the brake system of a WT (see **Figure 3.2**) includes a rotor lock and a rotor brake. From **Figure 3.2** it can be seen that the rotor lock is placed close to the blades (between the hub and the nacelle) and the rotor brake behind the gearbox. For this reason and taking into account that the authors of [14] have placed the assembly "Other Blade Brake" under "Rotor & Blades", it is assumed that the authors have referred to "Other Blade Brake" as being the rotor lock. The rotor lock is physically connected to the hub.

Nacelle
The nacelle is an enclosed space on top of the tower that accommodates the components which are responsible for converting mechanical energy into electrical energy [21][22]. These components are carried by the nacelle base frame and mounted in line behind the rotor. The nacelle also houses the yaw system, which forms the transition from the nacelle to the tower. Parts of the components of the yaw system are integrated into the nacelle and some in the tower.

Drive train
In the case of a geared WT, the main/low-speed shaft is one of the first assemblies to be mounted behind the rotor. It is located in the nacelle [22] and connected to the hub and gearbox - the hub is installed on the low-speed shaft. Therefore it rotates due to the rotation of the hub (and blades) [22]. It is further supported by the main bearing(s) [23][25]. The gearbox is further connected to

the high-speed shaft, which is aligned and coupled with the generator (shaft) [22]. The high-speed shaft is also connected to the mechanical brake, which is also called the rotor brake [21]. To address the physical connection of the assembly "bearings" (see **Figure 3.1**), it should be noted that the blade bearings and main bearing(s) have been excluded from this term (see **Figure 3.1**). Other bearings to be present in a WT are the generator, yaw and gearbox bearings, which are all, respectively, part of the assemblies "generator", "yaw system" and "gearbox" themselves. For this reason, it is unclear which "bearings" are considered by the authors of [14]. Lastly, silent blocks are mechanical devices that are used for suspensions with pivoting and/or rotating movements, pivot points of connection rods and damping of high-frequency vibrations. They are made up of twee concentric steel bushings with a layer of rubber between them [29]. In WT applications, rubber bushings are generally placed at the gearbox. Worth mentioning is that when the WT has no gearbox, there is no high-speed shaft present as this is the assembly connecting the gearbox with the generator.

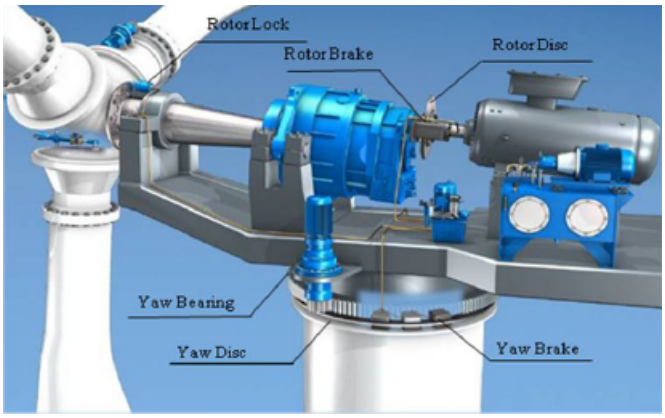

Figure 3.2: Braking system of a WT [27].

Power module + Control & Communications + Auxiliary System
According to [21], the electrical system of a WT " includes all components for converting mechanical energy into electric power as well as the electrical auxiliaries and the entire control and supervisory system". Based on the taxonomy in **Figure 3.1**, the electrical system is thus divided into the subsystem "Power module", "Control & Communications" and "Auxiliary System".

The power module is responsible for the production (generator), control (frequency converter) and supply (tranformer, power feeder cables) of the electrical power as well as the protection (switch gear, soft starter, power protection unit) of and power supply (power cabinet) to the electrical equipment. It is assumed that the physical connections of the power cabinet and the switch gear, for example, with the assemblies of the power module as well as other WT assemblies may differ per WT design and so this work shall only consider the physical connections of the generator and frequency converter as generally their arrangement remains the same for most configurations. For the case of the geared WT's the generator is physically connected to the high-speed shaft of the gearbox and the transformer. Further, the frequency converter is physically connected to the generator and transformer. A difference with the direct drive WT is that in this case the generator is directly connected to the hub through the main shaft.

Lastly, similar to the power cabinet and switch gear, the physical arrangements among the assemblies listed under the Control & Communications and the Auxiliary System may strongly differ per WT. However, from literature it can be derived that certain physical connections between the (assemblies of the) Control & Communications and the Auxiliary System and other assemblies generally are the same despite the type of HAWT. The pitch system, for example, is physically connected to the Control & Communications as the latter sends a signal to the pitch system for adjusting the blade pitch angle.

Further, the frequency converter is also physically connected to the Control & Communications due to the fact that the former adjusts the generator speed based on aninput signal received from the Control & Communications. Lastly, the mechanical brake and yaw system also receive an input signal from the Control & Communications. With regard to the physical connections between the Auxiliary System and other WT assemblies, the following exist: the pitch system, main bearing(s), gearbox, mechanical brake, generator and yaw system require cooling, hydraulic fluid and lubrication to function properly. Worth mentioning is that a "lubrication system" has not been included as an assembly of the subsystem "Auxiliary System". It is unclear why this has been done as the lubrication of WT bearings occurs in two ways, namely through an external oil supply system or through grease lubrication.

Structure
The tower holds the rotor and the nacelle in the air and must therefore be strong enough to carry the weights of the WT assemblies. Generally, a WT tower is integrated in a foundation, which is embedded in the ground [21].

Based on the theory studied above a general representation of the physical connections between the (sub-)assemblies of a HAWT is established. This is presented in ***Figure 3.3***. The gray (sub-)assemblies represent those which are not always present in a HAWT, for example a gearbox. Similarly, the gray arrows indicate physical connections which only exist in the case that the gray (sub-)assemblies are present in the WT under study. Since, based on the theory, the black colored (sub-)assemblies are always present in a HAWT the physical connections between them are represented by orange arrows.

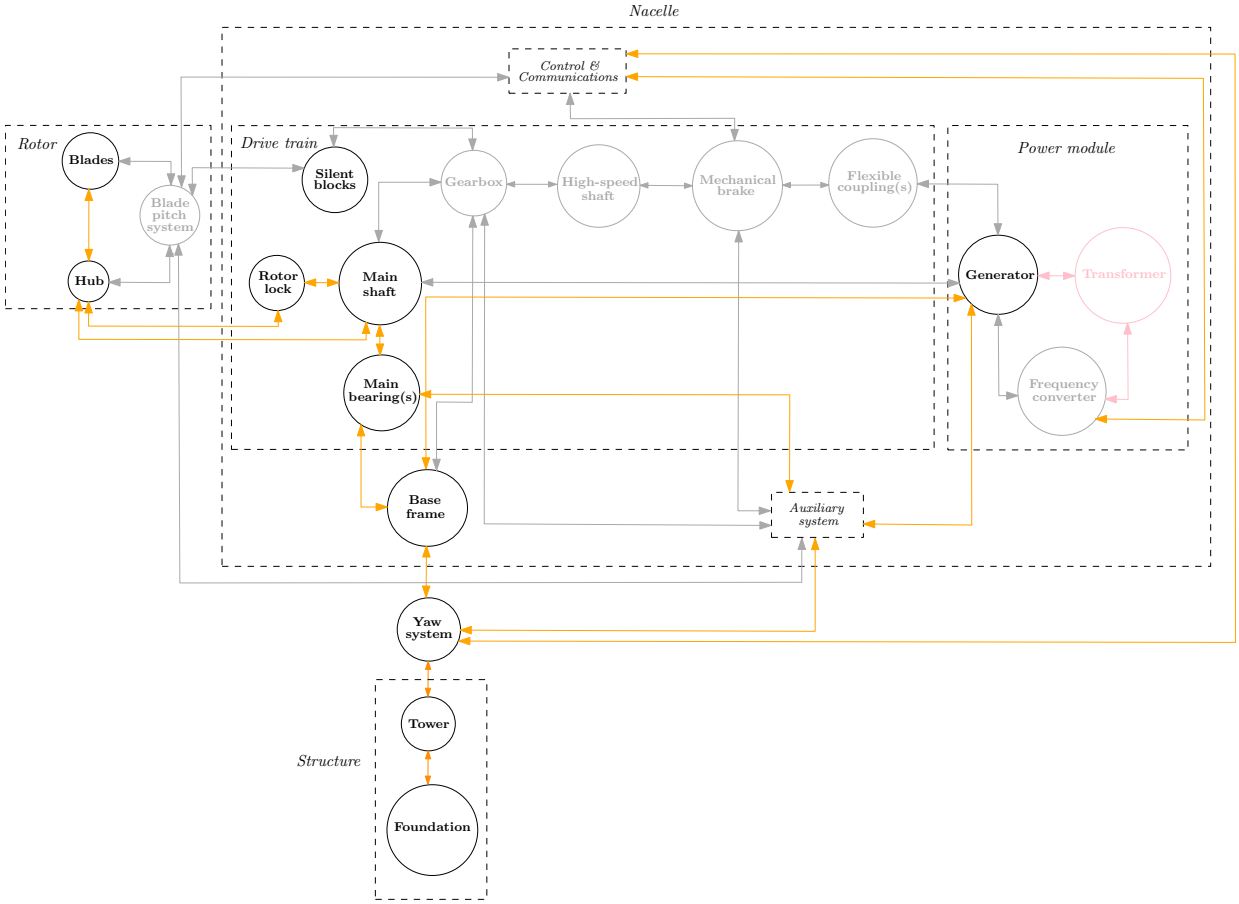

Figure 3.3: A simplified overview of the physical connections between the assemblies of a HAWT. The orange arrows indicate physical connections between (sub-)assemblies that are present in every HAWT, whereas the gray arrows refer to physical connections that depend on the WT-configuration.

3.3 General functional relations for HAWT's

Generally, in System Engineering the design of a system starts with identifying the functions and functional requirements which make up the system. Based on these, the physical solutions to provide for these functions are assigned. In the case of this work, the physical architecture of the system is already established. Therefore, to find the functional dependencies, the physical connections between the (sub-)assemblies have first been studied (see **section 3.2**) after which the functions of the (sub-)assemblies have been identified. The functionalities of the (sub-)assemblies are listed in **Appendix A**.

For this work, *a functional dependency is defined as the relation between subassembly X and Y such that the functionality of subassembly Y depends on or is controlled by input from subassembly X in order to function properly.* Taking this into account, the functional relations/dependencies between the (sub-)assemblies have been established. These are explained in **Table 3.1** and are graphically presented in **Figure 3.4**.

Assembly	Functional dependency	Description
Blades	Hub	The blades can only produce a torque from the wind if they are properly supported by the hub.
	Blade pitch system	The torque produced by the blades depends among others on the blade angle of attack, which is regulated by pitching the blades with the aid of the blade pitch bearings.
Blade pitch system	Auxiliary system	The blade pitch bearings require sufficient lubrication in order to function properly.
	Control & Communications	In order to adjust the pitch angles of the blades, the slewing gearboxes or hydraulic cylinders (in the case of an electric or hydraulic blade pitch drive) must receive a signal with the required pitch angle from the Control & Communications.
Hub	Main shaft	In order to be able to support the blades, the hub is mounted on the main shaft.
Main shaft	Main bearings	The rotational motion of the main shaft and the main shaft itself are supported by the main bearings.
	Gearbox (bearings)	Other functional dependencies present is the dependency between the gearbox bearings and the main shaft, since the rotation of the main shaft is not only supported by the main bearings, but also by a planet carrier bearing that supports the hallow input shaft in which the main shaft is mounted.
	Auxiliary System	In order to function properly, the main bearings require sufficient lubrication.
Gearbox	Auxiliary System	In order to ensure proper functioning of the gearbox, it must be cooled by a cooling system. Also, the bearings of the gearbox require sufficient lubrication.
	Silent blocks	The silent blocks of the gearbox absorb the torsional moment acting on the gearbox, due to the rotor torque, to prevent the gearbox from rotating.

Assembly	Functional dependency	Description
High-speed shaft	Gearbox (bearings)	The rotational motion of the high-speed shaft and the high-speed shaft itself are supported by the high-speed shaft bearings of the gearbox.
Mechanical brake	Auxiliary System	The calliper of the mechanical brake requires hydraulic oil for providing a braking force.
	Control & Communications	The flow of hydraulic oil to calliper is controlled via a control valve that receives a signal from the Control & Communications.
Generator	High-speed shaft	The torque required for generating electrical energy is transmitted via the high-speed shaft to the generator.
	Main shaft (in the case of gearless WT)	*The torque required for generating electrical energy is transmitted via the main shaft to the generator.*
	Flexible coupling	The torque required for generating electrical energy is transmitted via the high-speed shaft further to the flexible coupling and ultimately to the generator shaft.
	Auxiliary System	Similar to the gearbox, the generator requires cooling in order to be able to function properly. Also, the bearings of the generator require sufficient lubrication.
	Frequency converter	Between cut-in and rated wind speed, the generator speed and thus the power output of the generator is controlled by the frequency converter.
Frequency converter	Control & Communications	In order to control the generator speed, the frequency converter must first receive a signal containing the required generator speed from the Control & Communications.
Yaw system	Auxiliary System	The calliper of the yaw brake system requires hydraulic oil in order to provide a clamp force to the brake disc. Moreover, the yaw bearing and yaw ring gear require sufficient lubrication.
	Control & Communications	The yaw motor must receive a signal from the Control & Communications containing the wind direction prior to rotating the nacelle.

Table 3.1: The functional dependencies of a HAWT.

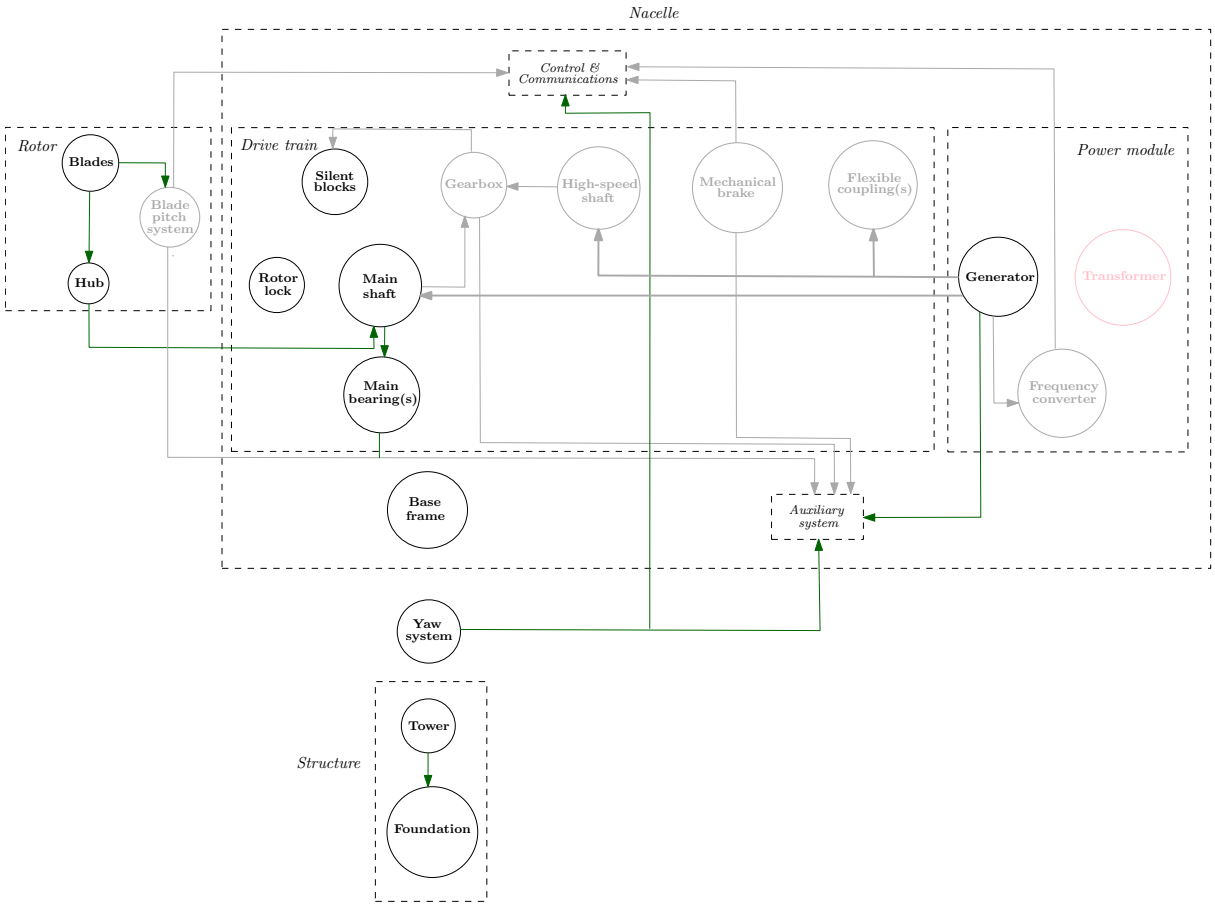

Figure 3.4: A simplified overview of the functional connections between the assemblies of a HAWT. The green arrows indicate functional dependencies between (sub-)assemblies that are always present in a HAWT, whereas the gray arrows represent functional relations between (sub-)assemblies which may not always be present for a certain WT-configuration. *Note that an arrow comes from the (sub-)assembly which functionally depends on the (sub-)assembly at which the arrow points*.

3.4 Existing methods regarding the application of SCADA-parameters

According to [4] several approaches using SCADA-data for failure detection currently exist. The authors of [4] have reviewed recent approaches using SCADA-data and have categorized them as i. trending, ii. clustering, iii. normal behavior modelling, iv. damage modelling and v. assessment of alarms and expert systems.

Trending methods include plotting SCADA-parameters against each other and interpreting the behaviors of these graphs in order to detect upcoming failures. The authors of [4] have pointed out that even though trending can reveal upcoming failures, various studies have shown that observed deviations are case dependent making interpretations of such changes difficult. The authors of [4] also mentioned the visual interpretation of trends may be difficult for large fleets of WTs as generally WTs operate under very different conditions. Therefore, research on the application of SCADA-data shifted to clustering algorithms for automating the classification of normal and faulty behaviors. In this regard, machine learning techniques are used for grouping normal and faulty data into clusters. [4] mentioned that the clustering of faulty and healthy data has not shown a clear advantage compared to trending algorithms. Another approach for fault detection through SCADA-data is modelling the behavior of normal operation so that anomalies are detected in the data. Here, the residual

of the measured signal minus the modelled signal acts as an indicator for a possible fault. When the residual is equal to 0 normal conditions are assumed, while a residual unequal to 0 indicates a possible fault. Normal behavior modelling can be based on linear and polynomial models, Artificial Neural Networks (ANNs), fuzzy systems or other methods not covered under these categories. A disadvantage of normal behavior modelling is that thresholds are manually set, which leads to frequent false alarms [4]. Lastly, damage modelling has been proposed to better predict failures. This method is based on the interpretation of SCADA-parameter signals with the aid of physical models.

This work aims to analyze SCADA-parameters for failure detection based on the functional relations between WT (sub-)assemblies. This means that based on the functional relations, the relations between the SCADA-parameters are established and for each parameter set it will be studied whether deviations are visible, i.e. whether failure can be detected. However, given that WT (sub-)assemblies may be monitored by multiple parameters, a main challenge in this regard is understanding which of these parameters can be used for detecting failure. From the literature review it was found that most works do not provide a method for understanding why a specific set of parameters are plotted against each other for failure detection. Also, most works do not show how the deviations seen in the data can be explained. In order to overcome this challenge, this work takes into account the physics governing the energy conversion process of a HAWT.

3.5 Physics governing the energy conversion process of a HAWT

In literature, various SCADA-parameters are analyzed over time or against each other in order to detect failures. However, a reasoning for plotting specific parameters against each other and/or an explanation of the root(s) behind the deviations from their normal behavior, is often lacking. *As the SCADA-parameters are related to the physics and monitor various WT functionalities, knowledge of the load transfer supports arguing which WT functionalities and thus the SCADA-parameters that may be affected due to abnormal operation of the WT. Additionally, the physics behind the load transfer support understanding how the SCADA-parameters are related to each other and how they may be plotted against each other in order to detect deviations.*

Another advantage of studying the forces and/or moments is that:

iii. they allow arguing the functional relations established (in the previous sections) as well as aid in identifying additional functional relations that were neither found on the basis of the physical connections between the WT assemblies nor on the basis of their function descriptions;

This is true as fundamentally the tasks and arrangement of the assemblies is based on the requirement that they transmit, convert and/or absorb the reaction forces and/or moments that originate from the rotational motion of the rotor. This means that any disruptions in the physical connections of the assemblies and consequently in their functionalities can be explained by looking into the loads that they carry.

The following subsections intend to identify the forces and/or moments that generally act on the WT (sub-)assemblies.

3.5.1 Wind turbine loads

In this section, the term "loads" refers to the forces and moments that act upon a WT.

During operation, a WT experiences loads of varying nature. These loads arise due to various reasons, for example the interaction of the wind with the rotor and tower (aerodynamics), the dead weight of the turbine assemblies (gravity), the simultaneous motion of the rotor and nacelle (gyroscopics), the control actions of the turbine controller (actuation), etc.

According to [21] and [40], it is the loads acting on the rotor that are transferred to the rest of the turbine (assemblies). The authors of [21] even state that the loads acting on the rotor primarily determine the loading on these assemblies as compared to the rotor loads, "the loads originating directly from downstream components are less significant". Moreover, "discussions of the loads acting on a wind turbine can, therefore, be concentrated on the rotor and deal with it as being representative of all parts". With this being said, the current subsection studies how the forces and/or moments acting on the rotor are transferred to the rest of the energy converting assemblies and how these loads affect the SCADA-parameters selected for this work.

The analysis of the rotor loads shall be done from a *quasi-static* perspective. This means that high frequency fluctuations of loads, such as structure vibrations, are not studied in this work. The reason for this is two-fold:

i. the available data is also considered to be quasi-static in the sense that the SCADA-parameters are logged every 10-minutes for a long period of time: these 10-minute "snapshots" can be seen as a static representation of the parameter behaviors at a certain moment in time and when plotted for the entire monitored period present the (slowly) fluctuating behavior of the parameters over time. Moreover, as these snapshots are the average value for a 10-minute time interval it is not possible to study the parameter behaviors, and thus the existing operating conditions, within this interval;
ii. this work does not intend to calculate the actual loads experienced by the WT assemblies: the objective is to fundamentally understand how the assemblies and thus the SCADA-parameters are affected by the presence of a certain force. For this it is sufficient to study the physics governing the energy conversion process in a basic way, since the fundamental principle of the energy conversion process (and thus the transfer of the loads required for/during this process) remains the same either from a static or dynamic perspective. Worth mentioning is that once the load path has been established for the static case, it is possible to extend this framework for a dynamic case as this would include adding other forces to the load path.

3.5.2 Rotor loads

The loads acting on the blades are transferred to the hub and from here to the rest of the assemblies in the nacelle and ultimately to the tower foundation. According to [22][40][41], the main sources of blade loading are among others **aerodynamic**, **gravity**, **centrifugal**, **inertial** and **actuation** forces. Since this work applies quasi-static analysis to the loads, inertia and actuation forces are *neglected*. As regards actuation forces, their occurrence during WT operation is temporary and therefore they are not taken into account. Also, gyroscopic loads are the result of a high yawing (= actuation) rate and are often mentioned in literature as a source of rotor blade loading. According to [21], yawing is normally done at low rates and so gyroscopic loads are neglected in this work.

From here on, the rotor loads are briefly introduced and thereafter the load path/flow from the blades to the rest of the WT assemblies is described.

Aerodynamic loads
As the wind flows over the turbine blades, the blades experience a force from the wind. This force pushes the blade back as well as lifts it and is called the aerodynamic force. The aerodynamic force can be decomposed in a *lift* force, F_l, and a *drag* force, F_d. These forces can be further decomposed into a *normal* force, F_n, and *tangential* force, F_t. The normal force produces a *thrust* force on the rotor, while the tangential force is responsible for *torque* generation. Worth mentioning is that due to the nature of the wind this thrust and torque force alternate during one revolution. This is explained in **section 3.5.3**.

In addition to the lift and drag force, the wind causes a moment *in* the airfoil [40]. This moment is

called the *(aerodynamic) pitching moment* and causes *twisting* of the blade. Generally, M_p is defined about a certain point along the chord line and is calculated as the sum of the moment of the lift force and an additional pure moment about this point. Further, it is considered positive when it tends to turn the nose of the airfoil in clockwise direction [30]. Similar to the lift and drag force, M_p alternates during one revolution as it depends on v_{rel}. This will be explained in **section 3.5.3**.

Gravitational loads
Due to the dead weight of the blades and their rotation in earth's gravity field, the blades of a WT are subject to a gravity force, F_G, that is always directed in downward direction. Depending on the position of the blades, F_G generates pressure and tensile forces along the longitudinal axis of the blades and bending moments in the chordwise and flapwise direction of the blades. These forces and moments alternate during one revolution, since the direction of F_G remains unchanged for every position of the blades.

Centrifugal loads
Due to the circular motion of the blades they experience a centrifugal force, F_C, that is directed outward along their longitudinal axis. In contrast to the aerodynamic and gravitational loads, this force does not alternate during the rotation of the blades.

In the following section the transfer of the abovementioned loads to the rest of the WT (assemblies) is explained in several steps.

3.5.3 Load analysis

As mentioned earlier, due to the nature of the wind the thrust and torque alternate during one revolution. Generally, the wind is variable in nature [22][32][43]. At the Earth's surface the actual wind speed ($\mathbf{V_{wind}}$) varies with height above the ground [22][32] due to surface friction [43]. Farther away from the Earth's surface the wind speed increases, however at a certain height, surface friction has a negligible effect and the wind is assumed to have constant speed [22]. The variation of the actual wind speed with height is called the *vertical profile of the wind speed* or *vertical wind shear*. **Figure 3.5** shows an example of a vertical profile of the actual wind speed. From this figure it can be seen that the flow toward a WT is essentially turbulent [47] (the explanation regarding the origins of turbulence is out of scope of this work) and that $\mathbf{V_{wind}}$ varies in direction (and time) around a mean value [32].

The actual wind speed at a fixed point can be split into two components, namely a *quasi-steady wind speed*, usually called mean wind speed ($\mathbf{V_{mean}}$, see **Figure 3.5**), and the *atmospheric turbulence*. According to [43], the mean wind speed is obtained as the average of the instantaneous wind speed over a period of usually 10 to 20 minutes and thus it can be concluded that this is the average ambient wind speed that is typically monitored by a WT SCADA-system. Lastly, the atmospheric turbulence represents fluctuations around the mean wind speed.

Given all of the above it is now clear that the magnitude of $\mathbf{V_{wind}}$, represented as v_{wind}, varies - i.e. increases - along the height of the turbine. This means that as a blade (segment) rotates it shall *experience* a cyclic wind speed, i.e. $\mathbf{V_{rel}}$ is periodic in nature during one revolution. This causes the lift and drag force, and thus F_n and F_t, for that segment to be periodic during a revolution. **Figure 3.6** shows an example of the periodic behavior of the torque due to the variation of the mean wind speed with height.

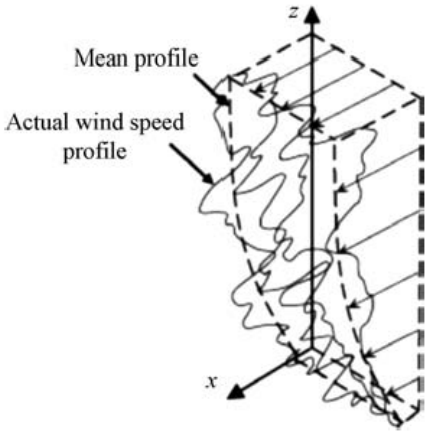

Figure 3.5: Example of vertical profile of the wind speed [32].

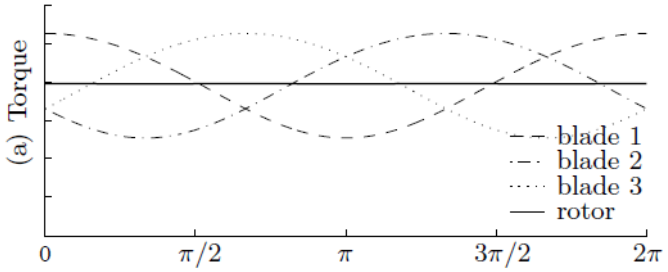

Figure 3.6: Cyclic torque fluctuations due to variations of the mean wind speed in height [43].

As the blade of a WT is twisted and the circumferential blade speed, $\mathbf{V_{blade}}$, varies along the blade span, a WT blade is, for analyses purposes, generally assumed to be made up of an arbitrary number of segments. This allows studying the effect of the wind on each segment: for each segment the aerodynamic force is decomposed into a F_l and F_d. F_l acts *perpendicular* to the direction of the *relative* wind speed, $\mathbf{V_{rel}}$, and F_d acts in the direction of or *parallel* to the relative wind speed (see **Figure 3.7**), where $\mathbf{V_{rel}}$ is the wind speed that the rotor blades *experience* as a result of their movement relative to the wind. In other words, $\mathbf{V_{rel}}$ is the difference between the actual speed of the incoming wind, $\mathbf{V_{wind}}$, and $\mathbf{V_{blade}}$. When the lift and drag force are decomposed in reference to the plane of rotation of the blades F_n and F_t are obtained.

Figure 3.7 shows the aerodynamic forces, gravitational force and centrifugal force acting on a blade-segment of an airfoil including a *velocity triangle* that explains how $\mathbf{V_{rel}}$ is determined. The F_n, F_t, M_p, F_g, and F_c of each segment are transferred to the blade root. To simplify the analysis, the transmission of the blade segment loads is studied for their *resultant* loads that act on the entire blade.

Resultant loads

Normal and tangential forces and pitching moments

The normal and tangential force F_n and F_t acting on a blade segment is calculated as follows:

$$F_n = F_l \cos\theta + F_d \sin\theta \tag{3.1}$$

$$F_t = F_l \sin\theta - F_d \cos\theta \tag{3.2}$$

where θ is the angle between $\mathbf{V_{rel}}$ and the rotation plane of the blades (see **Figure 3.7**), from here on called the *angle of relative wind* [33]. Here, F_l and F_d are calculated as follows:

$$F_l = \frac{1}{2}\rho {v_{rel}}^2 c C_l(\alpha) \tag{3.3}$$

$$F_d = \frac{1}{2}\rho {v_{rel}}^2 c C_d(\alpha) \tag{3.4}$$

where ρ is the air density, c is the blade chord length, v_{rel} is the magnitude of $\mathbf{V_{rel}}$ [30] and C_l and C_d the lift and drag coefficient of the airfoil, respectively.

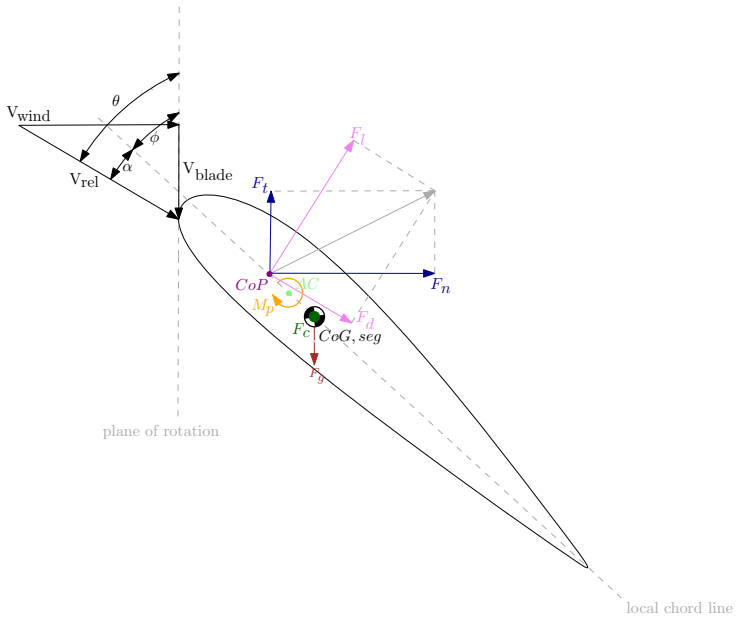

Figure 3.7: Loads acting on airfoil.

The normal and tangential forces of the blade segments produce a load distribution along the blade length of which their resultant forces, F_N and F_T, respectively, act at the *center of pressure (CoP)* of a certain blade cross-section - the *CoP* is also the point where F_n, F_t, F_l and F_d act (see **Figure 3.7**). As the location of the *CoP* of F_N and F_T is unknown, its location is chosen to coincide with the *center of gravity (CoG)* of the blade. Further, the *CoG* of the blade is assumed to act at a fixed distance R from the blade root.

For a certain position Φ (= the azimuth angle/position of the blade during rotation) of the blade, F_N and F_T can be obtained by integrating equations (3.1) and (3.2) over the length of the blade for $0 \leq r \leq R$, where R isthe length of the blade and r is the distance from a blade element to the axis of rotation. Namely, for each distance r the value of F_n and F_t is different due to the variation of v_{wind} along the height of the turbine and thus along the length of the blade. As mentioned earlier, this variation causes the magnitude of v_{rel} to be different along the blade length and as a result, the magnitude of F_l and F_d and thus F_n and F_t (see **equations 3.1** till **3.4**).

Apart from the distance r along the blade, from **equations (3.3)** and **(3.4)** it can also be seen that the magnitude of F_l and F_d and ultimately F_N and F_T depend on the *(local) angle of attack*, α, which is the angle between the line of chord and $\mathbf{V_{rel}}$ (see **Figure 3.7**). The angle of attack depends on i) θ and ii) the *(local) pitch angle* of the blade, ϕ. This is the local angle between the chord of the airfoil and the plane of rotation [30].

The next step in the analysis is to determine the resultant of all pitching moments, M_p. Previously it was stated that M_p is defined about a point along the chord line of the airfoil. Generally, M_p changes when α changes. This is because when α changes, the point of action of the lift force changes and as a consequence its moment changes. However, there is a point along the chord line where the M_p no longer changes with α [35]. This point lies at approximately $c/4$ of the chord from the leading edge of the airfoil and is called the *aerodynamic center (AC)*. The formula for calculating M_p for a blade segment, i.e. per meter, is given below:

$$M_p = \frac{1}{2}\rho {v_{rel}}^2 c^2 C_m(\alpha) \tag{3.5}$$

where C_m is called the pitching moment coefficient [34] and depends on the angle of attack. Similar to the normal and tangential forces, the resultant pitching moment, M_P, is obtained by integrating **equation 3.5** over the length of the blade.

Gravitational and centrifugal force
The resultant of the gravitational forces acting on the blade segments, F_G, generally already acts in the *CoG* of the blades. F_C, which is taken as the resultant of the centrifugal forces acting on the blade segments is, similar to F_N and F_T, also assumed to act in the *CoG*. The magnitude of the centrifugal force acting on a blade segment depends on the angular speed of the rotor, ω, and the distance r from the axis of rotation as follows:

$$F_c = m\omega^2 r \tag{3.6}$$

The resultant, F_C, is found by integrating **equation 3.6** over the entire blade length for $0 \leq r \leq R$.

Given that only F_N, F_T and M_P depend on the wind profile, their behavior is periodic, while the behavior of F_G and F_C on the other hand are constant for one revolution.

The following subsections explain how the above-mentioned resultant loads are transferred from the CoG of the blades to the blade root center.

3.5.3.1 Loads transfer from blade cross-section reference system to blade root reference system

The transfer of the resultant loads to the root is studied with the aid of two reference systems: the first reference system is applied at the *CoG* of the blade and the second is applied at the *blade root center* of the blades.

The axes of the blade cross-section reference system are oriented as follows:

i. x_{cross}-axis normal to plane of rotation of the blades (assuming zero tilt and cone angle) and positive towards the suction side of the airfoil;
ii. y_{cross}-axis directed tangential to the rotor plane (assuming zero tilt and cone angle) and positive in counter clockwise direction;
iii. z_{cross}-axis taken along the pitch axis of the blade and positive towards the tip of the blade.

For simplicity, this reference system is chosen to correspond with the direction of the normal and tangential forces, rather than with the chord line of the airfoil as has been done in literature and other works (see [38], [45] and [49]). This means that the reference system does not rotate with the *pitch angle* of the blade and is neither oriented by the *twist angle* of the blade cross-section.

For the blade root reference system the direction of its axes are chosen:

i. x_{root}-axis normal to plane of rotation of the blades (assuming zero tilt and cone angle) and positive along the rotor axis;
ii. y_{root}-axis directed tangential to the rotor plane (assuming zero tilt and cone angle) and positive in counter clockwise direction;
iii. z_{root}-axis taken along the pitch axis of the blade and positive towards the tip of the blade (assuming zero cone angle).

Similar to the blade cross-section reference system, this system does not rotate with the the pitch angle. Since this system is located in the blade root, the effect of the twist angle does not apply in this case.

For the analysis of the load flow the origin of the blade cross-section reference system is chosen at the *CoG* of the blade and the origin of the blade root reference system at the *blade root center* (see **Figure 3.8**). Given that the *CoP* was earlier chosen to coincide with the *CoG*, only M_P produces a reaction moment with respect to the blade cross-section reference system, while the reaction moments of F_N, F_T, F_G and F_C are zero. Further, the assumption is made that the *CoG* falls at the intersection of the *blade pitch axis* and the local chord line of the airfoil, where the intersection point is assumed to be located at a distance R (along the z_{root}-axis) from the blade root center. This assumption allows neglecting additional reaction moments of F_T, F_C and F_G that would be caused relative to the blade reference system due to their distance d (see **Figure 3.8**) from the blade root center.

Blade loads relative to blade cross-section reference frame
With M_P assumed positive in clockwise direction, its reaction moment, $M_{P_{cross}}$, acts along the $+z_{cross}$-axis (see **Figure 3.8**). Further, F_N, F_T, F_G and F_C create the reaction forces, $F_{N_{cross}}$, $F_{T_{cross}}$, $F_{G_{cross}}$ and $F_{C_{cross}}$ relative to the blade cross-section reference system.

Worth mentioning is that as the blades rotate the direction of F_G changes relative to the blade (see **Figure 3.9**). Moreover, with F_G always directed vertical and in downward direction, it does not "rotate" with the blade cross-section nor the blade root reference systems. Consequently, the moment that is created by F_G in the blade root depends on the position of the blade and is either due to F_G itself (position b) or due to its component $F_{G_{y_{cross}}}$ (position a).

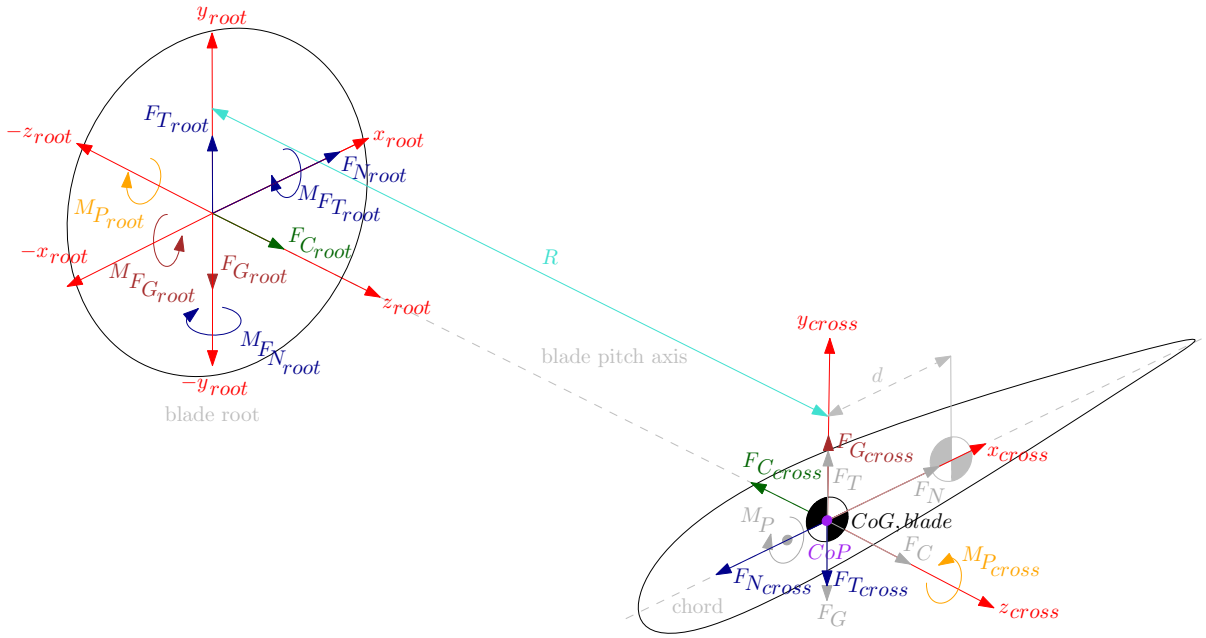

Figure 3.8: Load transfer from blade cross-section to blade root center.

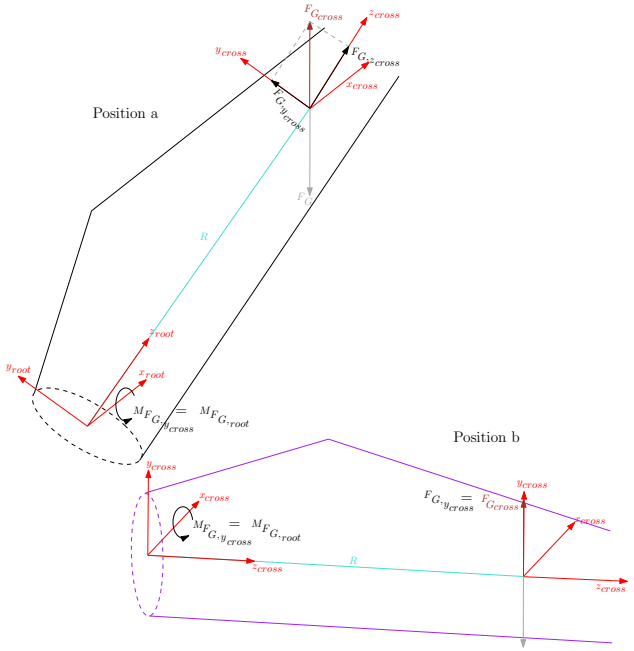

Figure 3.9: Moment of $F_{G_{cross}}$ in the blade root.

Blade loads relative to blade (root) reference frame

Now that the resultant blade loads are translated to the blade cross-section reference system, they can be transferred to the blade reference system, i.e the blade root (see **Figure 3.8**). Recall that the *CoG* was assumed to be located at a distance R from the blade root. Therefore, $F_{N_{cross}}$, $F_{T_{cross}}$ and $F_{G_{cross}}$ produce (bending) moments in the blade root. These moments are referred to as $M_{F_{N_{root}}}$, $M_{F_{T_{root}}}$ and $M_{F_{G_{root}}}$, respectively. As $F_{C_{cross}}$ is directed along - z_{cross}-axis, it does not create a moment in the blade

root. Further, $M_{P_{cross}}$ causes a (twisting) moment along the + z_{root}-axis. Lastly, the blade reference system sees the reaction forces of $F_{N_{cross}}$, $F_{T_{cross}}$, $F_{G_{cross}}$ and $F_{C_{cross}}$. These reaction forces point in the same direction as F_N, F_T, F_G and F_C.

Note that this load transfer is applied to all three blades. These loads flow from the blade roots to the hub and the rest of the WT assemblies, which means that the sum of the blade root loads of all blades form the loads seen by the hub [48]. For this reason the blade root loads must be transformed to a single reference system, placed in the hub, after which they can be summed.

3.5.3.2 Loads transfer from blade root reference system to hub reference system

The hub reference system is chosen to be fixed and its origin is placed at the hub center - this point aligns with the intersection point of the blade pitch axes. The hub center is further located on the centerline of the low-speed shaft and is assumed to be at a distance H from the blade root centers. Lastly, the axes of the hub reference system are taken as follows:

i. x_{hub}-axis normal to the rotation plane of the blades and positive along the rotor axis;
ii. y_{hub}-axis along the rotation plane of the blades and positive to the left;
iii. z_{hub}-axis along the rotation plane of the blades and directed vertical in upward direction.

In order to transform the loads from the blade (root) reference systems to the hub reference system, a rotation matrix is applied to the loads in the blade roots:

$$R(\Phi) = \begin{pmatrix} 1 & 0 & 0 \\ 0 & \cos\Phi & -\sin\Phi \\ 0 & \sin\Phi & \cos\Phi \end{pmatrix} \tag{3.7}$$

where $0 \leq \Phi \leq 2\pi$. The matrix R is used for rotating the root loads around the x_{root}-axis, since only the directions of the y_{root}- and the z_{root}-axis change as the blades rotate. The loads seen by the hub during one revolution can now be expressed with the following equations:

Blade 1:

$$\begin{aligned} \begin{pmatrix} F_{x_{hub,\ blade\ 1}} \\ F_{y_{hub,\ blade\ 1}} \\ F_{z_{hub,\ blade\ 1}} \end{pmatrix} &= \begin{pmatrix} 1 & 0 & 0 \\ 0 & \cos\Phi & -\sin\Phi \\ 0 & \sin\Phi & \cos\Phi \end{pmatrix} \begin{pmatrix} F_{x_{root}}(\Phi) \\ F_{y_{root}}(\Phi) \\ F_{z_{root}}(\Phi) \end{pmatrix}, \quad \text{for } 0 \leq \Phi \leq 2\pi \\ &= \begin{pmatrix} 1 & 0 & 0 \\ 0 & \cos\Phi & -\sin\Phi \\ 0 & \sin\Phi & \cos\Phi \end{pmatrix} \begin{pmatrix} F_{N_{root}}(\Phi) \\ [F_{T_{root}}(\Phi) + F_{G_{y_{root}}}(\Phi)] \\ [F_{G_{z_{root}}}(\Phi) + F_{C_{root}}(\Phi)] \end{pmatrix} \end{aligned} \tag{3.8}$$

$$\begin{aligned} \begin{pmatrix} M_{x_{hub,\ blade\ 1}} \\ M_{y_{hub,\ blade\ 1}} \\ M_{z_{hub,\ blade\ 1}} \end{pmatrix} &= \begin{pmatrix} 1 & 0 & 0 \\ 0 & \cos\Phi & -\sin\Phi \\ 0 & \sin\Phi & \cos\Phi \end{pmatrix} \begin{pmatrix} M_{x_{root}}(\Phi) \\ M_{y_{root}}(\Phi) \\ M_{z_{root}}(\Phi) \end{pmatrix}, \quad \text{for } 0 \leq \Phi \leq 2\pi \\ &= \begin{pmatrix} 1 & 0 & 0 \\ 0 & \cos\Phi & -\sin\Phi \\ 0 & \sin\Phi & \cos\Phi \end{pmatrix} \begin{pmatrix} [M_{F_{T_{root}}}(\Phi) + M_{F_{G_{root}}}(\Phi)] \\ M_{F_{N_{root}}}(\Phi) \\ M_{P_{root}}(\Phi) \end{pmatrix} \end{aligned} \tag{3.9}$$

Blade 2:

$$\begin{aligned}\begin{pmatrix} F_{x_{hub,\ blade\ 2}} \\ F_{y_{hub,\ blade\ 2}} \\ F_{z_{hub,\ blade\ 2}} \end{pmatrix} &= \begin{pmatrix} 1 & 0 & 0 \\ 0 & \cos\Phi & -\sin\Phi \\ 0 & \sin\Phi & \cos\Phi \end{pmatrix} \begin{pmatrix} F_{x_{root}}(\Phi+120°) \\ F_{y_{root}}(\Phi+120°) \\ F_{z_{root}}(\Phi+120°) \end{pmatrix}, \text{ for } 0 \le \Phi \le 2\pi \\ &= \begin{pmatrix} 1 & 0 & 0 \\ 0 & \cos\Phi & -\sin\Phi \\ 0 & \sin\Phi & \cos\Phi \end{pmatrix} \begin{pmatrix} F_{N_{root}}(\Phi+120°) \\ [F_{T_{root}}(\Phi+120°) + F_{G_{y_{root}}}(\Phi+120°)] \\ [F_{G_{z_{root}}}(\Phi+120°) + F_{C_{root}}(\Phi+120°)] \end{pmatrix}\end{aligned} \tag{3.10}$$

$$\begin{aligned}\begin{pmatrix} M_{x_{hub,\ blade\ 2}} \\ M_{y_{hub,\ blade\ 2}} \\ M_{z_{hub,\ blade\ 2}} \end{pmatrix} &= \begin{pmatrix} 1 & 0 & 0 \\ 0 & \cos\Phi & -\sin\Phi \\ 0 & \sin\Phi & \cos\Phi \end{pmatrix} \begin{pmatrix} M_{x_{root}}(\Phi+120°) \\ M_{y_{root}}(\Phi+120°) \\ M_{z_{root}}(\Phi+120°) \end{pmatrix}, \text{ for } 0 \le \Phi \le 2\pi \\ &= \begin{pmatrix} 1 & 0 & 0 \\ 0 & \cos\Phi & -\sin\Phi \\ 0 & \sin\Phi & \cos\Phi \end{pmatrix} \begin{pmatrix} [M_{F_{T_{root}}}(\Phi+120°) + M_{F_{G_{root}}}(\Phi+120°)] \\ M_{F_{N_{root}}}(\Phi+120°) \\ M_{P_{root}}(\Phi+120°) \end{pmatrix}\end{aligned} \tag{3.11}$$

Blade 3:

$$\begin{aligned}\begin{pmatrix} F_{x_{hub,\ blade\ 3}} \\ F_{y_{hub,\ blade\ 3}} \\ F_{z_{hub,\ blade\ 3}} \end{pmatrix} &= \begin{pmatrix} 1 & 0 & 0 \\ 0 & \cos\Phi & -\sin\Phi \\ 0 & \sin\Phi & \cos\Phi \end{pmatrix} \begin{pmatrix} F_{x_{root}}(\Phi-120°) \\ F_{y_{root}}(\Phi-120°) \\ F_{z_{root}}(\Phi-120°) \end{pmatrix}, \text{ for } 0 \le \Phi \le 2\pi \\ &= \begin{pmatrix} 1 & 0 & 0 \\ 0 & \cos\Phi & -\sin\Phi \\ 0 & \sin\Phi & \cos\Phi \end{pmatrix} \begin{pmatrix} F_{N_{root}}(\Phi-120°) \\ [F_{T_{root}}(\Phi-120°) + F_{G_{y_{root}}}(\Phi-120°)] \\ [F_{G_{z_{root}}}(\Phi-120°) + F_{C_{root}}(\Phi-120°)] \end{pmatrix}\end{aligned} \tag{3.12}$$

$$\begin{aligned}\begin{pmatrix} M_{x_{hub,\ blade\ 3}} \\ M_{y_{hub,\ blade\ 3}} \\ M_{z_{hub,\ blade\ 3}} \end{pmatrix} &= \begin{pmatrix} 1 & 0 & 0 \\ 0 & \cos\Phi & -\sin\Phi \\ 0 & \sin\Phi & \cos\Phi \end{pmatrix} \begin{pmatrix} M_{x_{root}}(\Phi-120°) \\ M_{y_{root}}(\Phi-120°) \\ M_{z_{root}}(\Phi-120°) \end{pmatrix}, \text{ for } 0 \le \Phi \le 2\pi \\ &= \begin{pmatrix} 1 & 0 & 0 \\ 0 & \cos\Phi & -\sin\Phi \\ 0 & \sin\Phi & \cos\Phi \end{pmatrix} \begin{pmatrix} [M_{F_{T_{root}}}(\Phi-120°) + M_{F_{G_{root}}}(\Phi-120°)] \\ M_{F_{N_{root}}}(\Phi-120°) \\ M_{P_{root}}(\Phi-120°) \end{pmatrix}\end{aligned} \tag{3.13}$$

Total hub loading:

$$\begin{pmatrix} F_{x_{hub,\ total}} \\ F_{y_{hub,\ total}} \\ F_{z_{hub,\ total}} \end{pmatrix} = \begin{pmatrix} F_{x_{hub,\ blade\ 1}} \\ F_{y_{hub,\ blade\ 1}} \\ F_{z_{hub,\ blade\ 1}} \end{pmatrix} + \begin{pmatrix} F_{x_{hub,\ blade\ 2}} \\ F_{y_{hub,\ blade\ 2}} \\ F_{z_{hub,\ blade\ 2}} \end{pmatrix} + \begin{pmatrix} F_{x_{hub,\ blade\ 3}} \\ F_{y_{hub,\ blade\ 3}} \\ F_{z_{hub,\ blade\ 3}} \end{pmatrix}, \text{ for } 0 \le \Phi \le 2\pi \tag{3.14}$$

$$\begin{pmatrix} M_{x_{hub,\ total}} \\ M_{y_{hub,\ total}} \\ M_{z_{hub,\ total}} \end{pmatrix} = \begin{pmatrix} M_{x_{hub,\ blade\ 1}} \\ M_{y_{hub,\ blade\ 1}} \\ M_{z_{hub,\ blade\ 1}} \end{pmatrix} + \begin{pmatrix} M_{x_{hub,\ blade\ 2}} \\ M_{y_{hub,\ blade\ 2}} \\ M_{z_{hub,\ blade\ 2}} \end{pmatrix} + \begin{pmatrix} M_{x_{hub,\ blade\ 3}} \\ M_{y_{hub,\ blade\ 3}} \\ M_{z_{hub,\ blade\ 3}} \end{pmatrix}, \text{ for } 0 \le \Phi \le 2\pi \tag{3.15}$$

From **equations 3.8 - 3.13** it can be seen that due to the rotation of the blades, the hub forces and moments are calculated for every angle Φ. Also, since the blades are separated by an angle of 120°, the total loading of the hub at each instant is found by summing the transformed forces and moments for $\Phi_{\text{blade 1}} = \Phi$, $\Phi_{\text{blade 2}} = \Phi + 120°$ and $\Phi_{\text{blade 3}} = \Phi - 120°$.

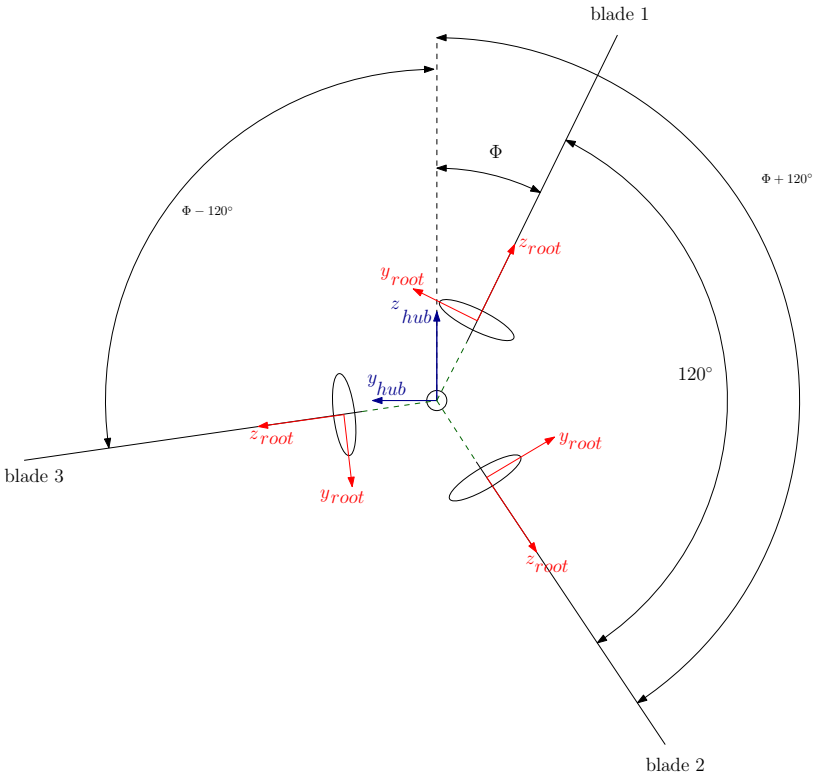

Figure 3.10: Summation of the blade root loads at an instant in time.

To summarize, the load analysis shows that the blade loads fundamentally depend on the position of the blades - and thus the magnitude of the incoming wind speed - and the blade pitch angles. Considering the case that all blades have the *same* blade pitch angle, the loads on each blade are still different in magnitude due to the position of the blades. When the blades are positioned at the "top" of the wind profile they experience higher loads compared to when they are positioned at the "bottom" of the wind profile - this is because of higher incoming wind speeds at the top of the wind profile. As each blade has different load magnitudes, the resultant of all blade loads, i.e. the hub loads, is actually never equal to 0. The analysis also showed that the hub forces and moments directed along the x_{hub}-axis are the *summation* of the transformed x_{root}-loads, e.g. $M_{x_{hub,total}}$ is the summation of the transformed moment of $[M_{F_{T_{root}}} + M_{F_{G_{root}}}]$ of each blade, while the hub loads acting along the y_{hub}-axis and z_{hub}-axis are the resulting loads after *subtraction* of all other transformed blade loads, e.g. $M_{y_{hub,total}}$ is the result of subtracting the transformed bending moment of $M_{F_{N_{root}}}$ of each blade, from each other.

When one of the blades has a *different* blade pitch angle, the magnitude of the loads of this blade changes even further (in **Appendix B.1** it is explained that the effect of pitch failure due to one blade is similar in nature compared to pitch failure of two or three blades, however smaller in magnitude). If, for example, the blade pitch angle of one blade is larger than the remaining two blades the resulting loads along the x_{hub}-axis decrease, while the loads along the y_{hub}-axis and z_{hub}-axis increase. On the other hand, if the blade pitch angle of this blade is smaller the resultant loads along all three axes increase. This implies that deviating blade pitch angles will either cause

an increase or decrease in the hub loads directed along the x_{hub}-axis, while the hub loads directed along the y_{hub}-axis and z_{hub}-axis will always increase.

As an example, the above is illustrated for the aerodynamic torque, $M_{F_{T_{root}}}$, and the bending moment $M_{F_{N_{root}}}$:

Generally, $F_{T_{root}}$ and $F_{N_{root}}$ are proportional to ${v_{rel}}^2$ based on **equations 3.2 - 3.4**. As v_{rel} depends on v_{wind}, $F_{T_{root}}$ and $F_{N_{root}}$ are proportional to ${v_{wind}}^2$.

Given that the wind speed varies with height, the authors of [43] have derived a formula that allows calculating the wind speed that is seen by a blade element that is located at a height h_r above the ground:

$$v_{wind}(h_r) = v_{wind}(h)\frac{\ln\left(\frac{h_r}{z_0}\right)}{\ln\left(\frac{h}{z_0}\right)} \tag{3.16}$$

where $h_r = h - r\cos\Phi$, h is the height of the tower, r is the distance from the blade element to the axis of rotation, Φ represents the azimuth angle/position of the blade during rotation and z_0 is the roughness length (this parameter has different values depending on the type of terrain [43]).

Taking $v_{wind}(h) = 1$, $h = 90$ meters, $r = R = 40$ meters, $h_r = 90 - 40\cos\Phi$ and $z_0 = 0.25$, **equation 3.16** becomes:

$$v_{wind}(h_r(\Phi)) = \frac{\ln\left(\frac{h_r(\Phi)}{0.25}\right)}{\ln\left(\frac{90}{0.25}\right)} \tag{3.17}$$

For $\Phi_{\text{blade 1}} = 0°$, $\Phi_{\text{blade 2}} = 120°$ and $\Phi_{\text{blade 3}} = -120°$, the resultant of $M_{F_{T_{root}}}$, $M_{x_{hub_{total}}}$, and of $M_{F_{N_{root}}}$, $M_{y_{hub_{total}}}$, becomes:

Pitch failure case	$M_{x_{hub,total}}$ (summation)	$M_{y_{hub,total}}$ (subtraction)
No pitch failure	2.52	0.30
One blade has smaller pitch angle	2.56 (increase)	0.42 (increase)
One blade has larger pitch angle	2.48 (decrease)	0.48 (increase)

Table 3.2: The effect of pitch failure on the hub loads.

Table 3.2 shows that pitch failure affects the resultant loads, in this case the torque and bending moment, in the hub center.

3.5.3.3 Loads transfer from hub to the rest of the WT assemblies

The loads seen by the hub center flow to the low-speed shaft, main bearings, gearbox, etc. For the analysis of the load flow through the drive train a configuration with two main bearings is chosen (see **Figure 3.11**). The reason for this is that even though generally different WT configurations are available [50], all are simplified versions of the "2-main bearing" configuration - this is explained in the work of [51]. The main bearings are assumed to be either ball or roller bearings, since these are widely used in the wind energy industry in, for example, main shaft mountings, gearboxes, generators, yaw systems, blade pitch systems, etc. [21][32].

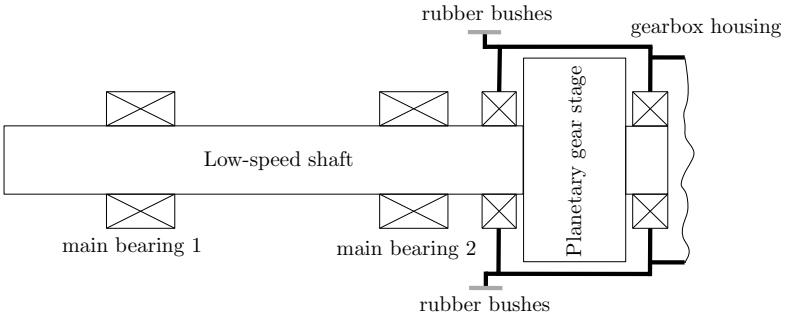

Figure 3.11: Schematic overview of a drive train configuration with two main bearings [51].

Low-speed shaft
At the front end of the low-speed shaft, the hub loads enter (see **Figure 3.12**). The hub forces are absorbed by the main bearings [53]. Together with the forces of the bending moments $M_{y_{hub,total}}$ and $M_{z_{hub,total}}$, the hub forces cause displacement of the shaft at the gearbox entrance. This displacement is in the z- and y-direction, respectively. In **Figure 3.12** the z-displacement is drawn as a green curve. Worth mentioning is that the displacement caused by the hub forces is larger than due to the forces of the bending moments, since the latter are the result of dividing the bending moments by a distance.

Main bearings
As mentioned earlier, the main bearings absorb the hub forces. They also have to compensate for the effect of the bending moments $M_{y_{hub,total}}$ and $M_{z_{hub,total}}$, which means that they experience an additional force due to these moments. Further, the main bearings support the weight of the shaft. Lastly, as shafts are generally supported by at least one fixed and loose bearing, the main bearings in **Figure 3.12** are drawn as fixed and loose. The fixed bearing fixes the shaft both radially and axially, while the loose bearing carries only radial loads.

Gearbox
Earlier it was mentioned that the hub forces and moments along the y_{hub} and z_{hub} direction cause a motion of the gearbox. To discuss this motion a coordinate system, of which the axes are in the same direction as the hub reference system, is assumed at the gearbox entrance. As the rotor torque is being transferred to the gearbox, it causes the gearbox to roll to its side - the direction of the tilt depends on the direction of the torque. Further, $M_{y_{hub,total}}$ causes the gearbox to pitch about the y_{gear}-axis, while $M_{z_{hub,total}}$ slightly yaws the gearbox about the z_{gear}-axis. It should be noted that the motion of the gearbox is determined by the stiffness of the rubber bushings and the magnitude of the rotor moments and forces (see **Figure 3.12**). As the rubber bushings allow movement of the gearbox, they are modelled as springs attached to the nacelle bed plate (see **Figure 3.12**).

High-speed shaft
While the gearbox moves the high-speed shaft undergoes the same motions. When the gearbox tilts to its side, the shaft moves vertically upward and horizontally to the left or right in the direction of the y_{gear}-axis. The pitching of the gearbox about this axis causes a vertical offset of the shaft. Further, when the gearbox yaws about the z_{hub}-axis the high-speed shaft displaces horizontally.

Flexible couplings
At the end of the high-speed shaft, a brake disk is installed. Between the brake and the generator either one or two flexible couplings can be mounted. These transmit the torque coming from the high-speed shaft and accommodate axial, angular and/or radial misalignment between the gearbox and the generator. When there is misalignment, the couplings produce forces and moments that are transmitted to the high-speed shaft and generator shaft [53][55]. The magnitude of these loads

depend on the amount of misalignment and the stiffness of the couplings. In **Figure 3.12** these couplings are replaced with springs.

Generator
The torque coming from the high-speed shaft passes through the flexible couplings and reaches the generator. Also, the loads due to the misalignment between the gearbox and generator are seen by the generator. More specifically, these loads must be carried by the generator bearings and thus the lifetime of the generator bearings ultimately depend on the misalignment between the gearbox and the generator. In general, the misalignment is not only caused by the motion of the gearbox. It can be a pre-existing condition or it can also be a result of the movement of the bedplate, as this also has a certain stiffness, and the motion of the generator due to its torque.

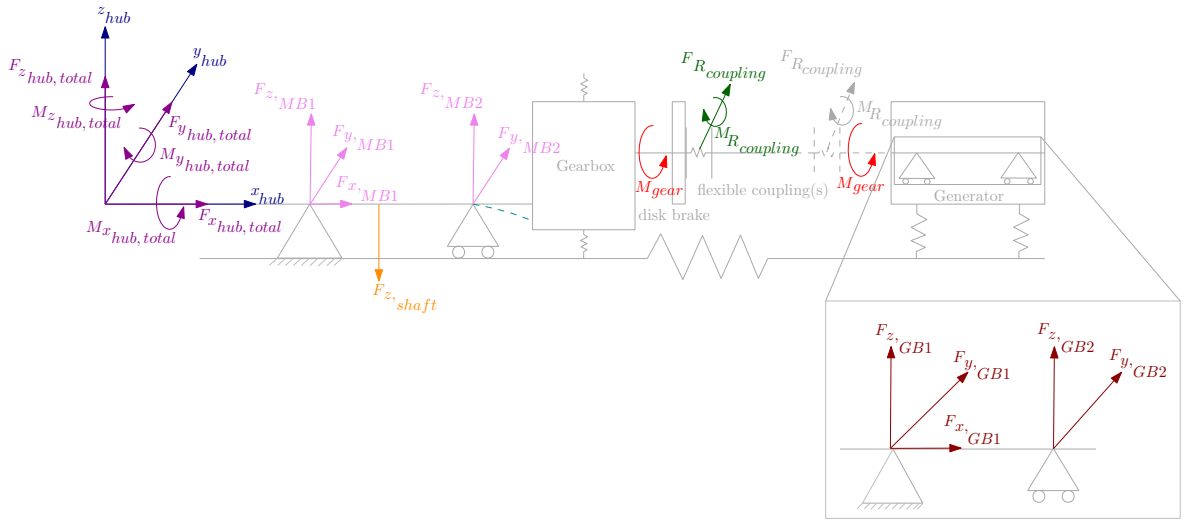

Figure 3.12: Load transfer from hub to generator bearings.

To summarize, the loads seen by the generator are primarily affected by the misalignment between the gearbox and generator. The compliance of the nacelle bed plate is not significant relative to the gearbox motion [53] and so the lifetime of the generator bearings is fundamentally affected by the stiffness of the rubber bushings of the gearbox and the hub forces and moments. Namely, the rubber bushings are intended to allow some displacement of the gearbox caused by the hub forces and bending moments. The displacement of the gearbox causes misalignment of the flexible coupling and as a result generates reaction loads in the coupling. Ultimately, the forces generated in the coupling cause reaction forces in the generator bearings.

Lastly, from statics it can be derived that the effect of the hub forces $F_{y_{hub,total}}$ and $F_{z_{hub,total}}$ on the gearbox movement is larger than due to the forces of the bending moments $M_{y_{hub,total}}$ and $M_{z_{hub,total}}$. This is because the forces due to the bending moments are smaller in magnitude, since they are obtained by dividing the bending moments by a distance.

Figure 3.13 presents a simplified overview of the load flow from the blades to the generator and WT foundation. The purple arrows indicate the load flow from the blades to the WT (sub-)assemblies which are generally present in a HAWT, while the gray arrows represent the load flow to/from WT (sub-)assemblies that do not exist in all HAWT-configurations.

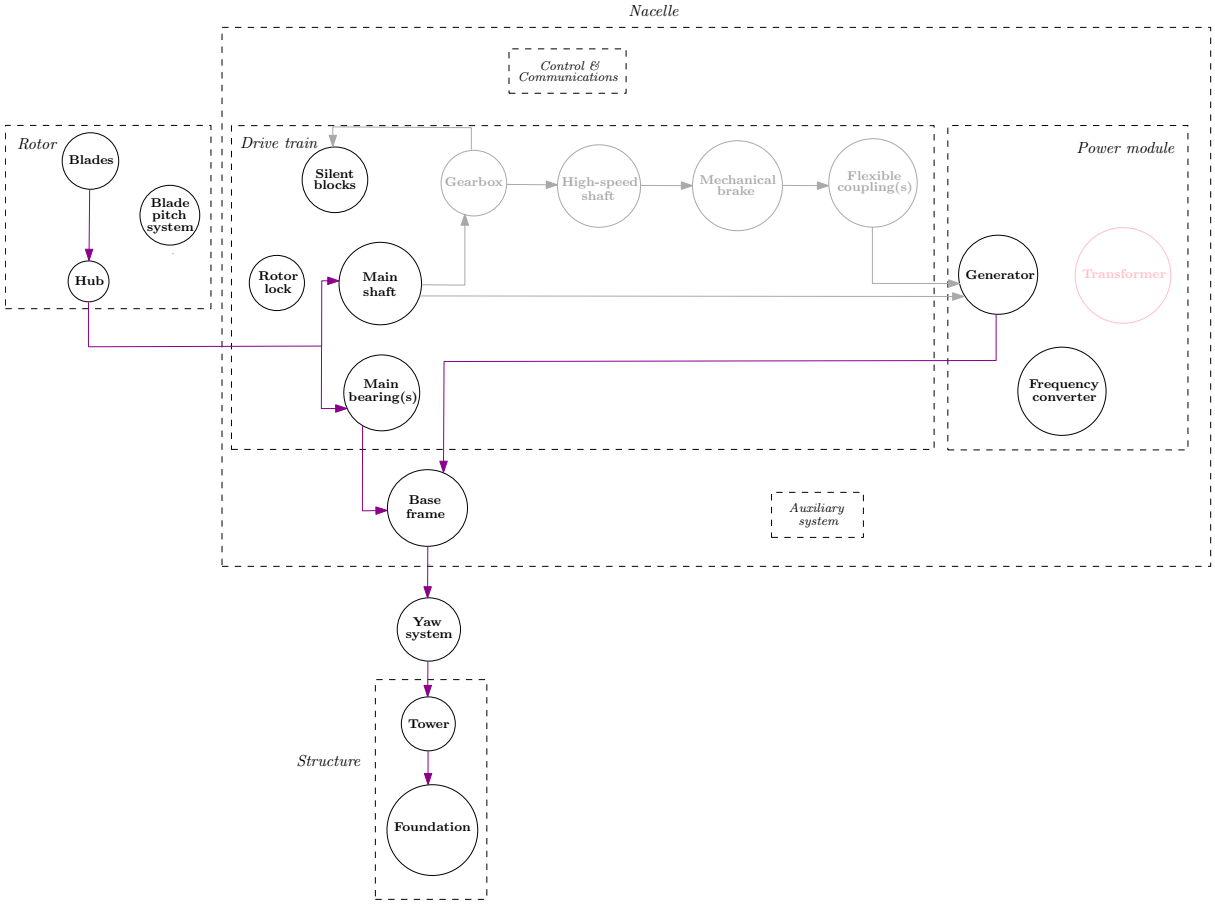

Figure 3.13: A simplified overview of the load flow from the blades to the foundation. The purple arrows indicate the load flow from the blades to those (sub-)assemblies which are generally present in a HAWT. The gray arrows represent the load flow to/from (sub-)assemblies that do not exist in all HAWT-configurations. *The direction of the arrow indicates the direction of the "flow" of the loads.*

To summarize, in the previous sections an extensive literature study was done in order to establish a **generic** representation of i. the physical connections between the (sub-)assemblies of a HAWT (see **Figure 3.3**), ii. the functional relations between these (sub-)assemblies (see **see Figure 3.4**) and iii. the load flow along them (see **Figure 3.13**). Recall that the loads were analyzed in order to gain insight into which SCADA-parameters may be plotted against each other in order to detect deviations.

Chapter 4

Case study

This chapter is intended to verify whether/to what extent the established functional failure effects, according to the functional tree, of WT sub-assemblies correspond with observations from field data. The intention of this comparison is to establish the identifiers for a certain WT sub-assembly failure in order to allow the detection of its failure.

The main selection criterion for the case study used in this work, is the number of failures that occurred in a specific WT. It is assumed that the operational data of a WT turbine with more failures in the past contains more deviating parameters compared to a WT with less failures and thus supports a better evaluation of the identifiers of a WT sub-assembly failure.

4.1 Background information of the WT

The WT under study, from here on referred to as WTA4, is a Vestas V90 onshore HAWT with a Doubly-Fed Induction Generator (DFIG) and a rated capacity of 3000 kW.

According to a Performance Analyses Report of the wind farm, WTA4 showed lower than expected energy yield in the first year of operation. In this report two steps were taken in order to identify the possible root cause(s) of the lower energy yield. As a first step the availability of all turbines was calculated by using the time as registered by the SCADA counters in order to identify the months with characteristically lower availability. Here, it was mentioned that WTA4 had experienced a generator bearing failure. In the second step the power curve, control strategy (i.e. blade pitch angles and rotor speed) and power coefficient were additionally studied. From these analyses it was found that the power output of WTA4 was lower than expected, the blade pitch angles of WTA4 were increased late and that the measured wind speeds were not correctly measured.

Following are i. a derivation of the functional relations applicable to WTA4 based on knowledge of the physical connections between the (sub-)assemblies and ii. the load flow occurring in WTA4.

4.2 Physical decomposition WTA4

The WTA4 is, as mentioned earlier, a V90 WT and has one main bearing. The main bearing is integrated into the gearbox and the hub is connected directly to the gearbox input shaft, which is connected to the main bearing. The turbine is further equipped with a hydraulic pitch system for each blade. The blade bearings are grease lubricated, while the main bearing is forced oil lubricated. Further, the generator bearings are lubricated with grease, which is supplied from an automatic lubrication unit. Lastly, the gearbox is forced lubricated without the use of an integrated oil sump. **Figure 4.1** presents an overview of the physical connections between the assemblies of WTA4. The orange arrows indicate the physical connections that are in accordance with **Figure 3.3**, while the

dark cyan arrows represent the physical connections that differ from the general representation established from theory.

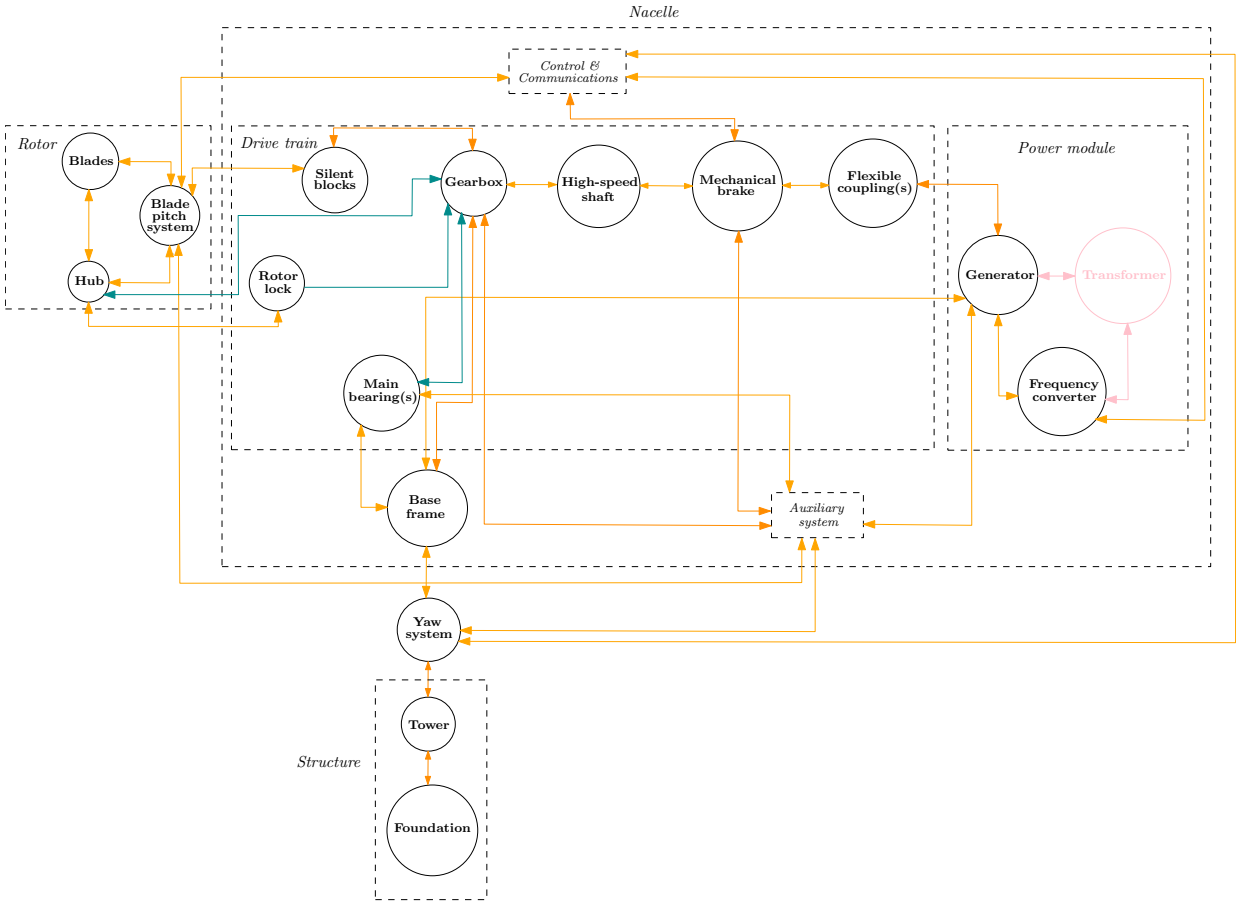

Figure 4.1: A simplified overview of the physical connections between the assemblies of WTA4. The orange arrows indicate the physical connections that are in accordance with those generally existing in a HAWT, while the dark cyan arrows represent the physical connections that are different.

4.3 Functional dependencies WTA4

Based on the physical connections between the assemblies of WTA4, the functional relations have been derived. These are presented in **Figure 4.2**. Compared to **Figure 3.3**, the functional dependencies between the (sub-)assemblies of WTA4 are the same except for the *Hub - Gearbox* and *Gearbox - Main bearing* dependency. Namely, the functionality of the hub, which is to support the turbine blades, depends on the gearbox input shaft, since for WTA4 there is no main shaft. Also, the rotation of the gearbox input shaft is supported by a main bearing. The functional dependencies of WTA4 which correspond with **Figure 3.3** are marked with green arrows and those which differ are represented with dark cyan colored arrows.

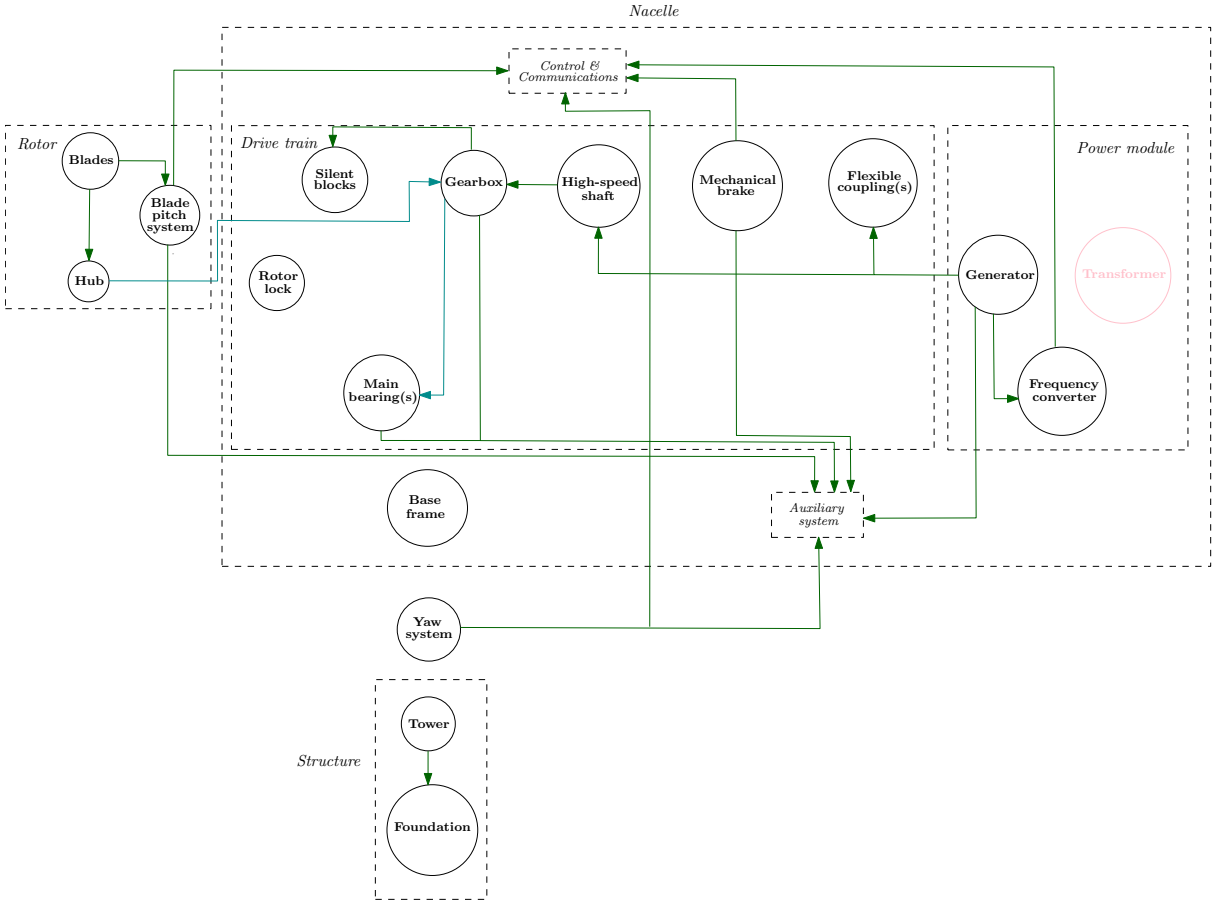

Figure 4.2: A simplified overview of the functional connections between the assemblies of WTA4. The green arrows indicate functional relations in accordance with those that generally exist in a HAWT. Dark cyan arrows represent those that differ.

4.4 Fault detection blade pitch system failure WTA4

Previously it was mentioned that WTA4 suffered from generator bearing and blade pitch failure. The choice is made to first analyze the failure of the blade pitch system, since from the load flow (see **section 3.5.3.3**) it was found that this assembly sees the WT loads prior to the generator.

In this section the failure mode(s), causes and effects of blade pitch system failure of WTA4 are identified based on knowledge of the functional dependencies and the load flow between the WT (sub-)assemblies. Hereafter, it is studied which SCADA-parameters are expected to be affected and how they are theoretically expected to behave in this regard. These results are then compared with the field data in order to determine to what extent the functional approach and knowlegde of the load flow provide insight into upcoming failures.

Various SCADA-parameters have been measured, however, for the majority of them the descriptions are impossible to decipher without consultation from experts. Given that such expertise was not available during this research, this work will focus solely on i) parameters that are commonly monitored by the SCADA-system of a WT and ii) those parameters of which the descriptions could easily be derived. Generally, a wide range of parameters are monitored by the SCADA-system of a WT, however the authors of [1] mention that "wind speed and direction, pitch and yaw angles, rotational speed, power output and ambient temperature are always monitored. Additionally, tem-

peratures of parts in the drive train are often measured - although with different levels of detail, e.g. only a generator and a gearbox temperature in one setup or more than twenty temperatures at different locations at the shaft in a more detailed configuration." Taking this into account together with point i), a set of parameters are selected for this work. These are presented in **Table 4.1**.

Nr.	Parameter label	Description
1	Amb_Temp_Avg	Average ambient temperature
2	Amb_WindSpeed_Avg	Average ambient wind speed
3	Blds_PitchAngle_Avg	Average blade pitch angle
4	Gen_Bear_Temp_Avg	Average temperature generator bearing
5	Gen_Bear2_Temp_Avg	Average temperature generator bearing 2
6	Gen_CoolingWater_Temp_Avg	Average generator cooling water temperature
7	Gen_RPM_Avg	Average generator speed
8	Gen_SlipRing_Temp	Average generator slip ring temperature
9	Grd_Prod_Pwr_Avg	Average produced power
10	Hyd_Oil_Temp_Avg	Average hydraulic oil temperature
11	Nac_Temp_Avg	Average nacelle temperature
12	Rtr_RPM_Avg	Average rotor speed
13	Gear_Bear_Temp_HSMid_Avg	Average temperature intermediate gearbox bearing high-speed shaft
14	Gear_Bear_TempHSGenEnd_Avg	Average temperature generator end gearbox bearing high-speed shaft
15	Gear_Bear_TempHSRtrEnd_Avg	Average temperature rotor end gearbox bearing high-speed shaft
16	Gear_Oil_TempBasis_Avg	Average oil sump temperature

Table 4.1: Chosen set of SCADA-parameters.

4.4.1 Detection of the failure mode(s) blade pitch system WTA4

Based on the function description of the blade pitch system, the failure mode of this assembly is defined as "No/incorrect adjustment of the blade pitch angle". The question to answer in this regard is which SCADA-parameters instantly detect this failure mode itself, without yet considering the causes and its effects. In literature, the functionality of the blade pitch system has been studied by plotting the blade pitch angle against the wind speed [75]. However, as mentioned the measured wind speeds are lower than the actual wind speeds and therefore the measured wind speed, Amb_WindSpeed_Avg, cannot - in this work - be used as a parameter for detecting the failure of the blade pitch system.

4.4.2 Causes of blade pitch system failure WTA4

As mentioned earlier, the blades of WTA4 are individually pitched and have a hydraulic pitch system. In order to identify possible root causes of the failure of the blade pitch system itself, an Fault Tree Analysis was performed for the pitch system of WTA4 (see **Figure 4.3**). Worth mentioning is that the underlying failure events for the blade pitch system have been identified by considering the functional relations between the pitch system and other (sub-)assemblies.

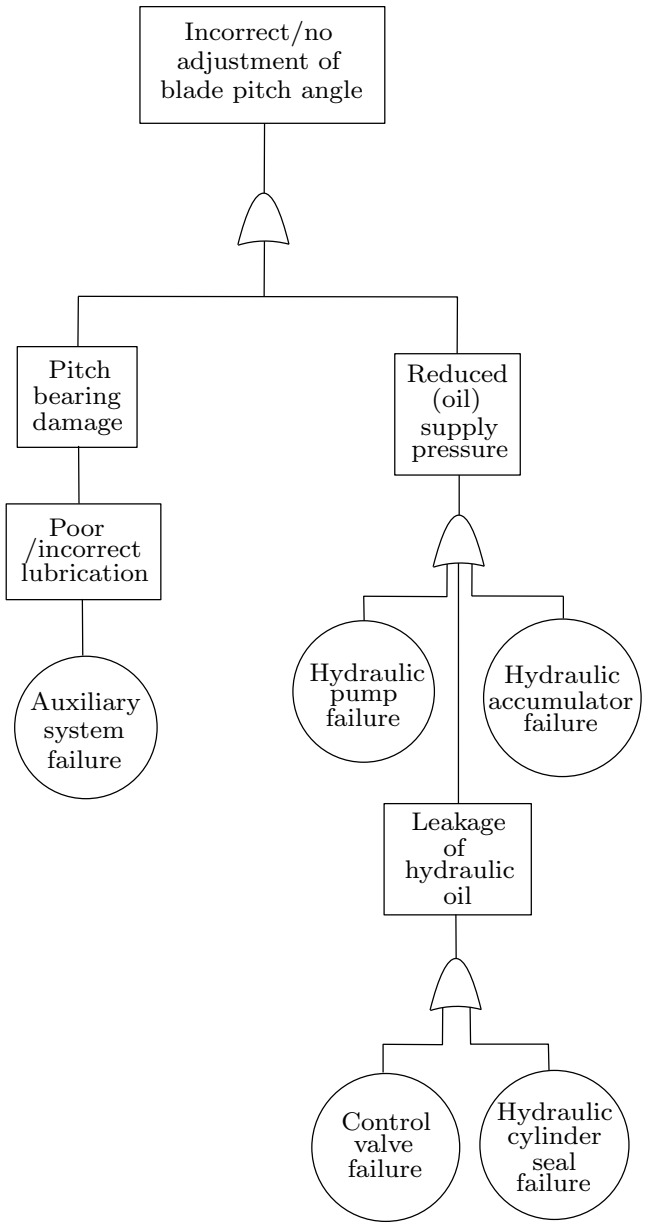

Figure 4.3: The Fault Tree Analysis for the blade pitch system of WTA4.

Pitch bearing damage
As the functionality of the pitch bearings is to rotate the blades, damage of this assembly will prevent that the blade pitch angles can be adjusted correctly or at all. Pitch bearing damage can be due to poor/incorrect lubrication.

Reduced (oil) supply pressure
Apart from pitch bearing failure, it is also possible that not enough hydraulic oil is supplied to the hydraulic cylinders. This can be due to i. failure of the hydraulic accumulator, ii. hydraulic pump, which is considered to be part of the Auxiliary System and provides hydraulic oil to the hydraulic accumulator, or iii. due to leakage of hydraulic oil. The latter is the result of i. failure of the control valve that regulates the amount of hydraulic oil to and from the pitch cylinders or ii. failure of the seal of the pitch cylinders.

Based on the list of monitored SCADA-parameters, it can be seen that no parameters related to the (sub-)assemblies that may cause blade pitch failure have been measured. Therefore, with the SCADA-system of WTA4 it is not possible to detect the failure events leading to pitch failure. Recall that these failure causes are based on the functional dependencies (and load flow) established through literature study. No expert knowledge has been included for the identification of these events and thus it is pointed out that this analysis may be incomplete and may contain some degree of uncertainty.

4.4.3 Expected effects of blade pitch system failure WTA4

As it is not possible to detect the failure mode and the underlying root causes of pitch failure with the current set of SCADA-parameters, it is possible that pitch failure may be detected based on the effects it has on other (sub-)assemblies. Similar to the root causes, these effects are studied through knowledge of the functional dependencies as well the load flow between the WT (sub-)assemblies. Later these effects are compared with field data in order to determine to what extent the functional approach and knowledge of the load flow provide insight into upcoming failure of the blade pitch system.

Pitch failure cases
Prior to studying the effects of pitch failure, the types of blade pitch failure are identified, namely:

1. the pitch system of one blade, two blades or all three blades fails, i.e. cannot provide sufficient power to increase or decrease the blade pitch angle(s). In the case of pitch failure of two blades it is assumed that the two blades have larger pitch angle than the third blade and that the pitch angles of these two are different. Lastly, if pitch failure of three blades occurs the assumption is made that all three blades have a different pitch angle;

2. Other possibilities of blade pitch failure is that there is a fault in the overall control system of the WT which causes the wrong signal to be sent to the individual pitch systems;

3. Lastly, it is also possible that a combination of case 1 and 2 occurs. With regard to case 2 it is assumed that sensor faults - for example no signal coming from the sensor, the sensor does not always give a signal, etc. - are detected on time by the control system, since such failures lead to incorrect control of the individual pitch systems and results in uncontrolled regulation of the dynamic blade loads (which are generally transmitted further along the drive train). The uncontrolled regulation of the blade loads is a very risky situation and should be avoided as this may lead to damage of the drive-train sub-assemblies. Therefore, *only the failure effects of case 1 are considered in this work.*

4.4.3.1 Effects of blade pitch system failure - part 1

From **Figure 4.2** it can be seen that only the blades depend on the functionality of the blade pitch system. *Therefore, it can be stated that purely based on the functional dependencies it is expected that only the functionality of the blades will be affected by blade pitch failure.*

Recall, however, that according to the Performance Report of the wind farm, generator bearing failure had also occurred in WTA4. Even though, purely based on their functional descriptions, there is no functional relation between the generator and blade pitch system, *from the load flow analysis in **section 3.5.3.3** it was concluded that the functionality of the generator is also affected by the blade pitch system*. Namely, the generator bearings are affected by the gearbox-generator misalignment, which is fundamentally caused by the rotor moments. These moments, as explained in **section 3.5.3.3**, depend on the angle of attack and thus on the blade pitch system.

Preliminary conclusion 1
Based on the above it can thus be stated that knowledge of the functional relations does not fully describe the effects of a certain (sub-)assembly failure on other (sub-)assembly functionalities. This means that a functional approach alone does not fully support the detection of failures.

4.4.3.2 Effects of blade pitch system failure - part 2

Another option to *support* understanding how the WT (sub-)assemblies are affected due to the failure of a certain (sub-)assembly, in this case the blade pitch system, is by taking into account the loads that the (sub-)assemblies experience, i.e. *the load flow*. Namely, application of the load flow gives insight into how the forces and moments seen by the (sub-)assemblies changes when a certain (sub-)assembly no longer functions properly.

Failure effects based on functional dependencies and load flow
In this section the affected (sub-)assembly functionalities, and thus SCADA-parameters, due to pitch failure are studied based on the functional dependencies and additionally the load flow. **Figure 4.4** shows a complete overview of the relations between the (sub-)assemblies of WTA4 based on their functional descriptions and the load flow. The green arrows indicate the functional dependencies which are in accordance with the general functional relations, while the dark cyan arrows are those which are different, i.e. case-specific. Lastly, the purple arrow indicate the load flow that corresponds to the general load flow and the pink arrow represents the case-specific load flow. In this figure the SCADA-parameters have also been mapped (orange text) to the concerning (sub-)assemblies they monitor. Note that the parameters related to the ambient temperature, ambient wind speed and nacelle temperature cannot be assigned to a specific (sub-)assembly.

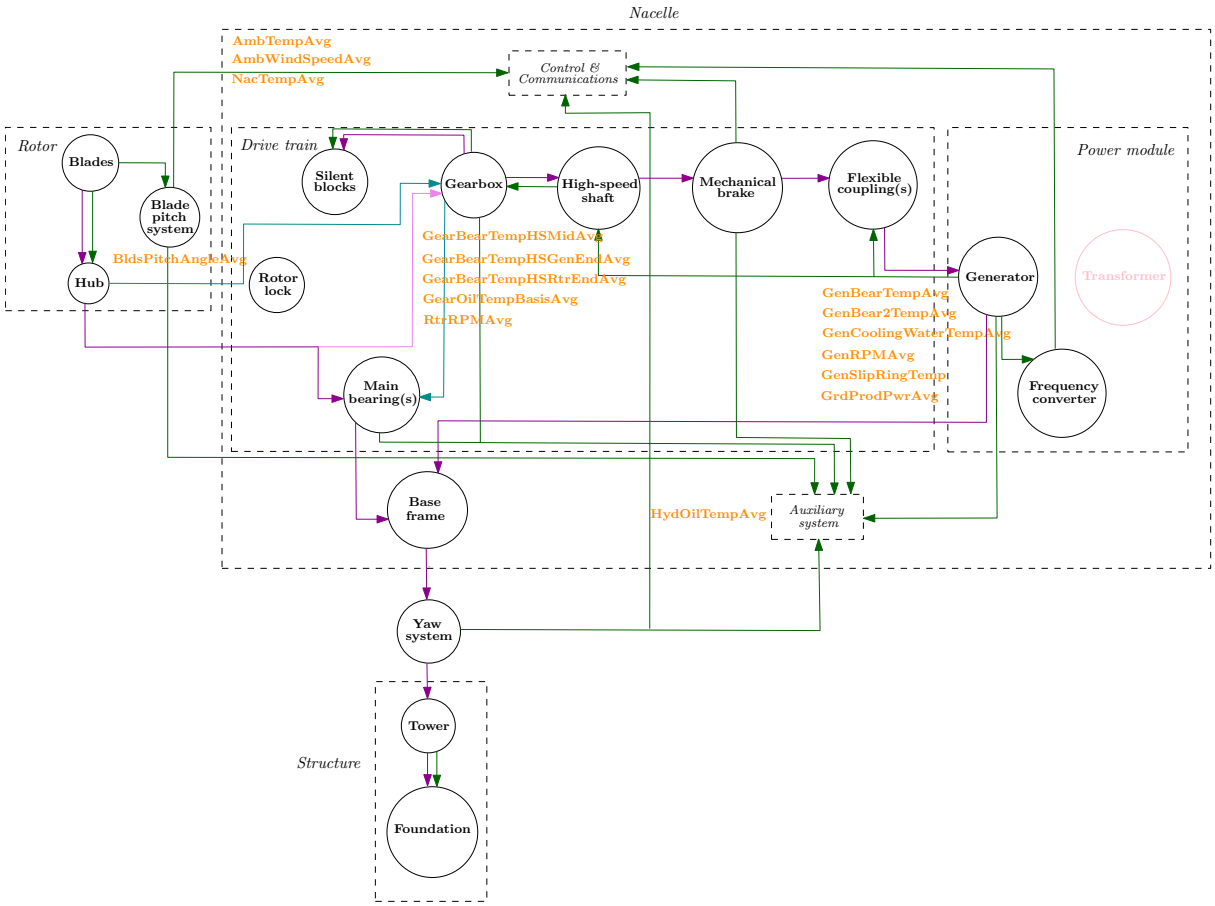

Figure 4.4: A complete overview of the functional dependencies and load flow from the blades to the foundation of WTA4. The green arrows are functional dependencies in accordance with the general functional relations established. Dark cyan are case-specific functional relations. Purple arrows indicate load flow following the general load path in a HAWT. Pink arrow indicates a case-specific load flow.

Next, the affected (sub-)assemblies due to pitch failure are studied with the aid of **Figure 4.4**, i.e. the functional dependencies and load flow.

Blades
As mentioned earlier, based on the functional dependencies the blades are expected to be affected by blade pitch failure. *There are, however, no SCADA-parameters available that monitor the blades*.

Hub
From **Figure 4.4** it can be seen that there is no functional relation between the hub and the pitch system. However, it can be seen that there is a load flow from the blades to the hub. Since the blade loads depend on the blade pitch system it can be argued that the hub *indirectly* functionally depends on the pitch system and it is thus expected that its functionality will be affected when pitch failure occurs. *There are no SCADA-parameters available that monitor the hub.*

Note: **Figure 4.4** only presents the functional relations that can *directly* be derived from the functional descriptions of the WT (sub-)assemblies.

Gearbox
Generally, the next assembly along the chain is the main shaft as this supports the hub. For WTA4,

however, there is no main shaft present and the hub is directly connected to the gearbox, where it is supported by the gearbox input shaft.

Based on the functional relations, the gearbox has no relation with the blade pitch system. However, from **Figure 4.4** it can be seen that there is a load flow from the hub to the gearbox - this is the overall aerodynamic torque that is generated by the blades and transferred to the gearbox in order to be converted to a lower torque for driving the generator. Given that the overall aerodynamic torque depends on the blade pitch angles and is transmitted to the gearbox, it can be argued that the functionality of the gearbox *indirectly* depends on the blade pitch system. *Therefore, it is expected that the functionality of the gearbox will be affected due to pitch failure and so will the parameters monitoring the gearbox*.

Note: From **Figure 4.4** it can be seen that there is a functional dependency and load flow from the gearbox to the silent blocks. The gearbox has its own silent blocks, which absorb the torsional rotor moment acting on the gearbox. Given their physical structure, it is expected that blade pitch failure cannot be detected by monitoring the silent blocks.

Main bearing
Similar to the gearbox, the main bearing has an *indirect* functional dependency with the pitch system. Namely, the loads it experiences depends on the pitch system as, according to the load flow, they originate from the blades. This was explained in **section 3.5.3.3**, where it was found that the main bearings absorb $F_{x_{hub,total}}$, $F_{y_{hub,total}}$ and $F_{z_{hub,total}}$ and additionally experience reaction forces due to $M_{y_{hub,total}}$ and $M_{z_{hub,total}}$.Thus it is expected that the functionality of the main bearings will be affected when pitch failure occurs. *There are no SCADA-parameters available that monitor the main bearings*.

High-speed shaft
From **Figure 4.4** it can be seen that the high-speed shaft functionally depends on the gearbox and that there is a load flow from the gearbox to the high-speed shaft - this is the increased rotor torque for driving the generator. Due to this load flow it can thus be stated that the high-speed shaft *indirectly* functionally depends on the blade pitch system and that that it is expected that its functionality will be affected when pitch failure occurs. *There are no SCADA-parameters available that monitor the high-speed shaft*.

Mechanical brake
The mechanical brake is a steel disc brake that is mounted on the high-speed shaft and is responsible for mechanically braking the rotor (torque), where braking is achieved through engagement of the brake calliper on the brake disc. Generally, the mechanical brake is applied after the shaft speed has been reduced (through feathering of the blades) - the mechanical brakes would otherwise wear too quickly if the rotor was stopped from full speed. When no braking occurs the mechanical brake allows the transmission of the rotor torque, $M_{x_{hub,total}}$, from the high-speed shaft to the generator.

As the mechanical brake has the function of fixing the rotor during maintenance, it can be stated that the mechanical brake will not be affected due to pitch failure. *There are no SCADA-parameters available that monitor the mechanical brake.*

Flexible coupling
Following the mechanical brake is the flexible coupling, which transmits the increased $M_{x_{hub,total}}$ from the high-speed shaft to the generator (see load flow in **Figure 4.4**). While doing so, the flexible coupling accommodates the misalignment between the gearbox and generator. In **section 3.4.3.3** it was explained that the misalignment is a result of the motion of the gearbox and that this motion depends on $M_{y_{hub,total}}$ and $M_{z_{hub,total}}$.Therefore, it can be stated that the flexible coupling *indirectly* functionally depends on the blade pitch system. *There are no SCADA-parameters available that monitor the flexible coupling.*

Generator
Lastly, from **Figure 4.4** it can also be seen that there exists a functional dependency between the generator and the high-speed shaft + the flexible coupling, since the converted overall aerodynamic torque is transmitted through the high-speed shaft + flexible coupling to the generator. As the generator converts this torque into electrical energy, it is clear that the generator functionally *indirectly* depends on the pitch system and *so it is expected that the parameters which monitor its functionality will be affected in case of pitch failure.*

To summarize, the load flow gave a full overview of all the (sub-)assemblies to be affected by blade pitch system failure. In this way a complete overview is achieved of the affected SCADA-parameters. Of all the affected (sub-)assemblies, only the gearbox and generator are monitored by the SCADA-system. Apart from providing a complete overview of the affected SCADA-parameters due to blade pitch failure, the load flow also complemented the functional approach in providing insight into *which* SCADA-parameters may be *related* in the case of blade pitch failure. For example, from the load flow it was found that the gearbox parameters are expected to be affected by blade pitch failure, since there is a load flow from the blade pitch system to the gearbox. Therefore, based on this it may be possible to plot the gearbox parameters against the parameter monitoring the blade pitch system. This can, however, not be derived from the functional relations as no functional relation exists between the blade pitch system and the gearbox. The same is also true for the generator parameters.

There are cases, however, where both the load flow and the functional relations show that the same (sub-)assemblies are related. This is found for the gearbox and the generator. Namely, based on the functional relations the generator is linked to the gearbox via the high-speed shaft, while the load flow from the gearbox to the generator indicates a indirect relation between the two.

Preliminary conclusion 2
From the figures representing the functional relations and load flow it is possible to create connections between a functional failure and its effects. However, from these figures it cannot be derived *how* the affected SCADA-parameters are *related*, and thus which SCADA-parameters can be plotted against each other in order to detect blade pitch failure. For this, in-depth knowledge of the physics is required. The physics can also be used for explaining deviations in parameter graphs.

Next, it is demonstrated how the physics can be applied for understanding how the gearbox and generator SCADA-parameters are related and explaining the deviations in the parameter graphs.

4.4.4 Application of the physics for understanding the relation between SCADA-parameters and explaining deviations

Generally, the total amount of energy available in the wind is equal to:

$$P_W = \frac{1}{2}\rho\pi R^2 {v_{wind}}^3 \tag{4.1}$$

where R is the radius of the WT rotor and v_{wind} is the magnitude of the incoming wind speed. From this amount only a portion is captured by a WT:

$$P_T = C_p(\lambda,\phi)\frac{1}{2}\rho\pi R^2 {v_{wind}}^3 \tag{4.2}$$

where C_p is the power coefficient and λ the tip-speed ratio. The tip-speed ratio is the ratio between the tangential speed of the tip of the blade and the magnitude of the incoming wind speed:

$$\lambda = \frac{\omega R}{v_{wind}} \tag{4.3}$$

where ω is the rotational speed of the rotor and R is the rotor radius.

The power coefficient generally describes the fraction of power extracted by a WT as:

$$P_T = C_p(\lambda, \phi)P_W \tag{4.4}$$

Equations 4.2 - 4.4 show that the C_p-value depends on the blade pitch angle, ϕ, the rotational speed of the WT-rotor, ω, and the incoming wind speed, v_{wind}. Ideally, the WT should operate at the maximum C_p-value. The operation of a WT consists of four different operating regions (see **Figure 4.5**):

Region 1: this is the region from 0 m/s up to cut-in wind speed. Wind speeds below cut-in wind speed are too low to start-up the WT. At cut-in wind speed the WT starts power production.

Region 2: is the region between cut-in wind speed and rated wind speed. In this region maximization of the power output is the main concern and therefore, ϕ is kept at 0°. The rated wind speed is the wind speed at which the WT reaches the maximum, i.e. rated, power output.

Region 3: is the region from rated wind speed up to cut-out wind speed, which is the wind speed at which the WT is shut down. In this region the power output is limited to the rated power in order to avoid overloading of the turbine.

Region 4: in this region wind speeds are very high and the WT does not produce power in order to prevent it from damage.

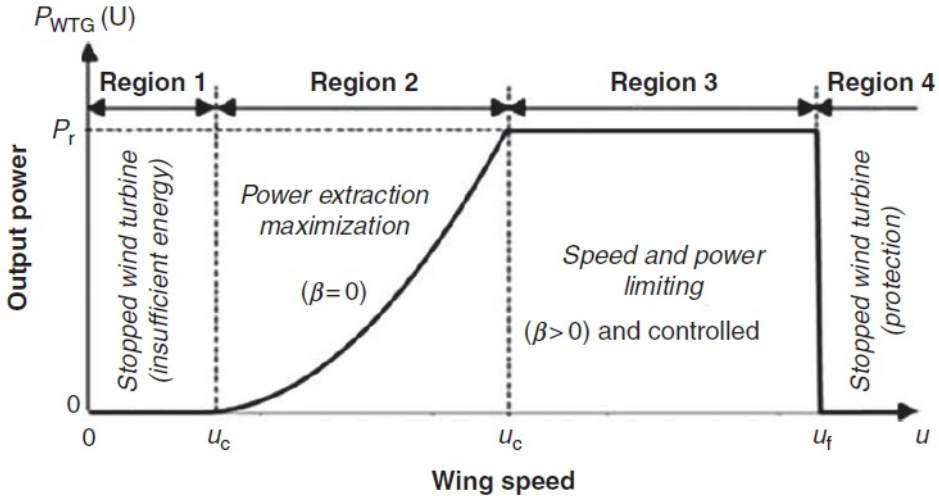

Figure 4.5: The different operating regions of a pitch-controlled variable-speed HAWT [77].

In region 1 and 3 the WT is pitch-controlled, i.e. the blade pitch angles of the blades are adjusted, and in region 2 it is speed-controlled, i.e. the rotor speed of the WT is adjusted. *Both pitch and speed control occur based on the rotational speed of the generator rotor*. With regard to pitch control, the control system measures the speed of the generator and compares the value with the reference generator speed. Based on the error in this value, a reference pitch angle is determined by the control system.

A similar approach applies to speed control, where the measured generator speed is compared with the WT characteristic curves. These curves present the power-rotor speed curves for different wind speeds and $\phi = 0°$. An example is presented in **Figure 4.6**. In this figure, the power is determined according to **equation 4.2** as follows: for a certain ω and $\phi = 0°$, a certain λ-value is obtained based on **equation 4.3**. With this λ-value, the optimum C_p-value is determined from a C_p-λ characteristic curve. An example of such curves is presented in **Figure 4.7**.

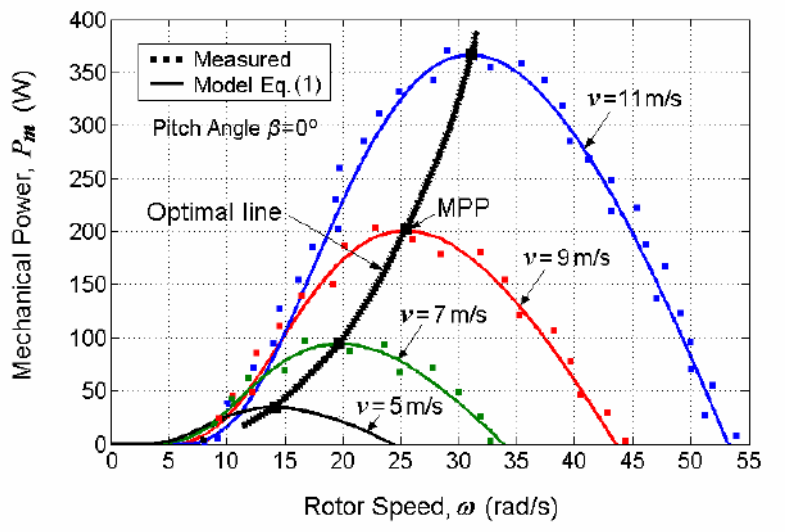

Figure 4.6: The power output captured by a WT-rotor v.s. the WT-rotor speed for different wind speeds [72].

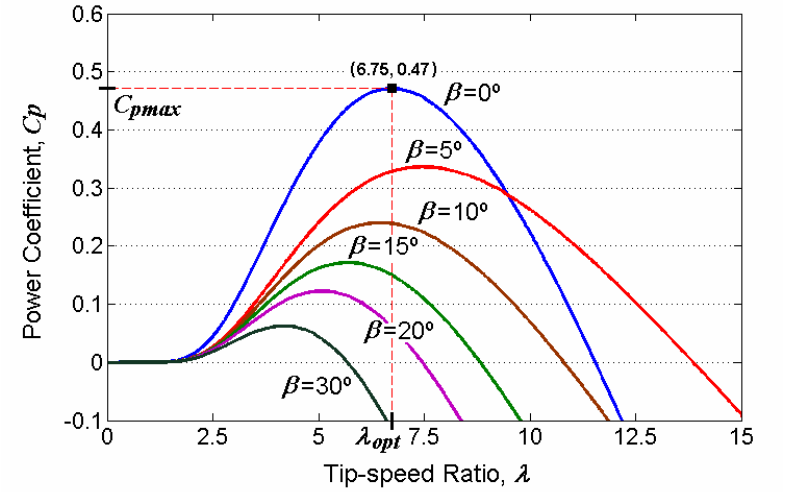

Figure 4.7: The power coefficient v.s. λ for various ϕ [72].

Coming back to speed control, for the measured generator speed and a certain wind speed, the Maximum Power Point (MPP) is determined from the power output v.s. rotor speed curve (**Figure 4.6**). This power output is then used as the reference signal for adjusting the power output- control of the power output is performed by the frequency converter. Based on this reference signal, the frequency converter adjusts the current flowing through the generator rotor windings and as a result causes the magnetic field of the generator to change. As the generator rotor rotates in this magnetic

field, the torque exerted by the field on the rotor, i.e. the counter torque, is also changes and as a result the rotational speed of the rotor blades change. By changing the rotational speed of the blades, the power captured by the WT changes.

From the above it can be concluded that since the power output of the generator, Grd_Prod_Pwr_Avg, is determined by the power coefficient C_p (λ, ϕ) and the incoming wind speed, Grd_Prod_Pwr_Avg can be plotted against the blade pitch angle, Blds_PitchAngle_Avg. Also, as λ is affected by the rotational speed of the WT, Rtr_RPM_Avg, it also possible to plot Grd_Prod_Pwr_Avg against Rtr_RPM_Avg.

Grd_Prod_Pwr_Avg v.s. Blds_PitchAngle_Avg
In **Appendix C** it is extensively explained, using the physics, that when pitch failure occurs the power output above rated output increases more compared to the case of no pitch failure. Therefore, for the failing WT *larger pitch angles are measured for the same power output*.

Grd_Prod_Pwr_Avg v.s. Rtr_RPM_Avg
Earlier it was explained that when pitch failure of one blade occurs, the hub loads change. For the rotor torque, $M_{x_{hub,total}}$, it is expected that this will decrease. Therefore, pitch failure causes the power output of the generator to decrease and so for the failing WT *lower power outputs are measured for the same rotational speed of the rotor*.

In **section 3.5.3.3** it was explained that a deviation in the blade pitch angle affects the hub loads. As the hub loads change, the gearbox bearing loads, gearbox displacement and generator bearing loads will also change. Changes in the bearing loads cause the bearing temperatures to change due to a change in the amount of heat generated by the bearing. For ball bearings the generated heat is calculated according to the following equation:

$$H = \ 1.047 \cdot 10^{-4} \cdot n \cdot M \tag{4.5}$$

where H is the heat generated by a ball bearing (W), n is the rotational speed of the ball bearing (rev/min) and M is the total frictional torque acting on the ball bearing (N/mm). Here, the total frictional torque includes viscous friction torque, torque due to applied load and lastly, torque due to the spinning and gyroscopic force acting on the bearing balls [62]. For roller bearings the generated heat is calculated with the same formula, however, the total frictional torque is calculated on the basis of the viscous friction torque and torque due to applied load only. If the roller bearings are flanged, then there is also friction torque due to the flanges [76].

Equation 4.5 shows that bearing temperatures - Gear_Bear_Temp_HSMidAvg, Gear_Bear_Temp_HSGenEndAvg, Gear_Bear_Temp_HSRtrEndAvg, Gen_Bear_Temp_Avg and Gen_Bear2_Temp_Avg - can be plotted against the power, in this case Grd_Prod_Pwr_Avg, as $n \cdot M$ is equal to the transmitted power. As the rotational speeds of both the gearbox and generator are measured, it is also possible to plot the bearing temperatures against these parameters. Next, the generator bearing temperatures are plotted against the power. **Appendix B and C** present other analyses that were conducted for the gearbox and generator parameters, based on the physics.

Gen_Bear_Temp_Avg and Gen_Bear2_Temp_Avg v.s. Grd_Prod_Pwr_Avg
In **section 3.5.3.3** it was explained that the generator bearing loads are determined by the gearbox movement and coupling misalignment, which depend on the hub loads. In **Appendix B.2** it is explained that the coupling misalignment increases due to pitch failure and so the generator bearing loads are expected to increase. A statics analysis showed (see **Appendix C.2**) that the reaction forces in the second generator bearing are smaller than those in the first generator bearing. *This means that due to pitch failure higher temperatures are measured for bearings 1 and 2, where the temperatures measured for bearing 2 are lower compared to bearing 1*. The analysis also showed that when pitch failure occurs, the loads in bearing 1 increase more than the loads in bearing 2 and that bearing 2 is less sensitive to pitch failure. A remark in this regard is that as generally bearing temperatures are

affected by the ambient temperature, the temperatures of bearing 1 and 2 must be plotted relative to the ambient temperature, unless this temperature does not fluctuate. Note that for the generator bearings the ambient temperature refers to the nacelle temperature, Nac_Temp_Avg. From the data it was found that the nacelle temperature continuously fluctuates and so the bearing temperature must be plotted relative to this temperature. Note: the data showed that Amb_Temp_Avg is the temperature outside of the nacelle and is therefore not used in this work.

4.5 Results: SCADA-data analysis

In this chapter the field data is analyzed in order to identify to what extent the functional relations, load flow analysis and physics allow the detection of upcoming pitch failure. The field data is studied for a period of approximately one year, namely from the 6th of February 2010 until the 26th of January 2011. This is the period from the start of operation until the generator bearing was replaced.

Worth mentioning is that the blade pitch system of WTA4 had failed due to incorrect settings rather than due to failure of one of its components. This means that pitch failure was present from the start of operation and so deviations in the SCADA-data cannot be studied with reference to the first months of operation as is normally done in literature. For this reason, in this work the field data of WTA4 shall continuously be compared with a healthy/reference turbine, from now on referred to as WTA2, in order to spot deviations from the actual expected normal behavior. As the study period is approximately one year, plotting all data in one graph does not provide clarity in spotting deviations and therefore, the data is plotted for time intervals of one month. Worth mentioning is that only those plots that show clear deviations from the reference behavior are presented in this chapter, while the full set of plots can be found in the **Appendix C**.

Failure case WTA4
From a Performance Analyses Report of the studied wind farm, it was stated that WTA4 increased its blade pitch angles later than WTA2, since for the same wind speed the average blade pitch angle of WTA4 is lower than of WTA2. As mentioned earlier, it is assumed that pitch failure is due to failure of (one of) the individual blade pitch systems.

Next, the parameter relations established in the previous section are studied for failure detection.

Grd_Prod_Pwr_Avg v.s. Blds_PitchAngle_Avg
Figure 4.8 shows the Grd_Pwr_Avg v.s. Blds_PitchAngle_Avg graph for the months February and March. In the month March the healthy turbine shows deviating behavior. It seems that at around 400 kW, varying average blade pitch angles are measured. Compared to the month February, the power output of 400 kW is more or less the point where the blade pitch angles are no longer adjusted and the frequency converter takes over the power regulation. The data analysis showed that from the 13th - 22nd of March the average blade pitch angle at a power output of about 400 kW was higher than it should have been.

Worth mentioning is that the remaining months, see **Appendix C.2**, show a similar behavior as exhibited in the month February.

Figure 4.8 shows that for WTA4 the average blade pitch angle, at power outputs close to the rated power output, is larger for the same power outputs. *This is in accordance with the theory.* The remaining months show similar behavior.

Based on this it can be stated that plotting the power output against the average blade pitch angle fully provides insight into pitch failure.

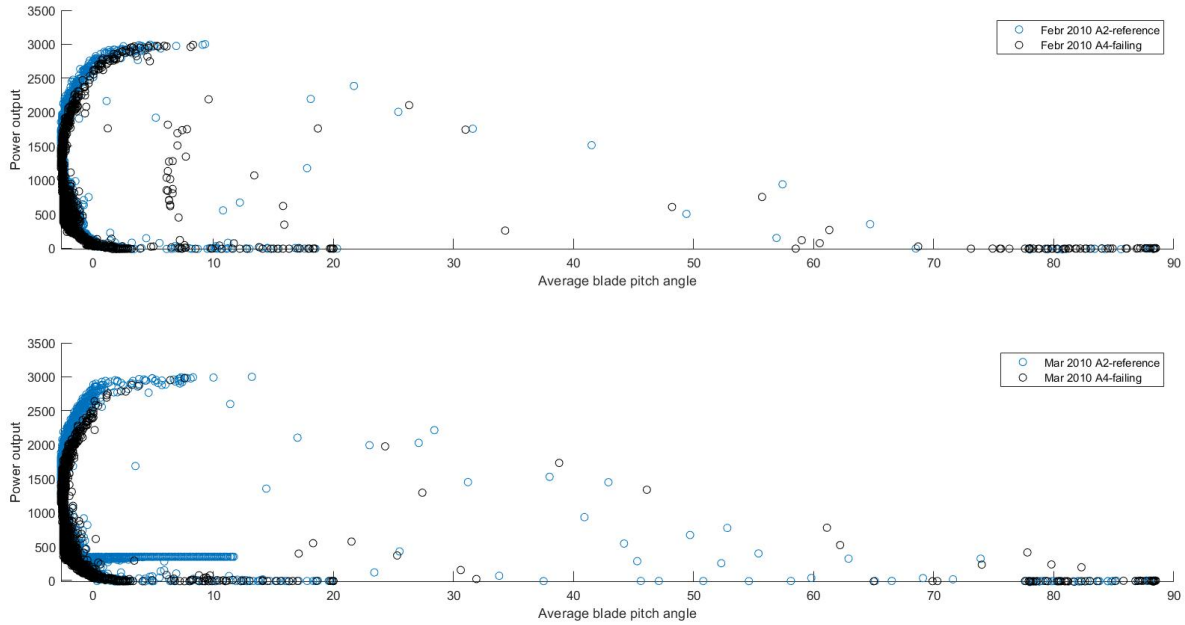

Figure 4.8: Comparison of power output v.s. average blade pitch angle of WTA4 with the reference WT for the months February 2010 and March 2010.

Grd_Prod_Pwr_Avg v.s. Rtr_RPM_Avg
Figures 4.9 - 4.10 show that for the failing WT the power output is indeed lower for the same rotor speed compared to the healthy WT. *This is in agreement with the theory*. The remaining months also show the same behavior.

In the months March and May, however, the healthy turbine shows some additional deviations. For the month March deviations were also visible in the Grd_Prod_Pwr_Avg v.s. Blds_PitchAngle_Avg graph. Here it was found that varying blade pitch angles were measured for the power output where the frequency converter takes over blade pitch control, i.e. start of power production. This power output is around 400 kW. **Figure 4.9** shows a similar behavior, where varying rotor speeds are measured at 400 kW. These rotor speeds are lower than they should be. This corresponds to the higher than usual blade pitch angles that were measured at 400 kW.

For the month March it can be seen that for the failing WT the rotor speed becomes constant for a smaller rotor speed compared to the healthy turbine. For the healthy WT the rotor speed remains constant at 16.7 rpm, while for the failing WT this is at around 16.7 rpm. However, from **Figure 4.11** it can be seen that for the months June and July the rotor speed also starts being constant at 16 rpm - this time also for the healthy turbine.

Based on this it can be stated that plotting the power output against the rotor speed fully provides insight into pitch failure.

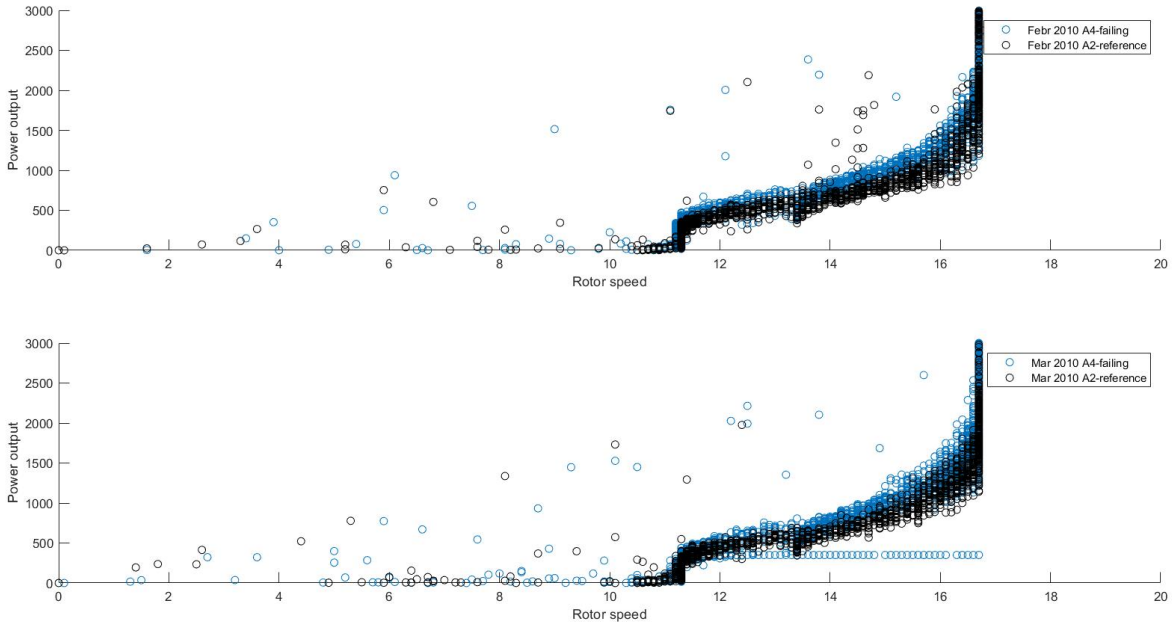

Figure 4.9: Comparison of the power output v.s. rotor speed data of WTA4 with the reference WT for the months February 2010 and March 2010.

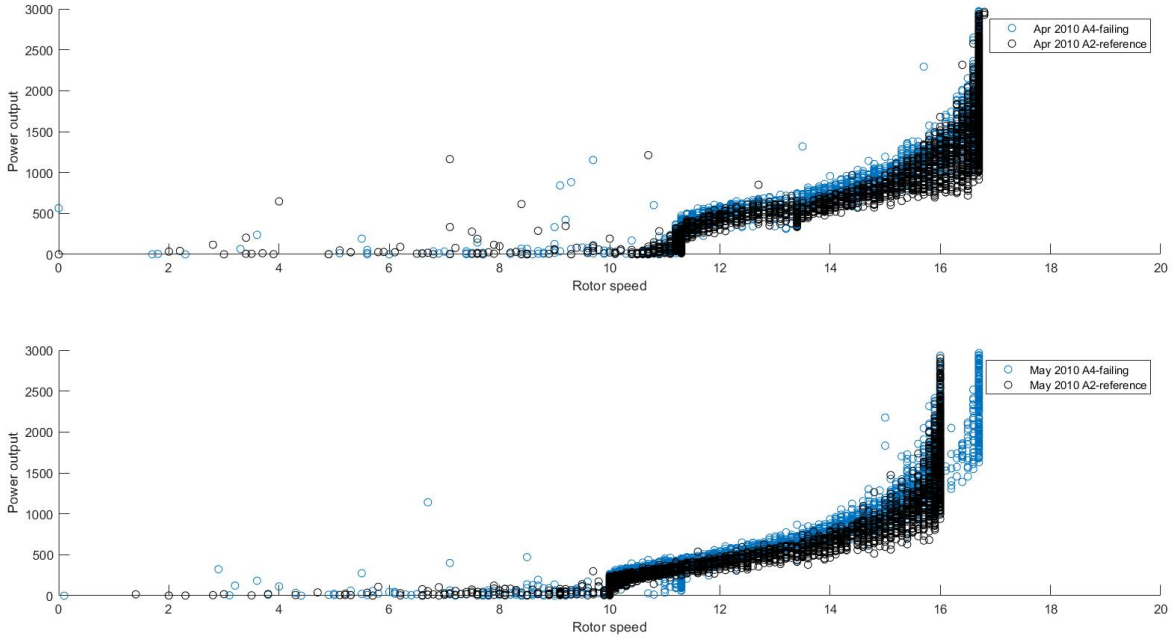

Figure 4.10: Comparison of the power output v.s. rotor speed data of WTA4 with the reference WT for the months April 2010 and May 2010.

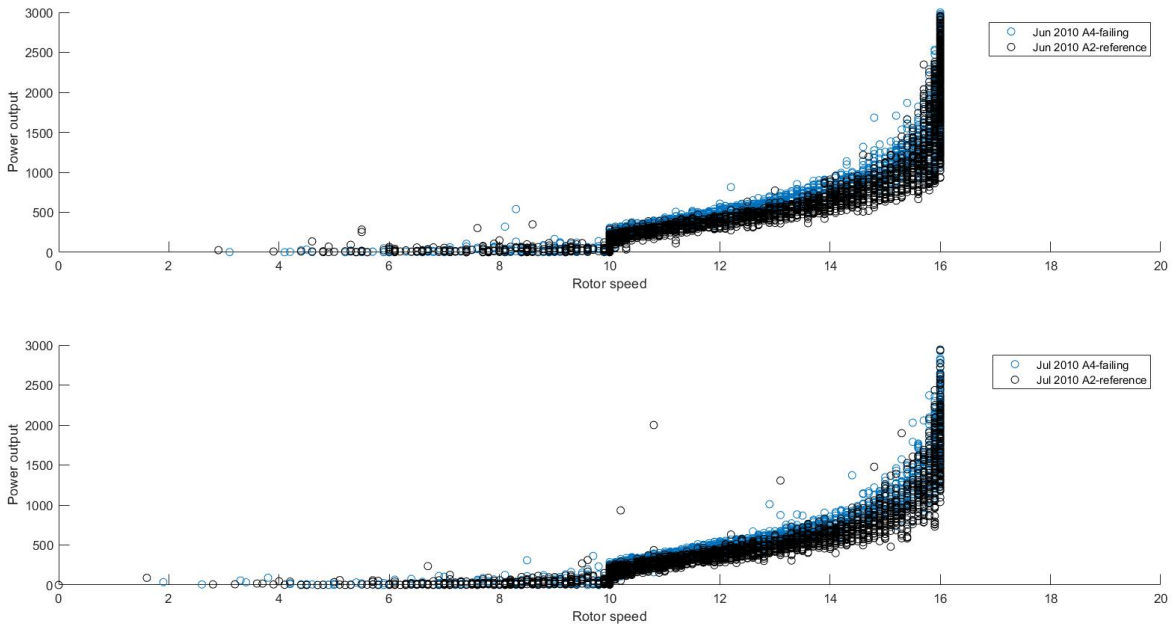

Figure 4.11: Comparison of the power output v.s. rotor speed data of WTA4 with the reference WT for the months Juni 2010 and July 2010.

Gen_Bear_Temp_Avg v.s. Grd_Prod_Pwr_Avg

From **Figure 4.12** it can be seen that during the first months of operation, i.e. February and March, the temperature of the bearing 1 of WTA4 overlaps with that of WTA2. *This is contradictory with theory*. However, over time the temperature of the bearing of WTA4 significantly increases, *which is in agreement with theory*, up until January 2011 (see **Appendix C.2**) when there is generator bearing replacement (Note: In the Performance Analyses Report of the wind farm it is not mentioned whether generator bearing 1 or bearing 2 was replaced). *This is in agreement with the expectations for pitch failure.*

Based on the above it can be stated that plotting delta T related to the temperature of generator bearing 1 against the power output does not fully provide insight into pitch failure.

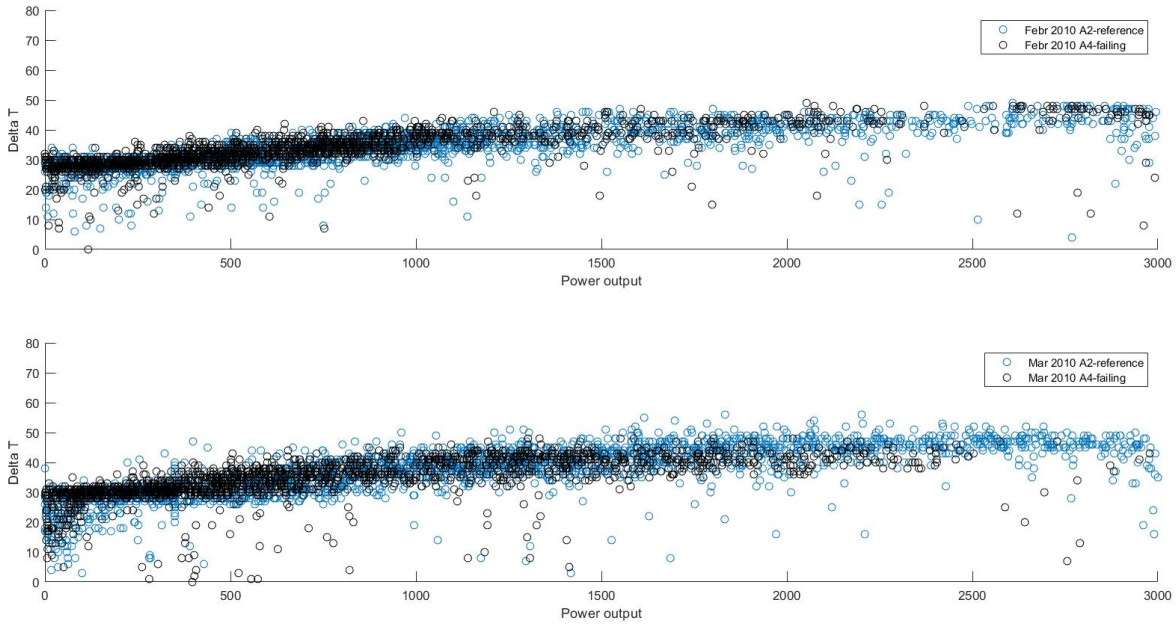

Figure 4.12: Comparison of $T_{temperature\ generator\ bearing\ 1}$ - $T_{nacelle}$ v.s. power output data of WTA4 with the reference WT for the months February 2010 and March 2010.

Gen_Bear2_Temp_Avg v.s. Grd_Prod_Pwr_Avg

Figures 4.9 - 4.10 show that for WTA4 delta T related to the temperature of generator bearing 2 for the months March and April 2010 is lower compared to WTA2. *This is in contradictory with the theory*. Lastly, it can be seen that for the months February and May 2010 no deviations are visible. *This is also in agreement with the theory, since the loads in bearing 2 increase less due to pitch failure and so it is possible that the loads do not increase enough to show deviations*. The remaining months also show no deviations.

Based on this it can be stated that plotting delta T related to the temperature of generator bearing 2 against the power output does fully provide insight into pitch failure.

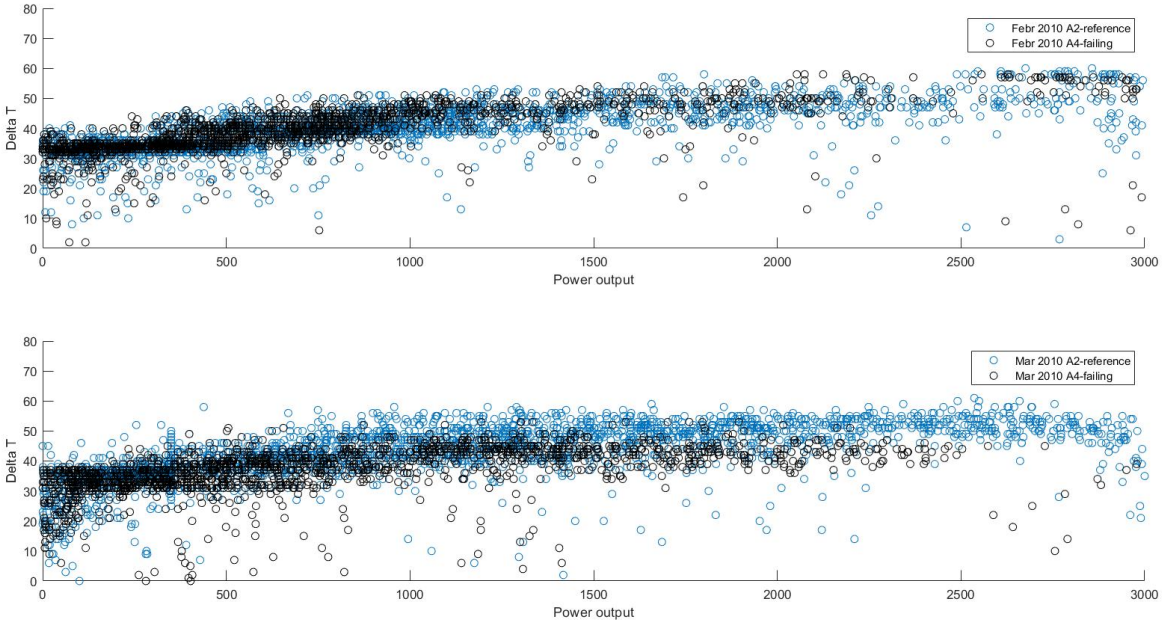

Figure 4.13: Comparison of $T_{generator\ bearing\ 2\ temperature}$ - $T_{nacelle}$ v.s. power output data of WTA4 with the reference WT for the months February 2010 and March 2010.

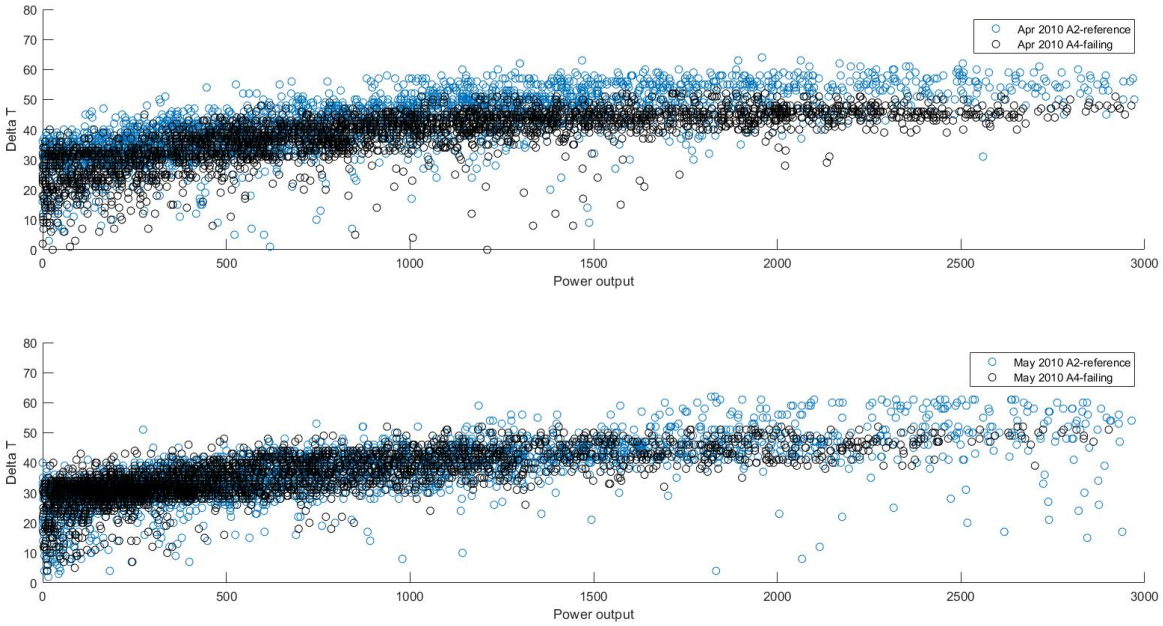

Figure 4.14: Comparison of $T_{generator\ bearing\ 2\ temperature}$ - $T_{nacelle}$ v.s. power output data of WTA4 with the reference WT for the months April 2010 and May 2010.

To summarize, in this section the SCADA-parameters related to the blade pitch system, gearbox and generator were plotted against each other based on the physical relations established in **section 4.4.3.2**. This section also demonstrated that knowledge of the physics supports explaining the deviations seen in the parameter plots, but that there are cases where observations from the field data do not match the theory.

4.6 Discussion

In this chapter firstly, the results presented in the previous section are interpreted more integrally in order to determine what they mean and what the limitations are and secondly, the findings are reviewed in the context of the literature.

The application of a functional approach for detecting WT failures was demonstrated on a case study that contained blade pitch system and generator bearing failure.

From the case study it was found that the functional approach did not fully support failure detection as it did not provide a full overview of the failure effects of blade pitch system failure. Namely, only the blades were expected to be affected, while generator bearing failure had also occurred. This means that not all affected SCADA-parameters could be captured. In order to be able to capture all the failure effects of the blade pitch system, it was proposed to additionally apply the load flow. With the load flow six affected (sub-)assemblies were identified, while based on the functional relations only one assembly was expected to be affected due to blade pitch failure.

Both the functional relations and the load flow showed which SCADA-parameters are affected and related, with the load flow providing a larger overview, but not how. In other words, they gave an *initial* indication of which parameters could be plotted against each other. For example, based on the functional relations the blade pitch system and blades are related and so their parameters are related to each other. The load flow additionally showed that the blade pitch system and gearbox are related and therefore so are their parameters. However, with one blade pitch parameter and five affected gearbox parameters and six generator parameters, it was difficult to identify which SCADA-parameters could be plotted against each other in order to detect deviations, i.e. blade pitch failure. This is where the application of the physics showed its value.

The physics immediately showed that one generator parameter, i.e the power output, could be related to the blade pitch angle. Also, the same generator parameter was related to four gearbox parameters, all related to temperatures in the gearbox, and two other generator parameters, i.e. the generator bearing temperatures (Note that of the six available generator parameters, two were not included in this work (see **Appendix B**)). Additionally, the physics helped explaining *beforehand* the expected deviations in the graphs of these parameter sets, due to pitch failure.

For the parameters sets studied in the previous section, the outcome of graphs showed that the field data matched the expectations. Namely, the parameter sets - chosen based on the physics- showed deviations and thus were indeed affected by pitch failure. Moreover, the behavior of these deviations matched what was theoretically expected for pitch failure. However, for some of the remaining parameter sets - see **Appendix C** - the behavior of the parameters did not match the theory for certain months. This demonstrates that the application of the physics does not always work.

From a generic point of view it can be stated that even though more failure effects were identified with the load flow, the load flow alone does not support failure detection. To be more specific, the root causes and failure effects of a certain (sub-)assembly can be traced back with the load flow alone. For example, the load flow showed that there is a load flow from the hub to the main bearing and so faulty operation of the main bearing may be traced back to the hub and blades (root causes).

However, there is also a functional dependency of the main bearing on the auxiliary system, i.e. its lubrication system, and thus it should be noted that failure of the auxiliary system could also be the cause of main bearing failure. This could not be found based on the load flow. Further, based on the load flow no (sub-)assemblies would be affected if the main bearing fails (Note that the base frame is not expected to be affected when the main bearings fail). The functional relations show that the gearbox depends on the main bearing and so it is possible that the failure of the main bearings affects the gearbox functionality. This implies that both the functional relations and load flow should be used in order to obtain a complete overview of the root causes and failure effects related to a (sub-)assembly.

In short, this work presented a structured analysis of SCADA-data for failure detection (of a certain (sub)assembly) by:

1. understanding the physical connections between the (sub-)assemblies of a HAWT and deriving the applicable physical structure with the aid of the general physical decomposition (see **Figure 3.3**);
2. from this structure and the general functional decomposition (see **Figure 3.4**) derive the functional relations between the (sub-)assemblies;
3. based on the physical structure and the generic load flow (see **Figure 3.13**) determine how the hub loads flow along the (sub-)assemblies;
4. with the functional relations and load flow determine the (sub-)assembly failures leading up to (= root causes) and affected by a certain (sub-)assembly failure (= effects).
5. through knowledge of the root causes and effects, identify the affected corresponding SCADA-parameters.
6. lastly, include the physics to identify the relations between the SCADA-parameters and which parameter sets can be used to detect a certain (sub-)assembly failure.

Given that steps 1-3 use a generic representation of the physical and functional relations in a HAWT, the proposed fault detection methodology can be applied to any HAWT. Also the identification of the affected SCADA-parameter (step 5) occurs based on the functional relations and the load flow, which are largely generic, and so this additionally shows the applicability of the method to any type of HAWT. The challenge, however, lies in step 2 as some technical system knowledge is required in identifying new functional relations between (sub-)assemblies in the case that the physical structure of a certain WT deviates from the general physical decomposition established in this work. Lastly, the physics used in this work are generic and apply to any HAWT.

Chapter 5

Conclusions & recommendations

This chapter is meant to provide an answer to the sub-research questions and ultimately the main research question.

This work explored the application of a functional approach in combination with SCADA-data for detecting failures of HAWTs. The application of a functional approach for SCADA-data analysis required the development of a functional decomposition of a HAWT such that it was generally applicable to all HAWTs and provided a structured method for relating SCADA-parameters to each other. Additionally, this work proposed taking into the load flow and physics for complementing the functional approach and supporting SCADA-data analysis.

The generic functional decomposition was obtained through an extensive literature review on current existing HAWT-configurations and existing WT taxonomies. In combination with the work of [14], first a generic physical decomposition of a HAWT was obtained and from this the generic functional connections between the WT (sub-)assemblies were derived. It was found that even since these decompositions are generic, there are cases where the decompositions must be slightly adjusted in order to be applicable to a case specific WT. This requires some technical system knowledge.

The analysis of the SCADA-parameters for the detection of certain (sub-)assembly failure required understanding which parameters are affected due to this failure and identifying which parameter sets will show deviations indicating (sub-)assembly failure. This work showed that the functional approach limits the identification of affected SCADA-parameters as it is not capable of capturing all root causesand failure effects. To overcome this challenge, it was proposed to include the loads seen by the various WT (sub-)assemblies. The load flow proved to identify additional failure effects, yet not all. For this the functional relations had to be included.

Even though the application of the functional approach and load flow supported identifying affected SCADA-parameters, they limited the data analysis as they did not provide insight into which parameters could be plotted against each other in order to detect deviations. This challenge was overcome by including the fundamental physics governing the energy conversion process. It was found that for the majority of the established parameter sets deviations were indeed detected. Moreover, the physics supported explaining these deviations.

Recommendations
Overall improvements for the proposed method are summarized below:

The set of SCADA-parameters chosen for this work currently contains only 16 parameters, while the original database has close to 130 parameters. Due to lack of expertise it was not possible to decode the remaining SCADA-parameters. In order to allow a better validation of the application of the physics in the detection of failures, the current set of parameters should be extended as more

parameters will be available for validation. For example, the main bearing temperature has not been measured and so the effect of pitch failure could not be validated for the main bearing. Also, with more SCADA-parameters available the identifiers of pitch failure can be extended. It should be noted, however, that of the decoded parameters not all provided usable inputs.

Given that this work only used SCADA-parameters for fault detection, future research can include the SCADA-alarm log. Connecting the alarms with the moment a deviation is observed can support establishing additional functional connections that might not have been established based on the functions and the load flow. This supports better detection of failures.

For future research it is also recommended to apply the proposed method to more case studies, i.e. other WT-types and other failures. This will aid in obtaining more generic outcomes regarding the SCADA-parameters supporting the detection of a certain failure.

Bibliography

[1] Tautz-Weinert, J. & Watson, S. J. (2017). Combining model-based monitoring and a physics of failure approach for wind turbine failure detection. *30th Conference on Condition Monitoring and Diagnostic Engineering Management (COMADEM 2017), University of Central Lancashire, UK*.

[2] Leahy, K., Gallagher, C., Bruton, K., O'Donovan P. & O'Sullivan, D. T. J. (2017). Automatically Identifying and Predicting Unplanned Wind Turbine Stoppages Using SCADA and Alarms System Data: Case Study and Results. *Journal of Physics: Conference Series 926 012011*.

[3] Gonzalez, E., Reder, M. & Melero, J. J. (2016). SCADA alarms processing for wind turbine component failure detection. *Journal of Physics: Conference Series 753 072019*.

[4] Tautz-Weinert, J. & Watson, S. J. (2017). Using SCADA data for wind turbine condition monitoring - a review. *IET Renewable Power Generation, 11 (4), pp. 382 - 394*.

[5] Zhao, Y., Li, D., Dong, A., Kang, D., Lv, Q. & Shang, L. (2017). Fault Prediction and Diagnosis of Wind Turbine Generators Using SCADA Data. *Energies 2017, 10, 1210*.

[6] Zhang, Z. & Wang, K. (2014). Wind turbine fault detection based on SCADA data analysis using ANN. *Adv. Manuf. (2014) 2: 70-78*.

[7] Koukoura, S., Carroll, J. & McDonald, A. (2018). An Insight into Wind Turbine Planet Bearing Fault Prediction Using SCADA Data. *European Conference of the Prognostics and Health Management Society 2018*.

[8] Zaher, A., McArthur, S. D. J., Infield, D. G. & Patel, Y. (2009). Online Wind Turbine Fault Detection through Automated SCADA Data Analysis. *Wind Energ. 2009; 12: 574-593*.

[9] Tchakoua, P., Wamkeue, R., Ouhrouche, M., Slaoui-Hasnaoui, F., Tameghe, T. A. & Ekemb, G. (2014). Wind Turbine Condition Monitoring: State-of-the-Art Review, New Trends, and Future Challenges. *Energies 2014, 7, 2595-2630*.

[10] McMillan, D. & Ault, G. W. (2007). Quantification of Condition Monitoring Benefit for Offshore Wind Turbines. *Wind Engineering 2007, Volume 3, No. 4*.

[11] Vazquez Hernandez, C., Telsnig, T. & Villalba Pradas, A. (2017). JRC Wind Energy Status Report - 2016 Edition. *EUR 28530 EN. Luxembourg: Publications Office of the European Union. JRC 105720; doi: 10.2760/332535*.

[12] Mwaniki, J., Lin, H. & Dai, Z. (2017). A Concise Presentation of Doubly Fed Induction Generator Wind Energy Conversion Systems Challenges and Solutions. *Hindawi, Journal of Engineering, Volume 2017, Article ID 4015102, 13 pages*.

[13] Kaidis, C., Uzunoglu, B. & Amoiralis, F. (2015). Wind turbine reliability estimation for different assemblies and failure severity categories. *IET Renew. Power Gener., pp. 1-8*.

[14] Reder, M., D., Gonzalez, E. & Melero, J., J. (2016). Wind Turbine Failures - Tackling current Problems in Failure Data Analysis. *Journal of Physics: Conference Series 753 072027*.

[15] Vazquez-Hernandez, C., Serrano-Gonzalez, J. & Centeno, G. (2017). A Market-Based Analysis on the Main Characteristics of Gearboxes Used in Onshore Wind Turbines. *Energies 2017, 10, 1686; doi:10.3390/en10111686*.

[16] Verma, N. & Pachori, A. (2015). Theoretical Approach for Comparison of Various Types of Wind Generator Systems. *International Journal of Recent Research in Electrical and Electronics Engineering, Volume 2, Issue 2, pp. 29-35*.

[17] Kadam, D., P. & Dr. Kushare, B., E. (2012). Overview of different wind generator systems and their comparisons. *International Journal of Engineering Science & Advanced Technology, Volume 2, Issue 4, pp. 1076-1081*.

[18] Beainy, A., Maatouk, C., Moubayed, N. & Kaddah, F. (2016). Comparison of Different Types of Generator for Wind Energy Conversion System Topologies. *3rd International Conference on Renewable Energies for Developing Countries (REDEC)*.

[19] Saini, S. (2013). Review of Doubly Fed Induction Generator Used in Wind Power Generation. *International Journal of Environmental Science: Development and Monitoring (IJESDM) ISSN No. 2231-1289, Volume 4 No. 3*.

[20] Murthy, J. (2013). A review on power electronics application on wind turbines. *IJRET: International Journal of Research in Engineering and Technology, Volume 2, Issue 11*.

[21] Hau, E. & von Renouard, H. (2006). *Wind Turbines. Fundamentals, Technologies, Application, Economics*. 2nd edition. Springer, Berlin, Heidelberg.

[22] Hemami, A. (2012). *Wind Turbine Technology*. 1st edition. Cengage Learning US.

[23] Zimroz, R., Bartelmus, W. & Urbanek, J. (2012). Wind Turbine Main Bearing Diagnosis - A Proposal of Data Processing and Decision Making Procedure under Non Stationary Load Condition. *Key Engineering Materials, doi: 10.4028*.

[24] Spinato, F., Tavner, P., J., van Bussel, G., J., W. & Koutoulakos, E. (2009). Reliability of wind turbine subassemblies. *IET Renewable Power Generation, Volume 3, Issue 4, pp. 1-15*.

[25] Perez, J., M., P., Marquez, F., P., G., Tobias, A. & Papaelias, M. (2013). Wind turbine reliability analysis. *Renewable and Sustainable Energy Reviews 23, pp. 463-472*.

[26] Tavner, P., J., Xiang, J. & Spinato, F. (2007). Reliability Analysis for Wind Turbines. *Wind Energy, 2007; 10: 1-18*.

[27] Kang, J. & Lee, H. (2017). The Development of Rotor Brakes for Wind Turbines. *International Journal of Applied Engineering Research, Volume 12, Number 15, pp. 5094-5100*.

[28] Licari, J., Ugalde-Loo, C., E., Ekanayake, J., B. & Jenkins, N. (2015). Comparison of the performance and stability if two torsional vibration dampers for variable-speed wind turbines. *Wind Energy, 2015; 18: 1545-1559*.

[29] Technirub Vizo International B.V. Silentblocks [*date accessed: 24-10-2018*]. https://www.technirub.nl/silentblocks.

[30] Hansen, M., O., L. (2008). *Aerodynamics of Wind Turbines*. 2nd edition. Earthscan.

[31] Babinsky, H. (2003). How do wings work?. *Physics Education, 38, 6, pp. 497-503*.

[32] Manwell, J., F., McGowan, J., G. & Rogers, A., L. (2009). *Wind Energy Explained - Theory, Design and Application*. Second Edition. John Wiley & Sons Ltd.

[33] A., R., S., Pandey, M., C., Sunil, N., N., S., S., Mugundhan, V. & Velamati, R., K. (2016). Numerical study of effect of pitch angle on performance characteristics of a HAWT. *Engineering Science and Technology, an International Journal 19, pp. 632-641*.

[34] Kandil, M., A., F. & Elnady, A., O. (2017). Performance of GOE-387 Airfoil Using CFD. *International Journal of Aerospace Sciences, 5, pp. 1-7*.

[35] Eliassen, L. Aerodynamic loads on a wind turbine rotor in axial motion. *PhD thesis, University of Stavanger, 2015*.

[36] Wang, C. & Chiang, M. (2016). A Novel Pitch Control System of a Large Wind Turbine Using Two-Degree-of-Freedom Motion Control with Feedback Linearization Control. *Energies, 9, 791, pp. 1-18*.

[37] Chehouri, A., Younes, R., IIinca, A. & Perron, J. (2015). Review of performance optimization techniques applied to wind turbines. *Applied Energy, Volume 142, pp. 361-388*.

[38] Isaza, A., V. Understanding the Mechanisms of Aero-Structural Optimization of a Wind Turbine Blade. *MSc thesis, Delft University of Technology, 2012*.

[39] Curtu, I., Stanciu, M., D., Titeiu, R. & Sturzu, T. (2015). The design of a test bench for wind blades bending with small dimension. *6th International Conference, "Computational Mechanics and Virtual Engineering", COMEC 2015, 15-16 October 2015, Braşov, Romania*.

[40] Söker, H. (2013). Advances in Wind Turbine Blade Design and Materials (2013). *Woodhead Publishing Series in Energy, pp. 29-58*.

[41] Schubel, P., J. & Crossley, R., J. (2012). Wind Turbine Blade Design. *Energies 2012, 5, pp. 3425-3449*.

[42] Jensen, C. Numerical Simulation of Gyroscopic Effects in Ansys. *MSc thesis, School of Engineering and Science, 2011*.

[43] Bianchi, F., D., De Battista, H. & Mantz, R., J. (2007). *Wind Turbine Control Systems. Principles, Modelling and Gain Scheduling Design*. Springer.

[44] Kim, B., Jin, J., Bitkina, O. & Kang, K. (2015). Ultimate load characteristics of NREL 5-MW offshore wind turbines with different substructures. *International Journal of Energy Research, doi: 10.1002/er.3430*.

[45] Van Rooij, R., P., J., O., M. (2001). Terminology, reference systems and conventions, Duwind 2001.004. *Vol. contract JOR3-CT98-0284., Delft University of Technology, Delft, 26 p*.

[46] Mamassis N., Efstratiadis A. & Apostolidou I. (2012). Topography-adjusted solar radiation indices and their importance in hydrology. *Hydrological Sciences Journal, 57 (4), 756-775*.

[47] Brand, A., J., Peinke, J. & Mann, J. (2011). Turbulence and wind turbines. *Journal of Physics: Conference Series 318 072005*.

[48] Rommel, D., P., Di Maio, D. & Tinga, T. Calculating Wind Turbine Component Loads for Improved Life Prediction. Submitted for publication.

[49] Popko, W., Thomas, P., Sevinc, A., Rosemeier, M., Bätge, M., Braun, R., Meng, F., Horte D., Balzani C., Bleich, O., Daniele, E., Stoevesandt, B., Wentingmann, M., Polman, J., D., Leimeister, M., Schümann, B. & Reuter, A. (2018). IWES Wind Turbine IWT-7.5-164 Rev 4. *Fraunhofer Institute for Wind Energy Systems IWES. Bremerhaven. https://doi.org/10.24406/IWES-N-518562*.

[50] Rommel, D. Load calculation at low and high speed gearbox shafts. Submitted for publication.

[51] Van Dasselaar, R., J. Load calculation drivetrain wind turbines. *MSc thesis, University of Twente, 2019*.

[52] Haastrup, M., Hansen, M., R. & Ebbesen, M., K. (2011). Modeling of Wind Turbine Gearbox Mounting. *Modeling, Identification and Control, Volume 32, No. 4, 2011, pp. 141-149*.

[53] Keller, J., Guo, Y. & Sethuraman, L. (2016). "Gearbox Reliability Collaborative Investigation of Gearbox Motion and High-Speed-Shaft Loads," National Renewable Energy Laboratory (NREL), Golden, CO, USA, NREL/TP-5000-65321, March, 2016, pp. 1- 41. Accessed on Jan. 14, 2019. [Online]. Available: https://www.nrel.gov/docs/fy16osti/65321.pdf.

[54] Dyachuk, E., Rossander, M., Goude, A. & Bernhoff, H. (2015). Measurements of the Aerodynamic Normal Forces on a 12-kW Straight-Bladed Vertical Axis Wind Turbine. *Energies 2015, 8, 8482 - 8496; doi:10.3390/en8088482*.

[55] Gibbons, C., B. (1976). Coupling misalignment forces. *Proceedings of the fifth turbomachinery symposium, pp. 111 - 116*

[56] Arabian-Hoseynabadi, H., Oraee, H. & Tavner, P., J. (2010). Failure Modes and Effects Analysis (FMEA) for wind turbines. *Electrical Power and Energy Systems, 32, pp. 817-824*.

[57] Tinga, T. (2013). *Principles of Loads and Failure Mechanisms. Application in Maintenance, Reliability and Design*. Springer.

[58] Eisa, S., A., Wedeward, K. & Stone, W. (2017). Time Domain Study of a Type-3 DFIG Wind Turbine's Dynamics: Q Drop Function Effect and Attraction vs Control Limits Analysis. *Conference Paper, doi: 10.1109/GreenTech.2017.57*.

[59] Bertagnolio, F., Sorensen, N., Johansen, J. & Fuglsang, P. (2001). Wind Turbine Airfoil Catalogue. *Riso National Laboratory, Roskilde, Denmark, Riso-R-1280(EN)*.

[60] Blaabjerg, F., Iov, F., Chen, Z. & Ma, K. (2014). Power Electronics and Controls for Wind Turbine Systems. *Department of Energy Technology, Aalborg University, doi: 10.1109/Energycon.2010.5771701*.

[61] Vásquez, S., Kinnaert, M. & Pintelon, R. (2017). Active Fault Diagnosis on a Hydraulic Pitch System Based on a Frequency-Domain Identification. *IEEE Transactions on Control System Technology, doi: 10.1109/TCST.2017.2772890*.

[62] Jeng, Y. & Huang, P. (2003). Predictions of Temperature Rise for Ball Bearings. *Triobology Transactions, 46:1, 49-56, doi: 10.1080/10402000308982599*.

[63] Jian, S., Xiaoqian, M., Shuying, C. & Huijing, G. (2015). Review of the Cooling Technology for High-power Wind Turbines. *5th International Conference on Advanced Design and Manufacturing Engineering (ICADME 2015)*.

[64] Neale, M., J. (2001). *The Tribology Handbook*. 2nd edition. Butterworth-Heinemann.

[65] Wang, Q. & Chung, Y. (*Editors*) (2013). *Encyclopedia of Tribology*. SpringerReference.

[66] Blaabjerg, F., Iov, F., Terekes, T., Teodorescu, R. & Ma, K. (2011). Power Electronics - Key Technology for Renewable Energy Systems. *2nd Power Electronics, Drive Systems and Technologies Conference, pp. 445-466, doi: 10.1109*.

[67] Spiteri Staines, C., Caruana, C., Licari, J. (2015). Review of Power Converters for Wind Energy Systems. *WINERCOST Workshop "Trends and Challenges for Wind Energy Harvesting", Coimbra*.

[68] Bang, D., Polinder, H., Shrestha, G. & Ferreira, J., A. Review of Generator Systems for Direct-Drive Wind Turbines. *Electrical Power Processing/DUWIND, Delft University of Technology, pp. 1-11*.

[69] Bang, D., Polinder, H., Shrestha, G. & Ferreira, J., A. Possible Solutions to Overcome Drawbacks of Direct-Drive Generator for Large Wind Turbines. *Electrical Power Processing/DUWIND, Delft University of Technology, pp. 1-10*.

[70] Wu, B., Lang, Y., Zargari, N. & Kouro, S. (2011) Power conversion and control of wind energy systems. *Wiley-IEEE press, pp. 16-35*.

[71] Tapre, P., C., Datkhile, S., N. & Veeresh, C. (2016) A Comparative Study of Constant Speed and Variable Speed Wind Energy Conversion Systems. *GRD Journals-Global Research and Development Journal for Engineering, Volume 1, Issue 10, pp. 19-24*.

[72] Molina, M., G. & Mercado, P., E. (2011) Modelling and Control Design of Pitch-Controlled Variable Speed Wind Turbines. *CONICET, Instituto de EnergÃ⬡a ElÃ́ctrica, Universidad Nacional de San Juan Argentina, doi: 10.5772/15880*.

[73] Iov, F., Ciobotaru, M., Sera, D., Teodorescu, R. & Blaabjerg, F. (2007) Power Electronics and Control of Renewable Energy Systems. *Aalborg University, Institute of Energy Technology, doi: 10.1109/PEDS.2007.4487668*.

[74] Ma, K. (2015). *Power Electronics for the Next Generation Wind Turbine System*. Springer International Publishing Switzerland.

[75] Chen, B., Matthews, P., C., & Tavner, P., J. (2013) Wind turbine pitch faults prognosis using a-priori knowledge-based ANFIS. *Expert Systems with Applications 40, pp. 6863 - 6876*.

[76] Takabi, J. (2015) On the Thermally Induced Failure of Rolling Element Bearings. *LSU Doctoral Dissertations. 1451*.

[77] El-Shimy, M. (2016) Wind Energy Conversion Systems: Reliability Perspective. *Encyclopedia of Energy Engineering and Technology, Second Edition, pp. 2184 - 2206*.

Appendix A

Functionalities HAWT-assemblies

ID	(Sub)Assembly	Function
1	Blades	Produce a torque from the aerodynamic forces exerted on the blades by the wind flow.
2	Hub	Provide structural support for the blades.
3	Blade pitch system	i. Control: Increase the pitch angle of the blades and thus decrease the angle of attack in order to control/limit the rotor speed/power output for wind speeds above rated wind speed; ii. Safety: Aerodynamically brake (feather) the rotor (blades) in case of extreme wind speeds.
3.1	Rotor blade/pitch bearings	i. Allow blades to turn around their longitudinal axis; ii. Carry the forces and moments acting at the blade root.
3.2**a**	Electric blade pitch drive	Move the rotor blades around their longitudinal axis by means of electrical motors.
3.2.1a	Controller(s)	Control the electric motors.
3.2.2a	Electric motors	Supply mechanical power to the slewing gearbox.
3.2.3a	Slewing gearboxes	Convert the high rotational speed of the electric drive motor into a slower torque for driving the pitch bearing.
3.2.5a	Power supply	Supply the drive motor with power.
3.2**b**	Hydraulic blade pitch drive	Move the rotor blades around their longitudinal axis by means of hydraulic cylinders.
3.2.1b	Control valves	Control the flow of hydraulic oil to and from the hydraulic cylinders.
3.2.2b	Hydraulic cylinders (alternative: Hydraulic motors + hydraulic slewing gearbox)	Vary pitch of the blade.

ID	(Sub)Assembly	Function
3.2.3b	Hydraulic accumulators	Store backup hydraulic pressure from the pump in case the pump fails or is switched off unexpectedly to bring the blades back to a safe out-of-wind mode.
4	Main shaft	i. Support the hub (and thus the blades); ii. Transmit/deliver the rotor torque to the gearbox.
5	Main bearings	i. Support the low-speed shaft along with the weight of the blades and hub; ii. Allow the rotational movement of the low-speed shaft; iii. Absorb radial rotor loads that are transferred from the blades to the hub and low-speed shaft.
6	Gearbox	Convert the rotational speed and torque of the rotor (received by the low-speed shaft) to the higher speed and lower torque of the generator, respectively.
6.1	Silent blocks	Absorb the movement caused by the rotational torque of the rotor as well as allow (some) displacement due to the rotor moments.
6.2	Bearings	Support the gearbox shafts, while allowing their rotational motions.
6.3	Gears	Convert torque and speed.
6.4	High-speed shaft	Transmit the converted mechanical power from the gearbox to the generator.
7	Brake system	Stop the operation of the WT.
8**a**	Mechanical brake	Mechanically brake the rotor during maintenance.
8a.1	Calliper + brake pads + disc	Provide braking force through engagement of the brake pads to (clamping of) the disc.
8a.2	Control valve	Control the hydraulic oil flow to the calliper.
8**b**	Rotor lock	Prevents the rotation of a stopped rotor, i.e. locks the rotor once it has been stopped.
9	Flexible coupling(s)	i. Connect the gearbox to the generator so that the torque and speed of the gearbox high-speed shaft can be transmitted to the generator input shaft; ii. Compensate for misalignment between gearbox and generator;

ID	(Sub)Assembly	Function
10	Generator	Convert mechanical energy captured by the blades into electrical energy.
10.1	Rotor	Cause excitation of the stator.
10.2	Stator	Rotate in the magnetic field of the rotor and provide electrical energy to the grid.
10.3	Bearings	Support and allow rotational movement of armature shaft.
11	Frequency converter system	Allow the generator to operate at variable speed for maximizing power extraction at wind speeds below the rated wind speed.
11.1	Capacitor bank	Compensate for the reactive power.
11.2	Rotor-side converter	Control the generator rotor speed and thus the active and reactive power by controlling the rotor currents.
11.3	Grid-side converter	Control the DC-capacitor voltage, i.e. keep the DC-capacitor voltage fixed.
11.4	Rotor-side controller	Control the rotor-side converter.
11.5	Grid-side controller	Control the grid-side converter.
12	Transformer	Increase the voltage and reduce the current of the electricity produced by the generator.
13	Yaw system	i. Orientate the WT into the wind direction to capture maximum wind power; ii. Turn the turbine out of the wind direction at high wind speeds; iii. Connect the nacelle and tower.
13.1	Yaw bearing	i. Allow the nacelle to rotate on the tower in order to align the blades into the wind direction; ii. Carry the wind and rotor loads, the weight of the nacelle and the weight of the assemblies enclosed by the nacelle.
13.2	Electric/Hydraulic yaw drives	Turn the ring gear and thus the yaw bearing to rotate the nacelle.
13.3	Ring gear	Allow rotation of the nacelle.
13.4	Yaw brakes	Fix the position of the nacelle after a completed yawing operation.

ID	(Sub)Assembly	Function
13.5	Yaw bearing clamp assembly (pre-tension system): spring and adjustment screw	Ensures that there is no looseness between the yaw bearing and ring gear.
14	Control & Communications	i. Maximize energy capture thereby taking into account the safe operation restrictions such as rated power, rated speed, cut-out speed; ii. Alleviate transient (low-frequency) loads that are induced by turbulence and gusts, mitigate high frequency cyclic loads caused by rotational sampling and avoid resonance of drive-train assemblies and the structure due to these cyclic loads; iii. Control the reactive power in order to attenuate frequency and voltage variations at the grid terminals and flicker on electrical lines.
15	Auxiliary System	Support the (functioning of the assemblies of the) energy conversion process, for example by supplying units with lubrication, cooling, heating, hydraulic pressure, detecting and suppressing fires, etc.
16	Base frame	i. Carry the assemblies of the nacelle; ii. Transmit the rotor loads absorbed by the main bearings and gearbox bushings through the yaw system to the tower.
17	Tower	Support the rotor, nacelle and the assemblies enclosed in the nacelle.
18	Foundation	Provide stability to the tower.

Table A.1: Function descriptions of HAWT assemblies.

Appendix B

Pitch failure effects on the SCADA-parameters

Hyd_Oil_Temp_Avg
There is a parameter measuring a hydraulic oil temperature of which it is unclear whether this relates to the blade pitch, mechanical brake or yaw system. As all three (sub-)assemblies do not operate continuously and the data points are taken every 10 minutes, it is expected that the hydraulic oil temperature will not support pitch failure detection. To be more specific, as these (sub-)assemblies do not operate continuously the hydraulic system is also not actuated continuously and therefore it is expected that in the time interval of 10 minutes the hydraulic oil has already cooled down to show any deviations.

B.1 Gearbox parameters

Rtr_RPM_Avg
The parameter Rtr_RPM_Avg is assumed to be the average rotational speed of the gearbox input shaft. Namely, as the hub is physically connected to the gearbox input shaft, the rotor speed is equal to the speed of the gearbox input shaft.

It is expected that Rtr_RPM_Avg can be used to detect pitch failure. When, for example, one blade has a larger ϕ and thus a smaller α, F_l of this blade decreases. As this blade has a lower F_l, the torque generated by this blade is smaller compared to the remaining two blades and consequently, the overall aerodynamic torque, $M_{x_{hub,\ total}}$ deviates compared to the case of no pitch failure. As a result the rotational speed of the gearbox input shaft will change.

With regard to the pitch failure case of WTA4, it cannot be stated beforehand how the rotational speed of the gearbox input shaft will change, since *several types of pitch failure* can occur of which the effects on the rotational speed must first be studied. These failure types are described next:

1. Generally, the blades are pitched below cut-in wind speed, which is around 3 - 4 m/s, and just before the rated wind speed is reached. As the wind speed increases from 0 m/s to the cut-in wind speed, the blade pitch angles are *decreased* from almost 90° (feathered position) to 0°, where the WT starts producing power. In this regard, the wind flows from the leading to the trailing edge and α is positive. Hereafter, the pitch angle of the blades are kept constant until just before the rated wind speed, i.e. the maximum allowable generator speed, is reached. The reason for pitching the blades slightly before the rated wind speed is reached is to prevent an abrupt change in the blade pitch angles so that the transient loads acting on the WT are kept at a minimum. Transient loads are the loads which are induced due to a temporary external event, e.g. wind gusts, turbulence, the application of the mechanical rotor brake, etc., and eventually decay [32][43]. Just below the rated

wind speed, the pitch angles are *increased* from 0° to almost 90°. The increase in the blade pitch angles is intended to maintain the power output of the WT at the rated value of the generator.

Given the above, pitch failure can thus occur i. *below cut-in wind speed*, where the blade pitch angles must be decreased or ii. *above the maximum allowable generator speed*, where the blade pitch angles should be increased.

2. Additionally, it is possible that during pitching a failure can occur in the blade pitch system of one, two or three blades and that as a result insufficient pitching power is delivered for adjusting the blade pitch angle(s). *The failure effects of the blade pitch system on the loads that enter the drive train, i.e. hub loads, shall for the remainder of this work only be discussed for the case of pitch failure of one blade*, since a larger effect is expected when pitch failure occurs for two or three blades. This is explained, as an example, for $F_{y_{root}}$:

Taking the azimuth angles of blade 1, 2 and 3 to be respectively 0°, 120° and -120° and assuming $F_{T_{root,\ blade\ 1}} = 2.2$, $F_{T_{root,blade\ 2}} = 1.8$, $F_{T_{root,blade\ 3}} = 2$ and $F_{G_{y,root}}$ for all blades $= 1$, the resulting hub loads in y_{hub}- and z_{hub} direction are:

Blade 1:

$$\begin{aligned}
\begin{pmatrix} F_{x_{hub,\ blade\ 1}} \\ F_{y_{hub,\ blade\ 1}} \\ F_{z_{hub,\ blade\ 1}} \end{pmatrix} &= \begin{pmatrix} 1 & 0 & 0 \\ 0 & \cos\Phi & -\sin\Phi \\ 0 & \sin\Phi & \cos\Phi \end{pmatrix} \begin{pmatrix} 0 \\ F_{y_{root}}(\Phi) \\ 0 \end{pmatrix}, \quad \text{for } 0 \leq \Phi \leq 2\pi \\
&= \begin{pmatrix} 1 & 0 & 0 \\ 0 & \cos\Phi & -\sin\Phi \\ 0 & \sin\Phi & \cos\Phi \end{pmatrix} \begin{pmatrix} 0 \\ [F_{T_{root}}(\Phi) + F_{G_{y_{root}}}(\Phi)]^1 \\ 0 \end{pmatrix} \\
&= \begin{pmatrix} 0 \\ \cos\Phi.[F_{T_{root}}(\Phi) + F_{G_{y_{root}}}(\Phi)] \\ \sin\Phi.[F_{T_{root}}(\Phi) + F_{G_{y_{root}}}(\Phi)] \end{pmatrix} \\
&= \begin{pmatrix} 0 \\ 3.2 \\ 0 \end{pmatrix}
\end{aligned} \tag{B.1}$$

Blade 2:

$$\begin{pmatrix} F_{x_{hub,\ blade\ 2}} \\ F_{y_{hub,\ blade\ 2}} \\ F_{z_{hub,\ blade\ 2}} \end{pmatrix} = \begin{pmatrix} 0 \\ 2.28 \\ 1.63 \end{pmatrix} \tag{B.2}$$

Blade 3:

$$\begin{pmatrix} F_{x_{hub,\ blade\ 3}} \\ F_{y_{hub,\ blade\ 3}} \\ F_{z_{hub,\ blade\ 3}} \end{pmatrix} = \begin{pmatrix} 0 \\ 2.44 \\ -1.74 \end{pmatrix} \tag{B.3}$$

The resultant hub loads due to $F_{y_{root}}$ of all blades becomes:

$$\begin{pmatrix} F_{x_{hub,\ total}} \\ F_{y_{hub,\ total}} \\ F_{z_{hub,\ total}} \end{pmatrix} = \begin{pmatrix} F_{x_{hub,\ blade\ 1}} \\ F_{y_{hub,\ blade\ 1}} \\ F_{z_{hub,\ blade\ 1}} \end{pmatrix} + \begin{pmatrix} F_{x_{hub,\ blade\ 2}} \\ F_{y_{hub,\ blade\ 2}} \\ F_{z_{hub,\ blade\ 2}} \end{pmatrix} + \begin{pmatrix} F_{x_{hub,\ blade\ 3}} \\ F_{y_{hub,\ blade\ 3}} \\ F_{z_{hub,\ blade\ 3}} \end{pmatrix} = \begin{pmatrix} 0 \\ 7.92 \\ -0.12 \end{pmatrix} \tag{B.4}$$

When pitch failure of blade 1 occurs below cut-in wind speed, $F_{T_{root,\ blade\ 1}}$ becomes for example = 1.9. The resultant hub loads then become:

$$\begin{pmatrix} F_{x_{hub,\ total}} \\ F_{y_{hub,\ total}} \\ F_{z_{hub,\ total}} \end{pmatrix} = \begin{pmatrix} 0 \\ 7.62 \\ -0.12 \end{pmatrix} \tag{B.5}$$

In the case that pitch failure of blade 1 and blade 2 occur, $F_{T_{root,\ blade\ 1}}$ becomes for example 1.9 and $F_{T_{root,\ blade\ 2}}$ becomes 1.3. The resultant hub loads are in this case:

$$\begin{pmatrix} F_{x_{hub,\ total}} \\ F_{y_{hub,\ total}} \\ F_{z_{hub,\ total}} \end{pmatrix} = \begin{pmatrix} 0 \\ 7.22 \\ -0.41 \end{pmatrix} \tag{B.6}$$

Equation B.4 - B.6 show that compared to no pitch failure, the resultant hub forces due to $F_{y_{root}}$ have decreased. When the blade pitch system of one more blade fails, the resultant hub forces decrease further. This illustrates that *the effect* of pitch failure on the hub forces *becomes larger* when pitch failure of more than 1 blade occurs.

Next it is studied how the aerodynamic torque, $M_{x_{hub,\ total}}$, and thus the rotational speed, Rtr_RPM_Avg, are affected for pitch failure case i. and ii.

i. Pitch failure below cut-in wind speed - one blade
In order to start up the WT at around 3 - 4 m/s, the blades are pitched from 90° to around 0° - here the WT should start producing power.

The blade pitch angles are decreased until the generator speed is no longer zero and the generator starts producing power. When failure occurs in the blade pitch system of one blade, it is assumed that insufficient pitching power is delivered for decreasing ϕ. This means that ϕ of this blade is *decreased insufficiently* and as a result the blade has a smaller α compared to the remaining two blades. Consequently, the pitch angles of the two remaining blades of the WT are *decreased more than usual* so that the minimum generator speed required for starting power production can be reached. In **section 3.5.3.2** it was explained that the blade pitch angle, ϕ, affects the hub loads - in this case $M_{x_{hub,\ total}}$. Generally, at start-up all blades have a blade pitch angle $\phi = 0°$ and the same power coefficient, C_p. In the case that pitch failure occurs, one blade has a different pitch angle compared to the remaining two blades and the blade pitch angles of the blades are larger than 0°. **Figure 4.7** shows that the C_p-value decreases for $\phi > 0°$. As the lift coefficient, C_l, depends on C_p it is expected that F_l of these blades will decrease and so $M_{x_{hub,\ total}}$ *also decreases*. Consequently, the power output of the generator will be lower due to pitch failure. *The rotational speed of the rotor, Rtr_RPM_Avg, is however not expected to change, since the control system continuously adjusts the rotor speed to the reference rotor speed.*

Based on the above explanation it can be concluded that when pitch failure occurs below cut-in wind speed, it is expected that the power output is lower (between cut-in and rated wind speed) and that the rotational speed of the rotor remains the same.

ii. Pitch failure slightly below rated generator speed - one blade
Another failure option is that the pitch system fails just before the maximum generator speed is reached. From this point on the blade pitch angles must be increased in order to limit and maintain the power output of the generator. If ϕ of one blade cannot be increased sufficiently, then its blade pitch angle is smaller compared to the remaining two blades. This blade will have a higher C_p-value than the remaining two blades and will thus produce a higher torque. The total torque generated by

the three blades, $M_{x_{hub,\ total}}$, will then be higher. However, the control system will then further adjust the blade pitch angles such that the power output of the generator is maintained at the rated value.

Based on the above explanation it can be concluded that when pitch failure occurs slightly below rated generator speed, both the power output and the rotational speed of the rotor will remain at the rated value and so no deviations will be visible. However, when the WT continues its operation and wind speeds reach values between cut-in and rated wind speed deviations will in this case be visible, i.e. the power output will be lower.

Gear_Bear_Temp_HSMid_Avg, Gear_Bear_TempHSGenEnd_Avg and Gear_Bear_TempHSRtrEnd_Avg
Table 4.1 shows that there are three parameters monitoring temperatures of three gearbox bearings. The operating temperature of the bearings is regulated by the cooling and lubricating system of the gearbox. The lubricating system of the gearbox is a pressure-fed, i.e. forced, system with an external oil sump. The heat generated by the bearings and (gears) is taken away by the (lubricating) oil, which is afterwards sent to the oil reservoir. An oil pump takes suction from the reservoir and sends the oil through a heat exchanger (i.e. cooler) to cool, after which it returns to the gearbox. This is regulated by a control unit or a switch. Both activate the cooling if the oil temperature is too high. Once the cooler is activated, the oil temperature is decreased until a certain minimum temperature. Then the cooler is switched off and the oil temperature starts to increase again until the maximum temperature, where the cooler switches again on. With such a system the goal is to maintain the bearing temperature at the required level, even when they start failing and so, theoretically the gearbox bearing temperatures would not give insight into pitch failure nor would they allow the detection of pitch failure.

Gear_Oil_TempBasis_Avg
There is also a parameter available which monitors the lubrication oil itself. It cannot, however, be said with certainty whether this is the temperature of the lubricating oil in the oil sump. The sump oil is responsible for absorbing the generated heat due to bearing friction and meshing of the gears. After the oil has passed through the gearbox bearings and gears, it flows to the oil reservoir and from here it is pumped through a filter. Depending on its temperature the oil returns back to the gearbox lubrication system. If the temperature has reached a certain maximum value, the oil flow is diverted to the cooler by a thermal valve (the oil has a maximum temperature that should not be exceeded in order to prevent fast deterioration of the oil). In this way the oil is forced to pass through the cooler before it can flow to the gearbox lubrication system. The expected behavior of the parameter Gear_Oil_TempBasis_Avg due to pitch failure is discussed next:

For the heat generated by the gearbox bearings, **equation 4.5** applies. With regard to the gears, the driving gear teeth push, i.e. exert a force on, the driven gear teeth. This is illustrated in the **Figure B.1**.

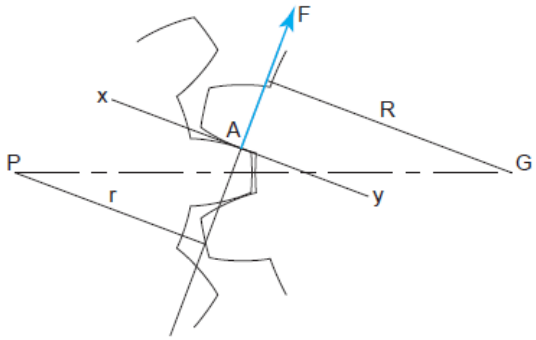

Figure B.1: Force exerted by driving gear teeth on driven gear teeth [22].

This force acts normal to the surfaces of the gears and its value generally depends on the torque transfer between the gears [22]. As the gears mesh, they slide over each other and cause a friction force. This friction force generates heat of which the amount of heat generation depends on the normal force and thus the torque transfer between the gears. As $M_{x_{hub,\ total}}$ is lower in the case of pitch failure, the gears will generate less heat compared to the case of no pitch failure.

To sum up, when pitch failure occurs it is expected that the gearbox bearings generate more or less the same amount of heat due to an increase in the bearing loads and a decrease in the transmitted torque. Due to the decrease in the transmitted torque the gears are expected to produce less heat and thus overall it is expected that the heat flow to the gear oil remains more or less the same.

B.2 Generator parameters

The current set of SCADA-parameters contains parameters measuring the average temperature of the generator cooling water, Gen_CoolingWater_Temp_Avg, and the average slip ring temperature, Gen_SlipRing_Temp. These parameters are not discussed in this work, because in-depth knowledge is required regarding the harmonics of the rotor current that adjusts the counter torque of the generator. As the focus of this work is primarily on the mechanical system of a HAWT, the harmonics due to the generator currents are out of scope of this work.

Gen_Bear_Temp_Avg and Gen_Bear2_Temp_Avg
In **section 3.5.3.3** it was explained that the reaction forces in the generator bearings are fundamentally caused by the displacement of the gearbox and that this displacement depends on the forces of the hub bending moments as well as the hub forces.

When pitch failure occurs, the forces of the bending moments and the hub forces are expected to increase. This causes increased motion of the gearbox and more misalignment of the flexible coupling. In **section 3.5.3.3** it was explained that due to the misalignment, reaction forces and moments are generated in the coupling. Consequently, the coupling reaction forces and moments cause reaction forces in the generator bearings. Due to the increased misalignment of the flexible coupling, the reaction forces in the generator bearings are expected to increase. *Below it is demonstrated that the reaction forces in the second generator bearing are generally smaller than in the first generator bearing.*

The reaction forces in generator bearing 1 are assumed to be $F_{x,_{GB1}}$, $F_{y,_{GB1}}$ and $F_{z,_{GB1}}$ and those in bearing 2 $F_{x,_{GB2}}$ and $F_{y,_{GB2}}$ (see **Figure B.2**). Further, $F_{R,coupling}$ and $M_{R,coupling}$ are assumed to act at a distance a from bearing 1 and a distance b from bearing 2.

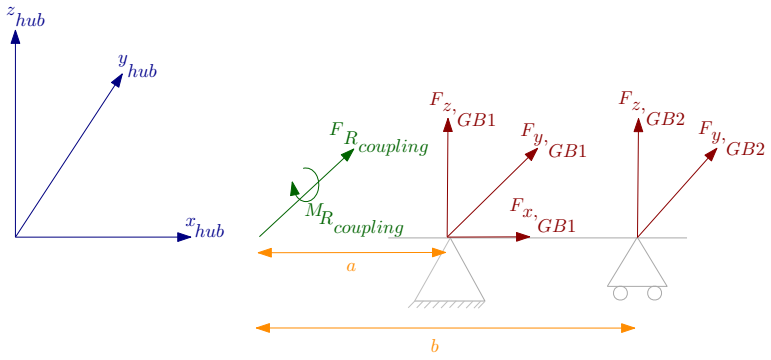

Figure B.2: Generator forces due to coupling reaction loads.

Through application of the equilibrium equations, the bearing reaction forces can be found:

$$
\begin{aligned}
&\Sigma\ F_{x_{hub}} = 0: \quad F_{x_{GB1}} = 0 \\
&\Sigma\ F_{y_{hub}} = 0: \quad F_{y_{GB1}} + F_{y_{GB2}} = -\ F_{R_{coupling}} \\
&\Sigma\ F_{z_{hub}} = 0: \quad F_{z_{GB1}} + \frac{M_{R_{coupling}}}{a} + F_{z_{GB2}} + \frac{M_{R_{coupling}}}{b} = 0 \\
&\Sigma\ M_{y_{hub}} = 0: \quad F_{z_{GB1}} \cdot a + F_{z_{GB2}} \cdot b = 0 \\
&\Sigma\ M_{z_{hub}} = 0: \quad F_{y_{GB1}} \cdot a + F_{y_{GB2}} \cdot b = 0
\end{aligned}
\tag{B.7}
$$

Assuming $F_{R_{coupling}} = 12$ and $M_{R_{coupling}} = 15$, a = 2 and b = 5, $F_{y_{GB1}} = 20$, $F_{y_{GB2}} = 8$, $F_{z_{GB1}} = 7.1$ and $F_{z_{GB2}} = 3.4$. When pitch failure occurs, the coupling misalignment increases and so do the coupling reaction forces. Assuming $F_{R_{coupling}}$ becomes 20 and $M_{R_{coupling}}$ becomes 23, $F_{y_{GB1}} = 33.3$, $F_{y_{GB2}} = 13.3$, $F_{z_{GB1}} = 11.1$ and $F_{z_{GB2}} = 5$. This shows that pitch failure causes the loads in bearing 1 to increase more than in bearing 2, which means that bearing 2 is less sensitive to pitch failure.

Gen_RPM_Avg
Another parameter that monitors the generator is the rotational speed of the generator. Previously it was explained that when pitch failure occurs, the rotational speed of the turbine rotor remains the same. Since the generator speed is proportional to the rotational speed of the turbine rotor, by the gearbox ratio, it is expected that the generator speed will (also) remain the same when pitch failure occurs.

Grd_Prod_Pwr_Avg
The last parameter to monitor the generator is the power output of the generator. Previously, it was explained that when pitch failure occurs, the power output is expected to be lower between the cut-in and rated wind speed and remains the same above rated wind speed.

Appendix C

SCADA-data analysis

C.1 Gearbox parameters

Gear_Oil_TempBasis_Avg
In **section B.1** it was explained that the temperature of the gear oil depends on the amount of heat generated by the bearings and gears. For the bearing it was explained that the heat generation, H, is a function of among others n, which is the rotational speed of the bearings. Based on this, delta T may be plotted against Rtr_RPM_Avg.

Gear_Oil_TempBasis_Avg v.s. Rtr_RPM_Avg
As the gear oil is in contact with the ambient temperature, part of the heat it has absorbed is dissipated to the surroundings, i.e. there is a heat flow from the bearings and gears to the gear oil as well as a heat flow from the gear oil to the surroundings. Therefore, the gear oil temperature must be plotted relative to the ambient temperature, unless this temperature does not fluctuate. From the data it was found that the nacelle temperature does fluctuate. Note that for the gearbox the ambient temperature refers to the nacelle temperature. From the data it was found that the nacelle temperature continuously fluctuates and so the gear oil temperature must be plotted relative to this temperature. As the gear oil temperatures are not expected to change, delta T is expected to be the same compared to the case of no pitch failure.

Figure C.6 shows that for the month December of 2010 and January of 2011 delta T of the failing WT is higher compared to the healthy WT. *This is contradictory to the theory.* The remaining months, however, *do indeed show that delta T for WTA4 overlaps with that of WTA2*.

Based on the above it can be stated that plotting delta T related to the gear oil temperature against the rotor speed does not fully provide insight into pitch failure.

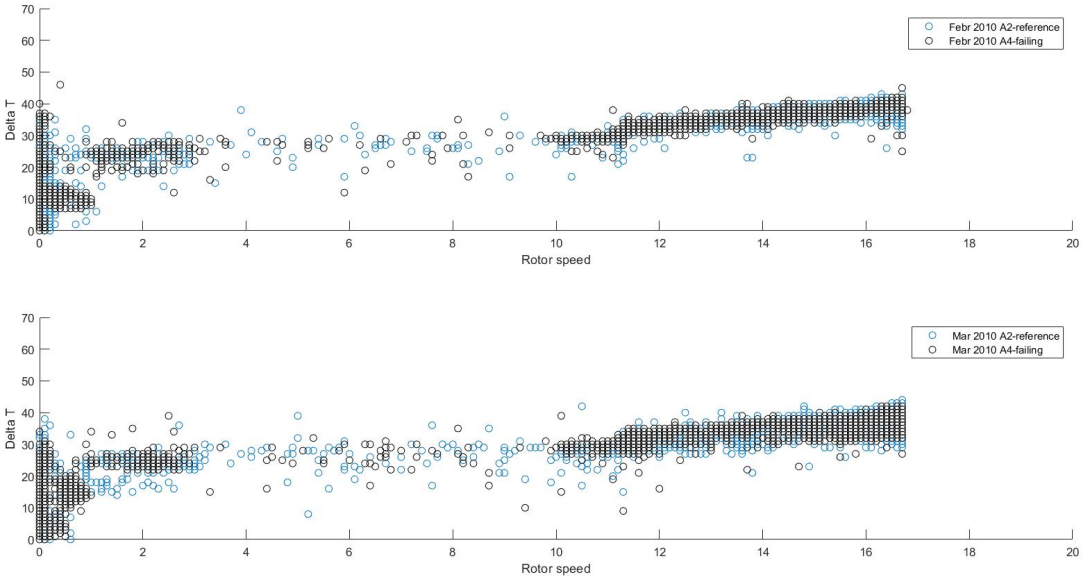

Figure C.1: Comparison of $T_{gear\ oil\ temperature}$ - $T_{nacelle}$ v.s. rotor speed data of WTA4 with the reference WT for the months February 2010 and March 2010.

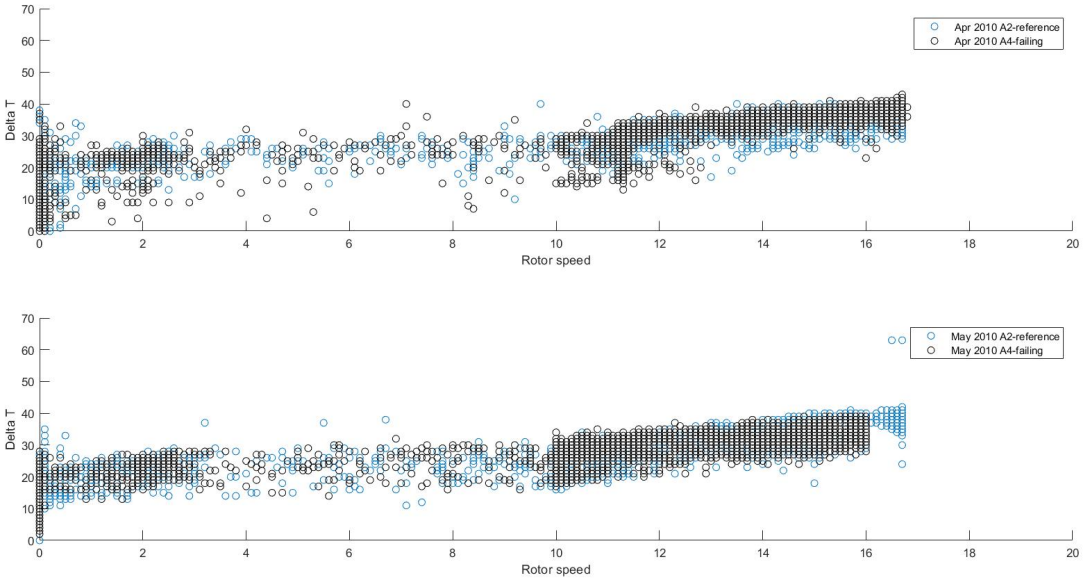

Figure C.2: Comparison of $T_{gear\ oil\ temperature}$ - $T_{nacelle}$ v.s. rotor speed data of WTA4 with the reference WT for the months April 2010 and May 2010.

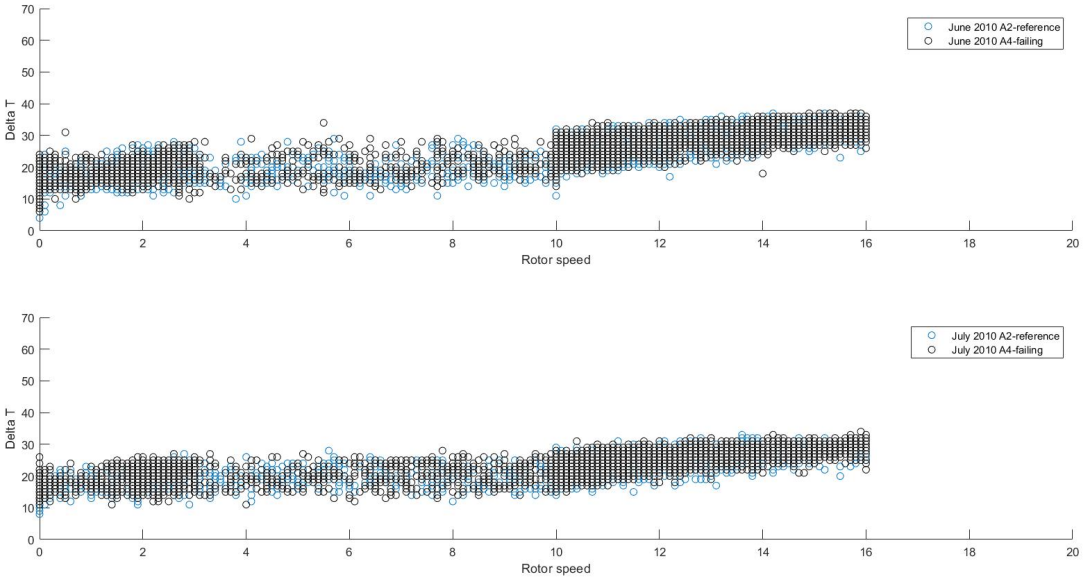

Figure C.3: Comparison of $T_{gear\ oil\ temperature}$ - $T_{nacelle}$ v.s. rotor speed data of WTA4 with the reference WT for the months Juni 2010 and July 2010.

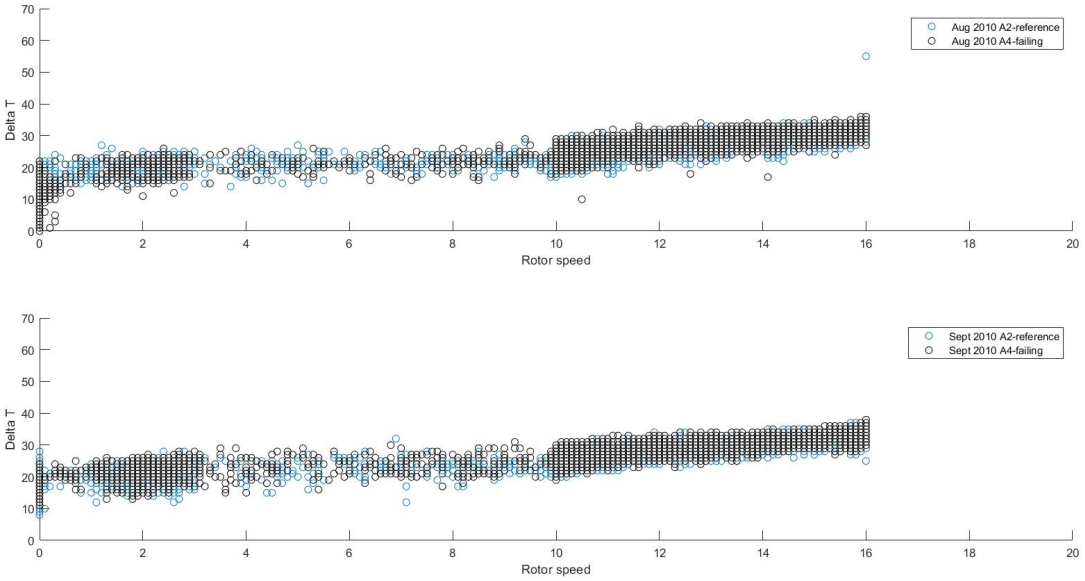

Figure C.4: Comparison of $T_{gear\ oil\ temperature}$ - $T_{nacelle}$ v.s. rotor speed data of WTA4 with the reference WT for the months Augustus 2010 and September 2010.

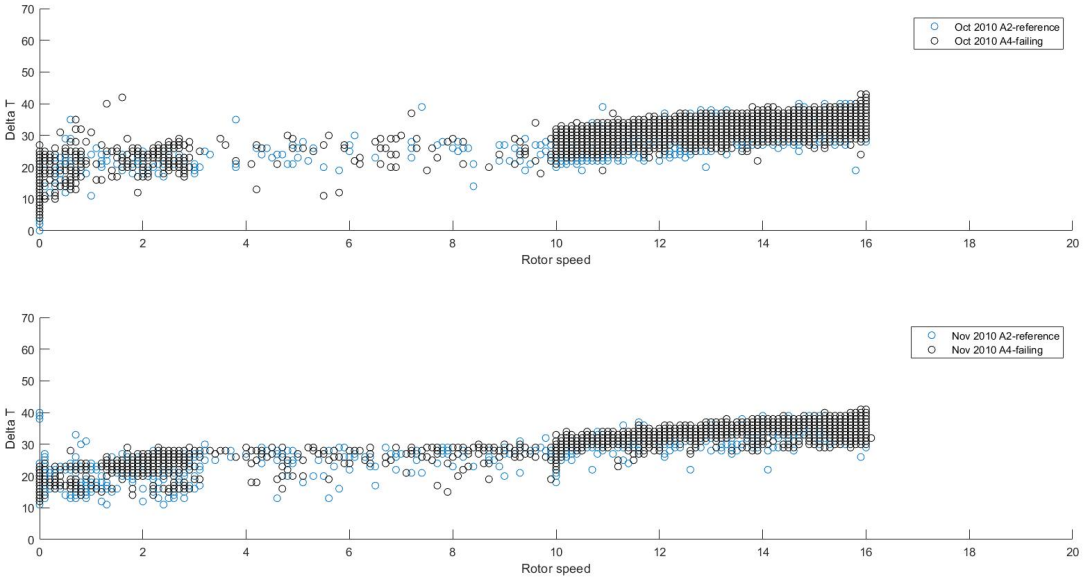

Figure C.5: Comparison of $T_{gear\ oil\ temperature}$ - $T_{nacelle}$ v.s. rotor speed data of WTA4 with the reference WT for the months October 2010 and November 2010.

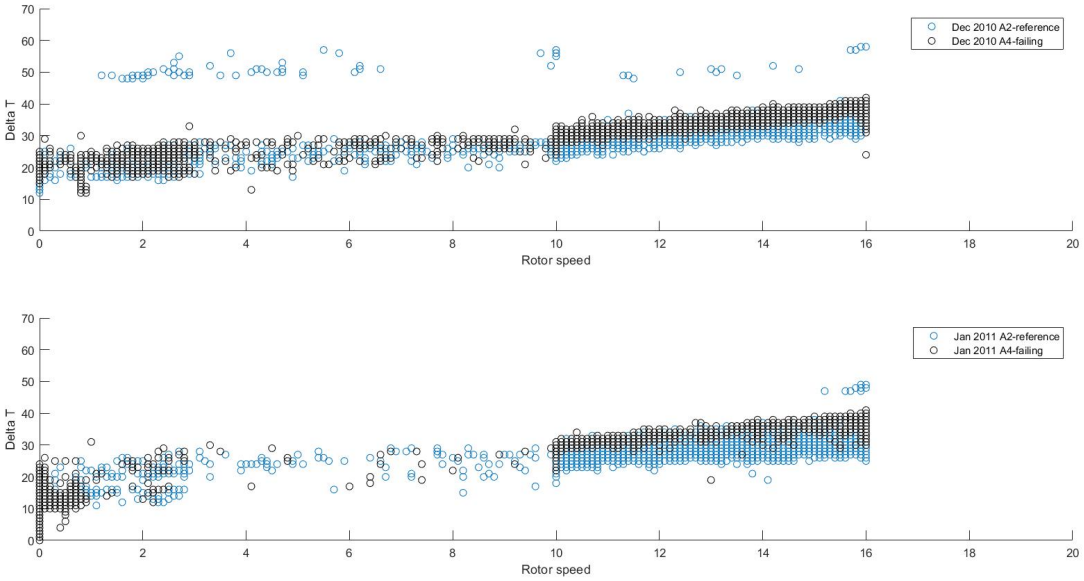

Figure C.6: Comparison of $T_{gear\ oil\ temperature}$ - $T_{nacelle}$ v.s. rotor speed data of WTA4 with the reference WT for the months December 2010 and January 2011.

Gear_Oil_TempBasis_Avg v.s. Grd_Prod_Pwr_Avg

Above delta T of Gear_Oil_TempBasis_Avg was plotted against Rtr_RPM_Avg based on **equation 4.5**. This equation also shows that Gear_Oil_TempBasis_Avg can be plotted against Grd_Prod_Pwr_Avg,

as $n \cdot M$ is equal to the transmitted power. In this regard it is expected that for the same power output, delta T will be the same for WTA4 compared to the reference WT.

In March of 2010 *delta T of WTA4 seems to be lower compared to the reference WT.* In the data it was found that for WTA4 454 data points were measured less and so this could a possible explanation for the "lower" delta T. In the months December and January, however, it was found that delta T of WTA4 was *higher* relative to WTA2. It was first checked whether WTA4 had less data points compared to WTA2 and the difference was only about 20 data points for the month January. *It can thus be concluded that delta T is indeed higher for WTA4. This is in agreement with the theory, as the gearbox bearing loads increase due to pitch failure.* For the remaining months, *delta T of WTA4 overlaps with that of WTA2 - which is also in agreement with the theory.*

Based on the above observations it can be stated that plotting delta T related to the gear oil temperature against the power output, to some extent provides insight into pitch failure (since delta T may remain constant even in the case of pitch failure).

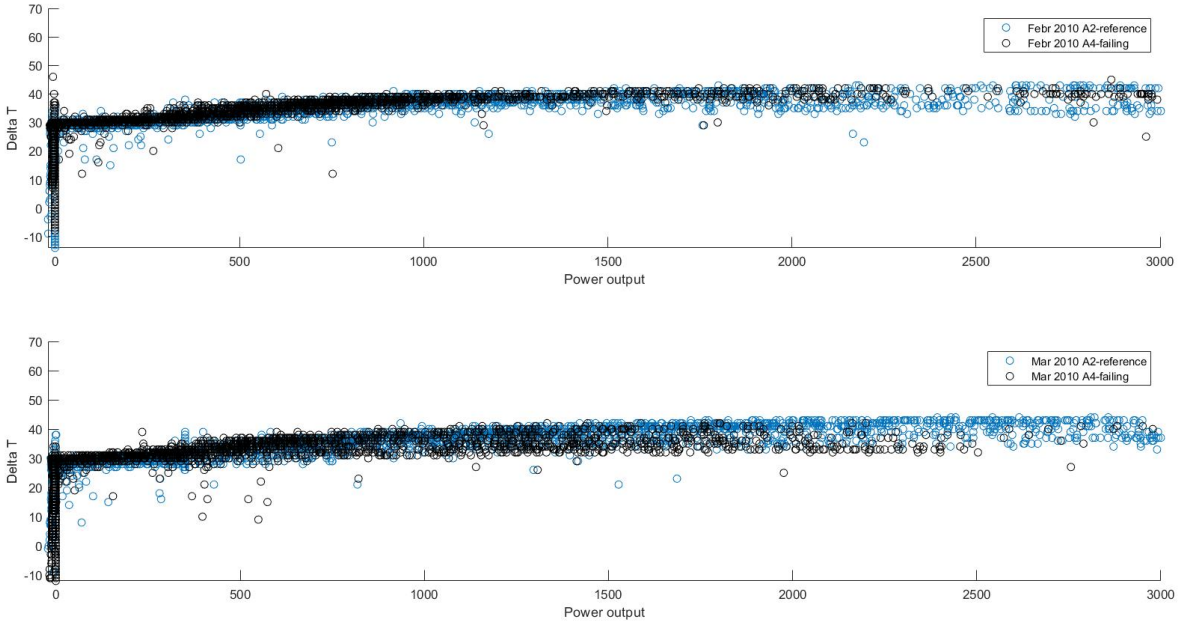

Figure C.7: Comparison of $T_{gear\ oil\ temperature}$ - $T_{nacelle}$ v.s. power output data of WTA4 with the reference WT for the months February 2010 and March 2010.

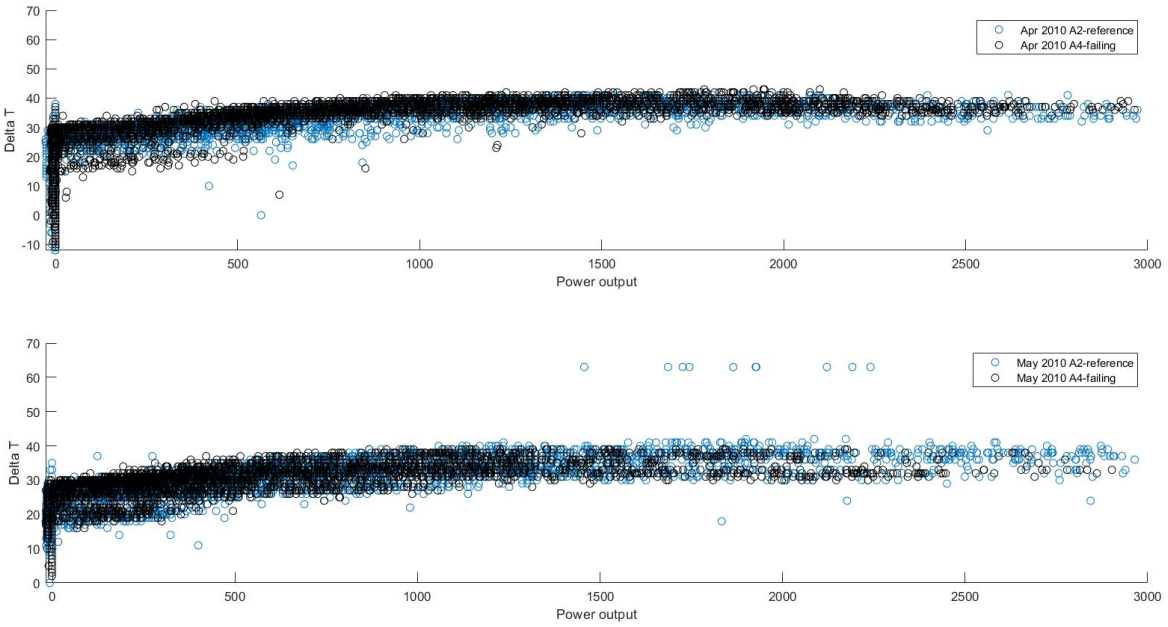

Figure C.8: Comparison of $T_{gear\ oil\ temperature}$ - $T_{nacelle}$ v.s. power output data of WTA4 with the reference WT for the months April 2010 and May 2010.

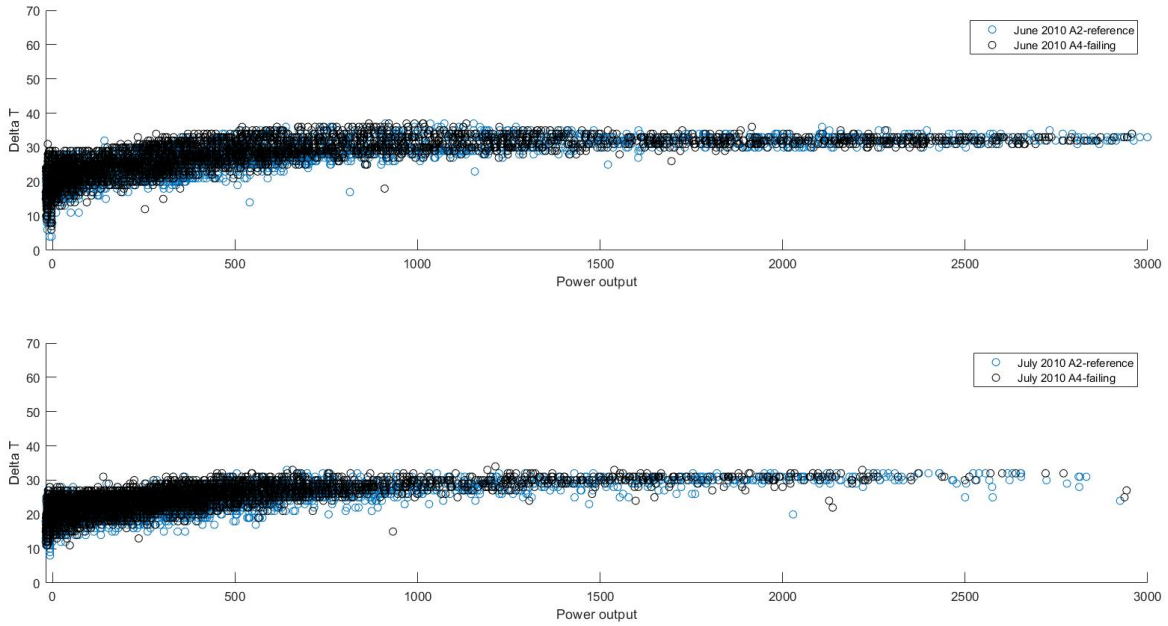

Figure C.9: Comparison of $T_{gear\ oil\ temperature}$ - $T_{nacelle}$ v.s. power output data of WTA4 with the reference WT for the months June 2010 and July 2010.

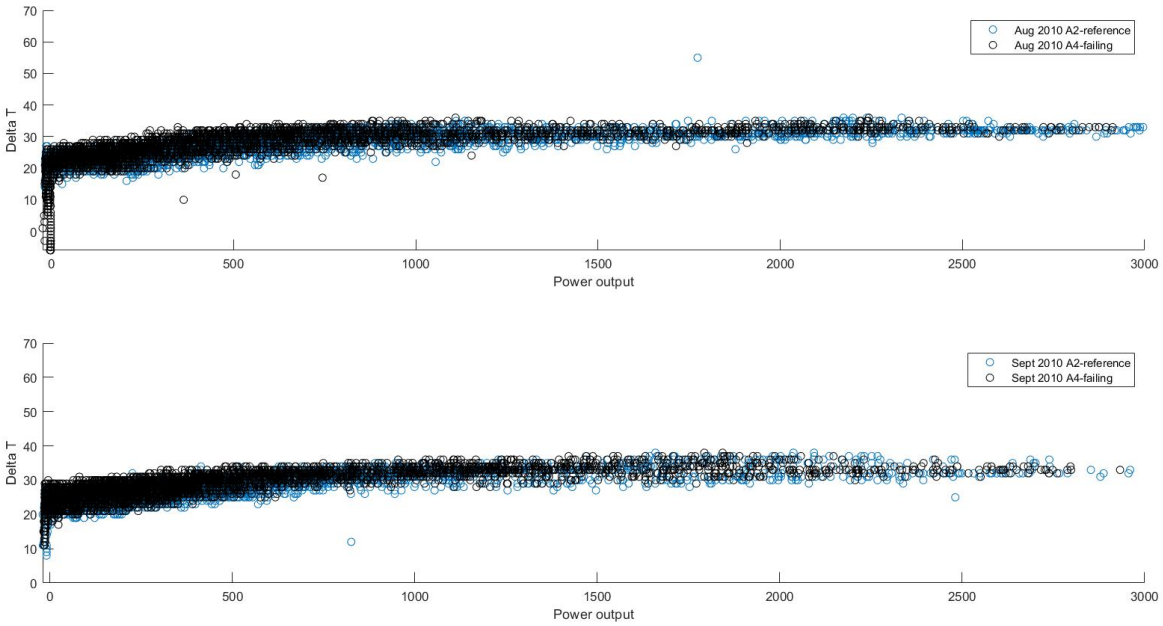

Figure C.10: Comparison of $T_{gear\ oil\ temperature}$ - $T_{nacelle}$ v.s. power output data of WTA4 with the reference WT for the months August 2010 and September 2010.

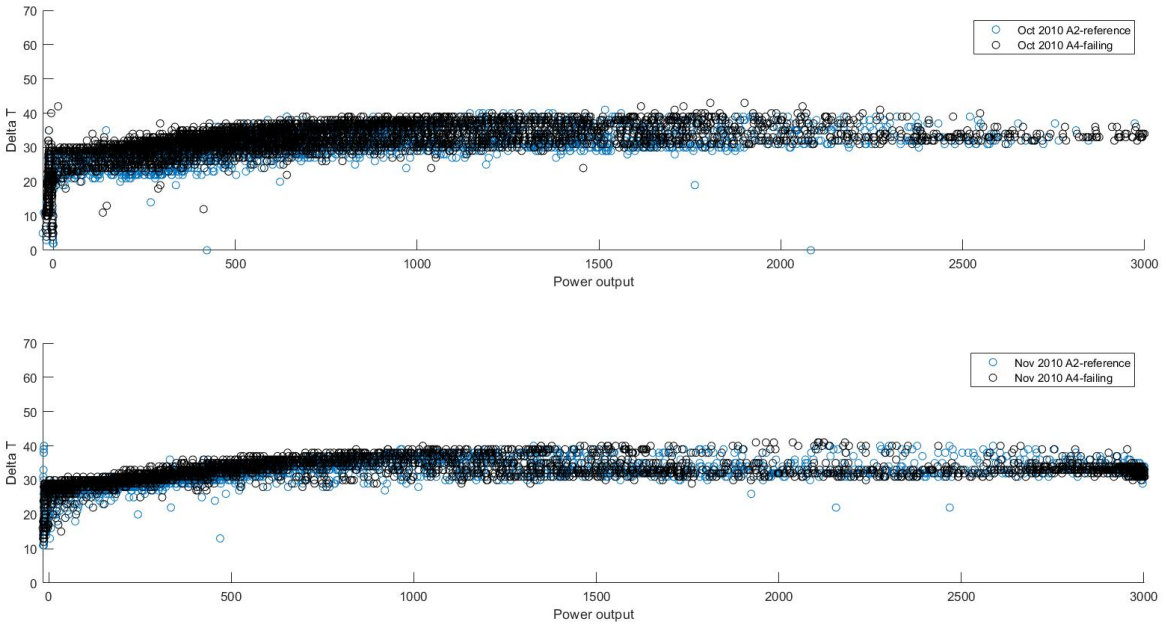

Figure C.11: Comparison of $T_{gear\ oil\ temperature}$ - $T_{nacelle}$ v.s. power output data of WTA4 with the reference WT for the months October 2010 and November 2010.

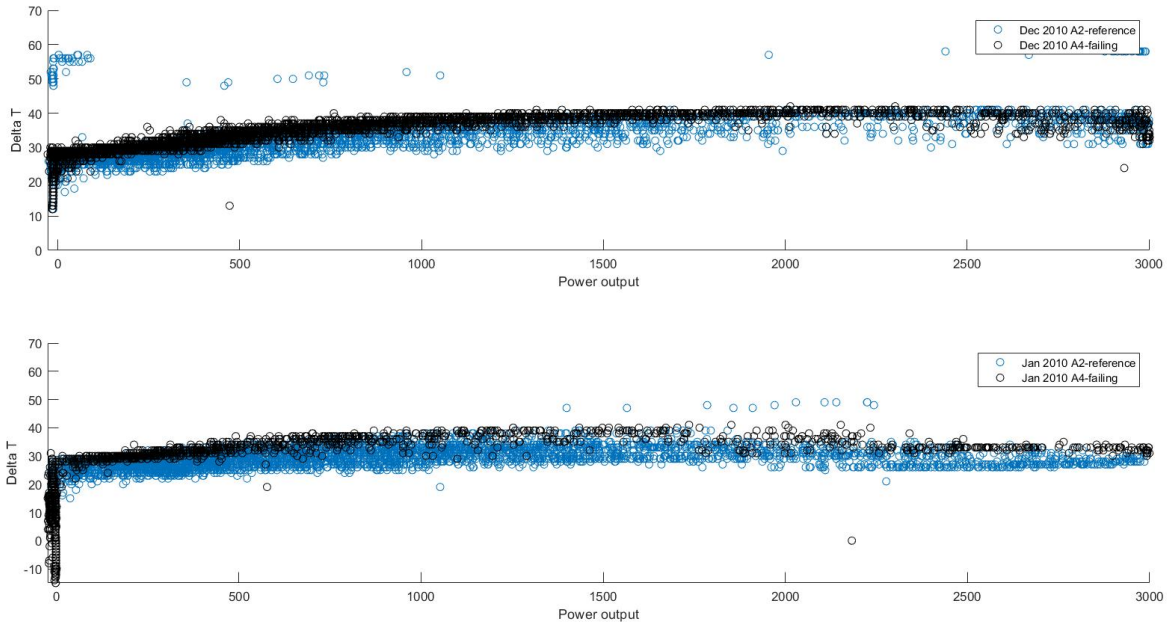

Figure C.12: Comparison of $T_{gear\ oil\ temperature}$ - $T_{nacelle}$ v.s. power output data of WTA4 with the reference WT for the months December 2010 and January 2011.

C.2 Generator parameters

Gen_Bear_Temp_Avg, Gen_Bear2_Temp_Avg
In **section B.2** it was explained that when pitch failure occurs the bearing reaction forces are expected to increase, which results in more heat generation H. Recall that H depends on n, the rotational speed of the bearing, and M, the frictional torque. This torque is a function of among others the applied load on the bearing. For the generator bearing this load fundamentally depends on ϕ and so Gen_Bear_Temp_Avg and Gen_Bear2_Temp_Avg are studied against Blds_PitchAngle_Avg. A remark in this regard is that as generally bearing temperatures are affected by the ambient temperature, the measured generator bearing temperatures must be plotted relative to the nacelle temperature.

Gen_Bear_Temp_Avg, Gen_Bear2_Temp_Avg v.s. Blds_PitchAngle_Avg
Given the above, it is expected that for the same average blade pitch angle delta T for WTA4 is higher than for WTA2. **Figures C.13 - C.18** are delta T v.s. Blds_PitchAngle_Avg graphs for generator bearing 1. From these graphs it can be seen that for the months May - December of 2010 delta T of WTA4 is *higher* compared to WTA2. *This is in agreement with theory.* For the remaining months the data points do not show a clear trend and so it is difficult to see deviations and make interpretations.

The delta T v.s. Blds_PitchAngle_Avg graphs for generator bearing 2 are presented in **Figures C.19 - C.24**. From these graphs it was found that for the months March, May, June, July August and December of 2010 delta T for WTA4 lies *lower* compared to WTA2. *This is in agreement with the expectations for pitch failure.* For the remaining months, the data more or less shows an overlaps. *This is also in agreement with the theory.*

Based on the above it can be stated that plotting delta T related to the temperature of generator bearing 1 and generator bearing 2 against the average blade pitch angle does not fully provide insight into pitch failure.

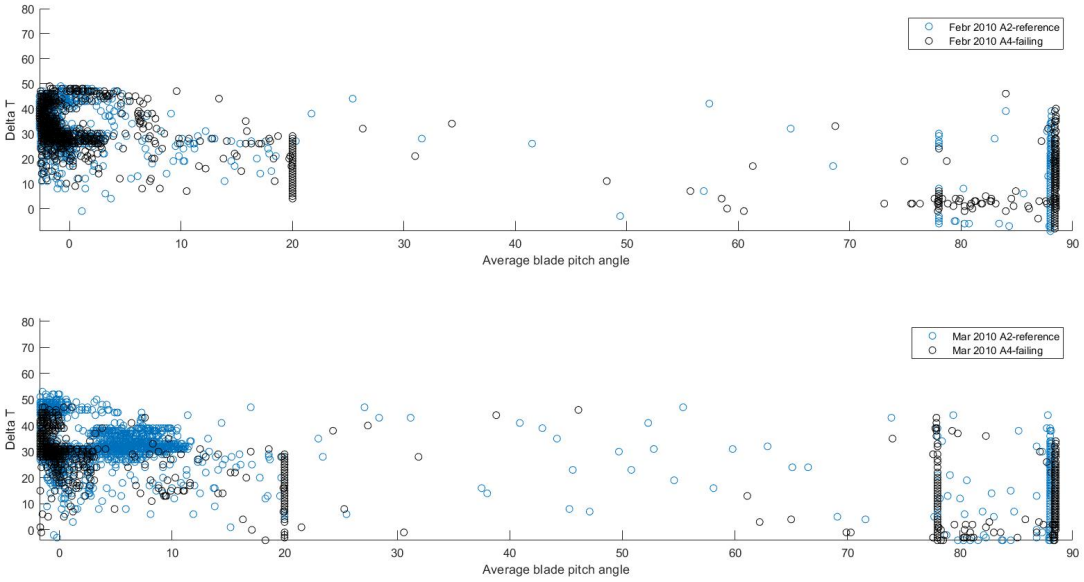

Figure C.13: Comparison of $T_{generator\ bearing\ 1\ temperature}$ - $T_{nacelle}$ v.s. average blade pitch angle data of WTA4 with the reference WT for the months February 2010 and March 2010.

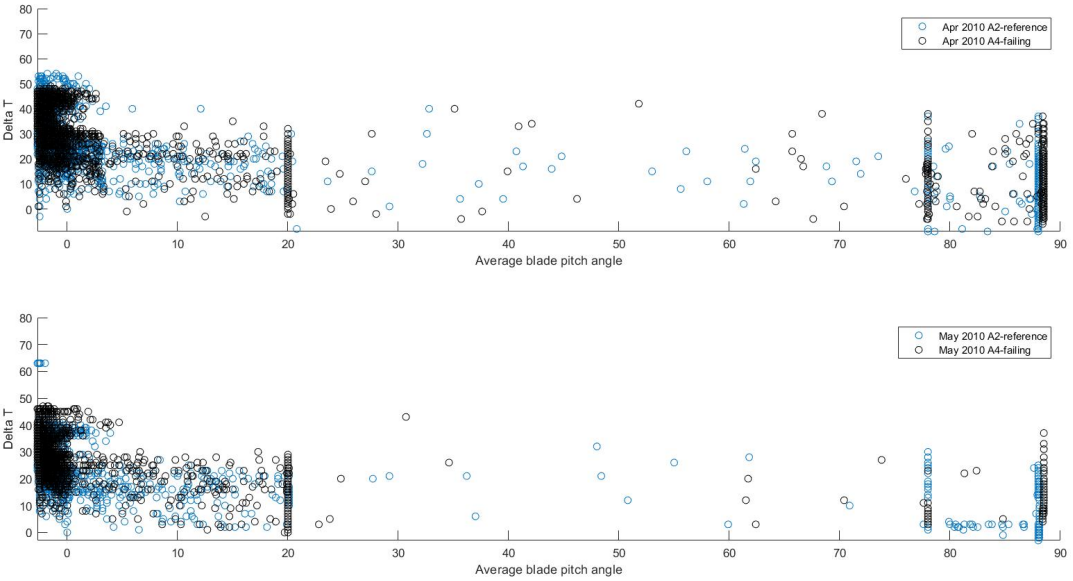

Figure C.14: Comparison of $T_{generator\ bearing\ 1\ temperature}$ - $T_{nacelle}$ v.s. average blade pitch angle data of WTA4 with the reference WT for the months April 2010 and May 2010.

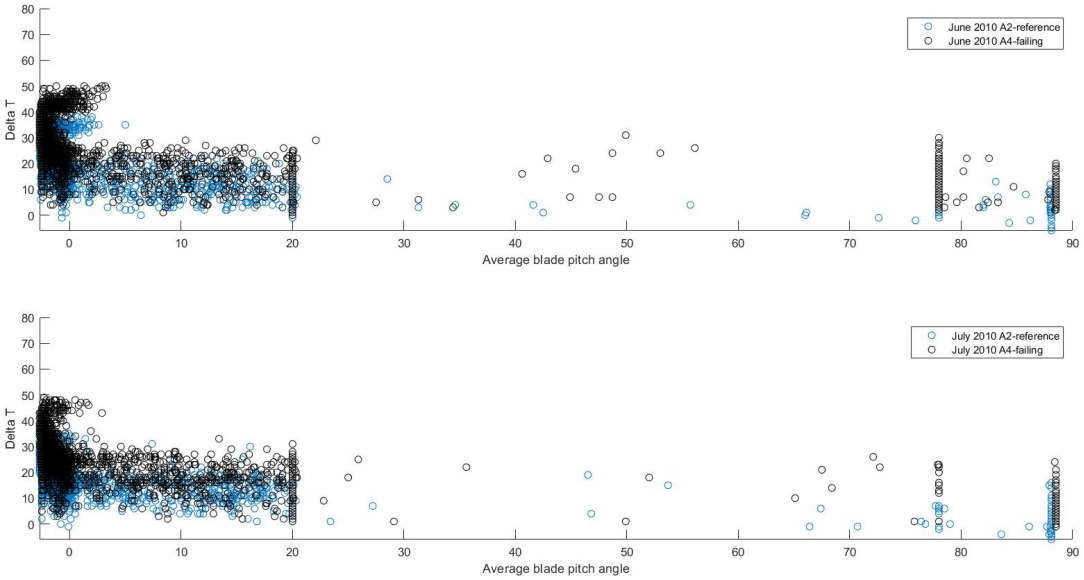

Figure C.15: Comparison of $T_{generator\ bearing\ 1\ temperature}$ - $T_{nacelle}$ v.s. average blade pitch angle data of WTA4 with the reference WT for the months June 2010 and July 2010.

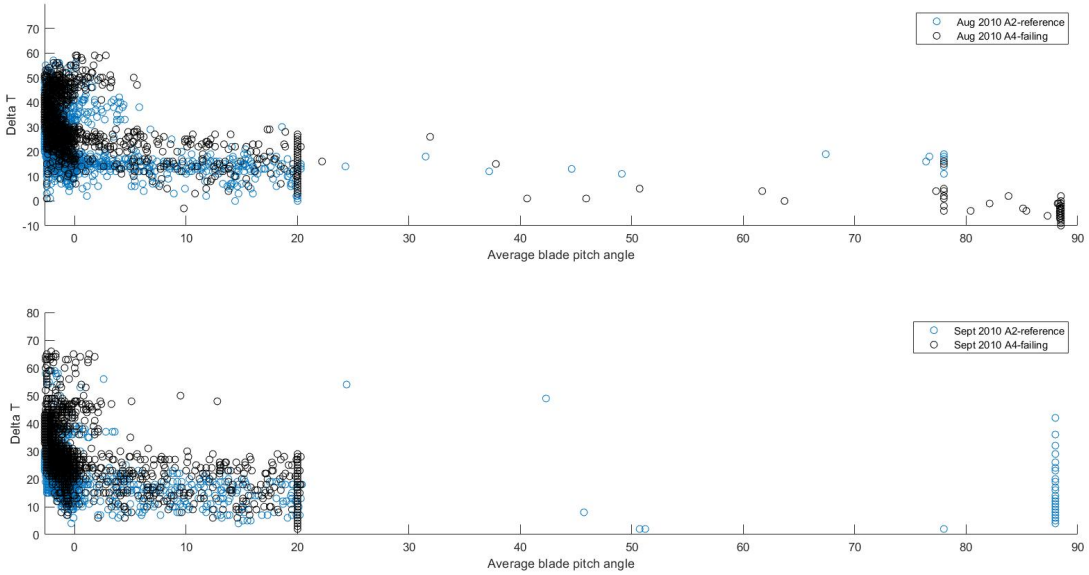

Figure C.16: Comparison of $T_{generator\ bearing\ 1\ temperature}$ - $T_{nacelle}$ v.s. average blade pitch angle data of WTA4 with the reference WT for the months August 2010 and September 2010.

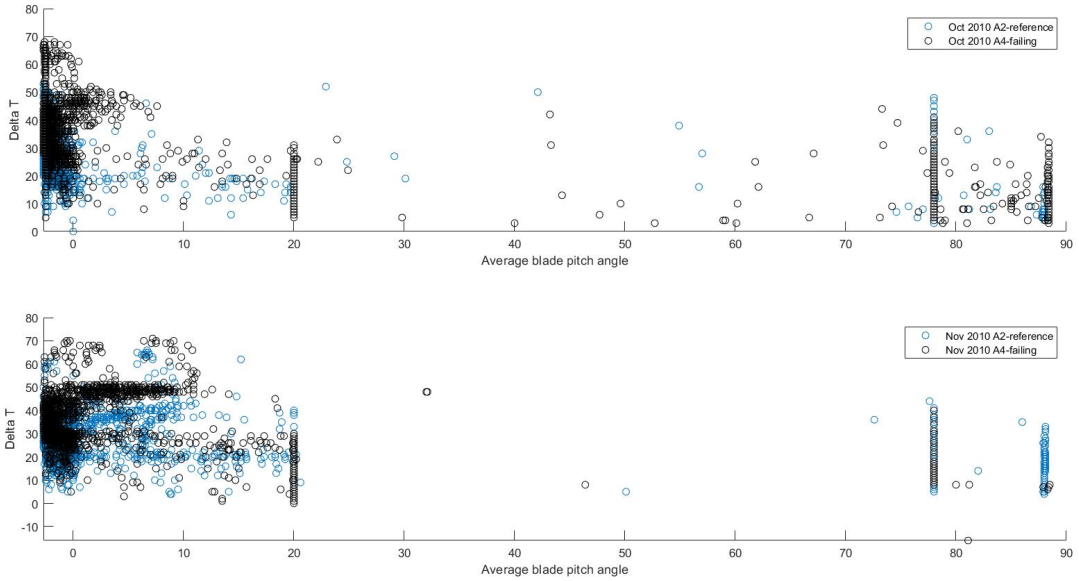

Figure C.17: Comparison of $T_{generator\ bearing\ 1\ temperature}$ - $T_{nacelle}$ v.s. average blade pitch angle data of WTA4 with the reference WT for the months October 2010 and November 2010.

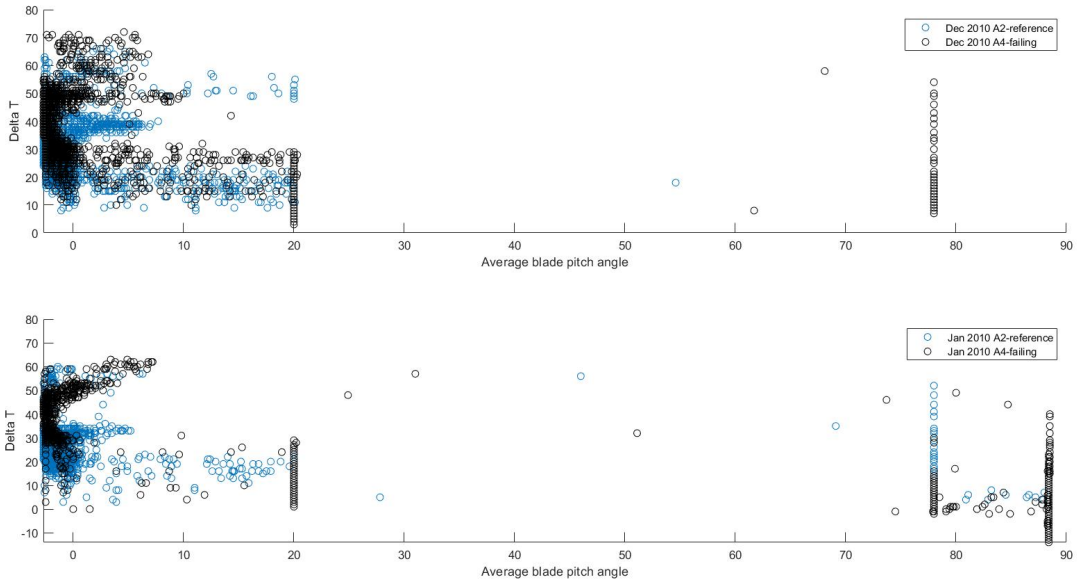

Figure C.18: Comparison of $T_{generator\ bearing\ 1\ temperature}$ - $T_{nacelle}$ v.s. average blade pitch angle data of WTA4 with the reference WT for the months December 2010 and January 2011.

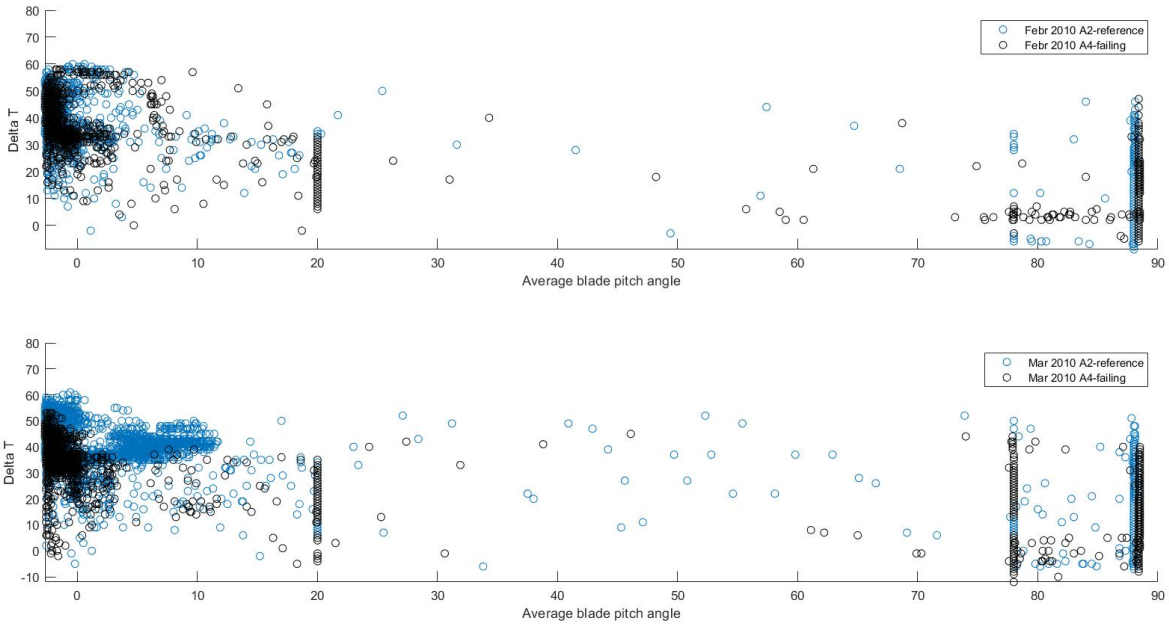

Figure C.19: Comparison of $T_{generator\ bearing\ 2\ temperature}$ - $T_{nacelle}$ v.s. power output data of WTA4 with the reference WT for the months February 2010 and March 2010.

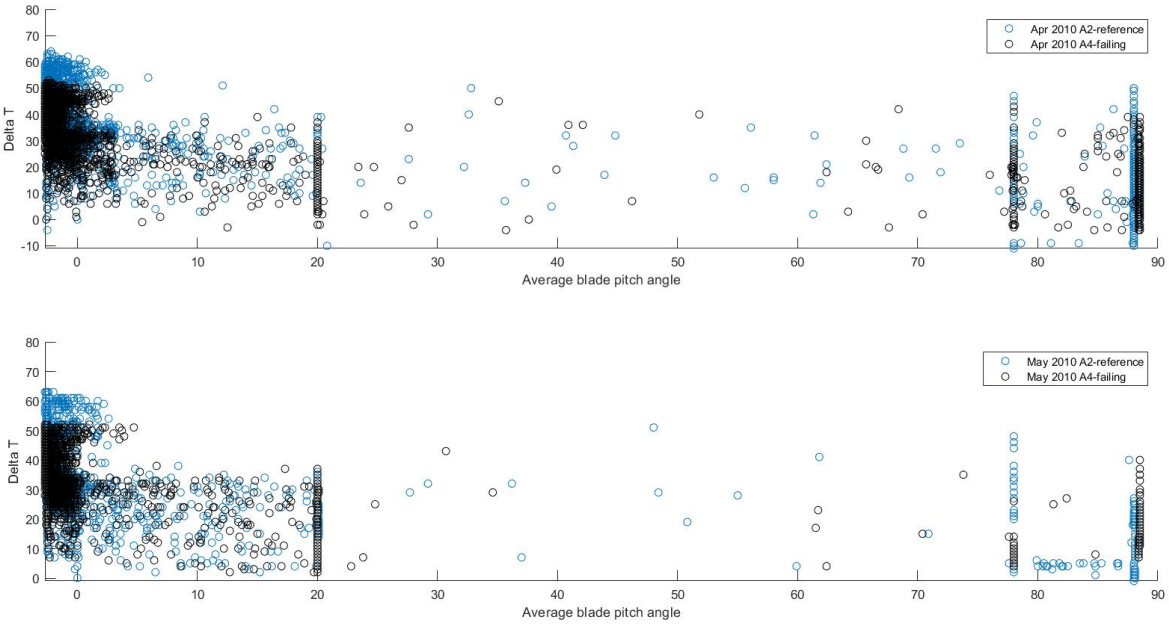

Figure C.20: Comparison of $T_{generator\ bearing\ 2\ temperature}$ - $T_{nacelle}$ v.s. power output data of WTA4 with the reference WT for the months April 2010 and May 2010.

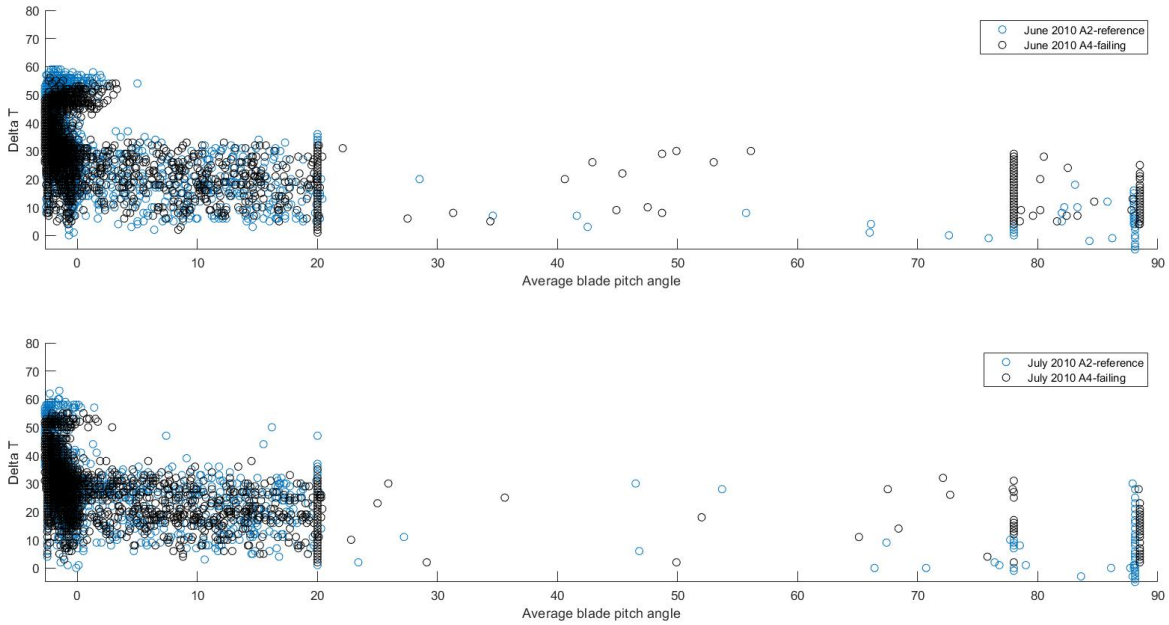

Figure C.21: Comparison of $T_{generator\ bearing\ 2\ temperature}$ - $T_{nacelle}$ v.s. power output data of WTA4 with the reference WT for the months June 2010 and July 2010.

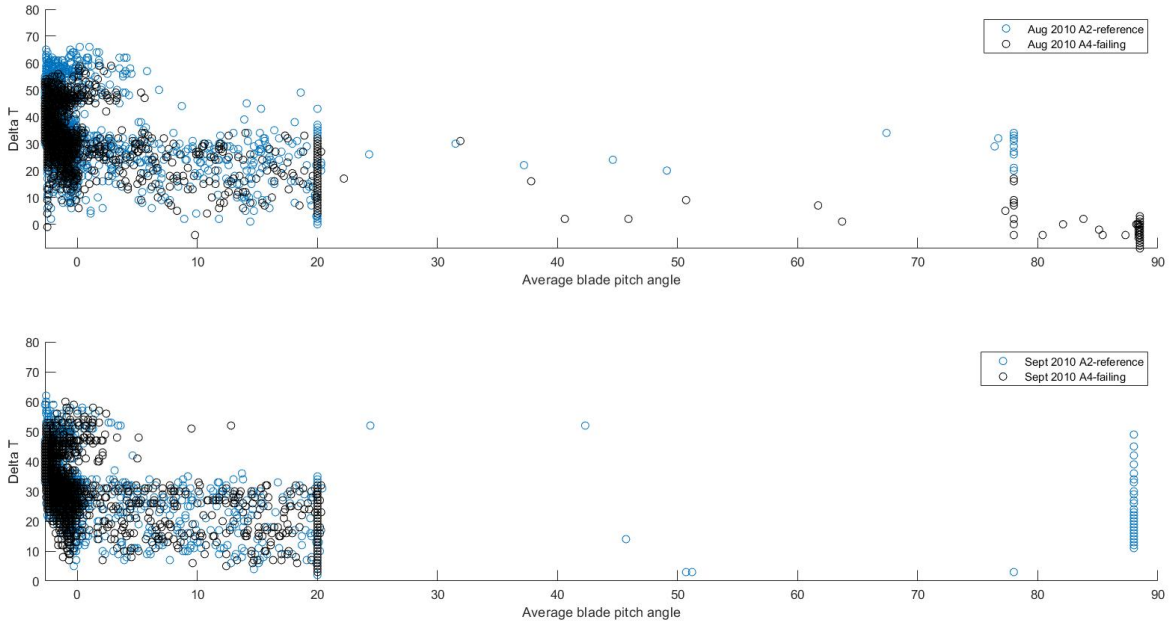

Figure C.22: Comparison of $T_{generator\ bearing\ 2\ temperature}$ - $T_{nacelle}$ v.s. power output data of WTA4 with the reference WT for the months Augustus 2010 and September 2010.

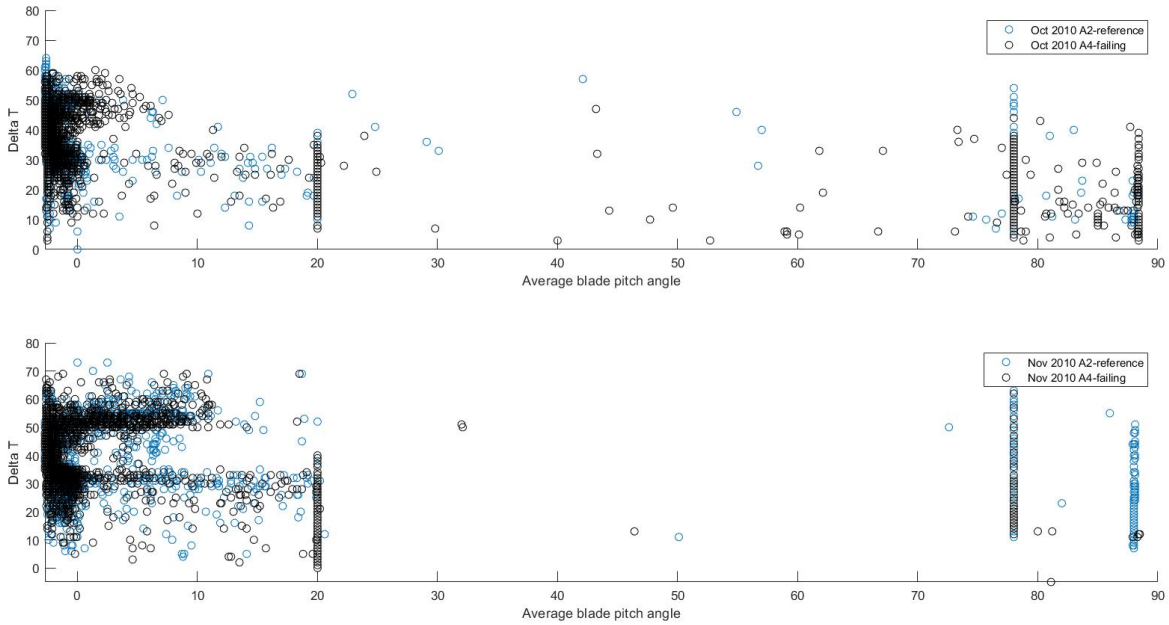

Figure C.23: Comparison of $T_{generator\ bearing\ 2\ temperature}$ - $T_{nacelle}$ v.s. power output data of WTA4 with the reference WT for the months October 2010 and November 2010.

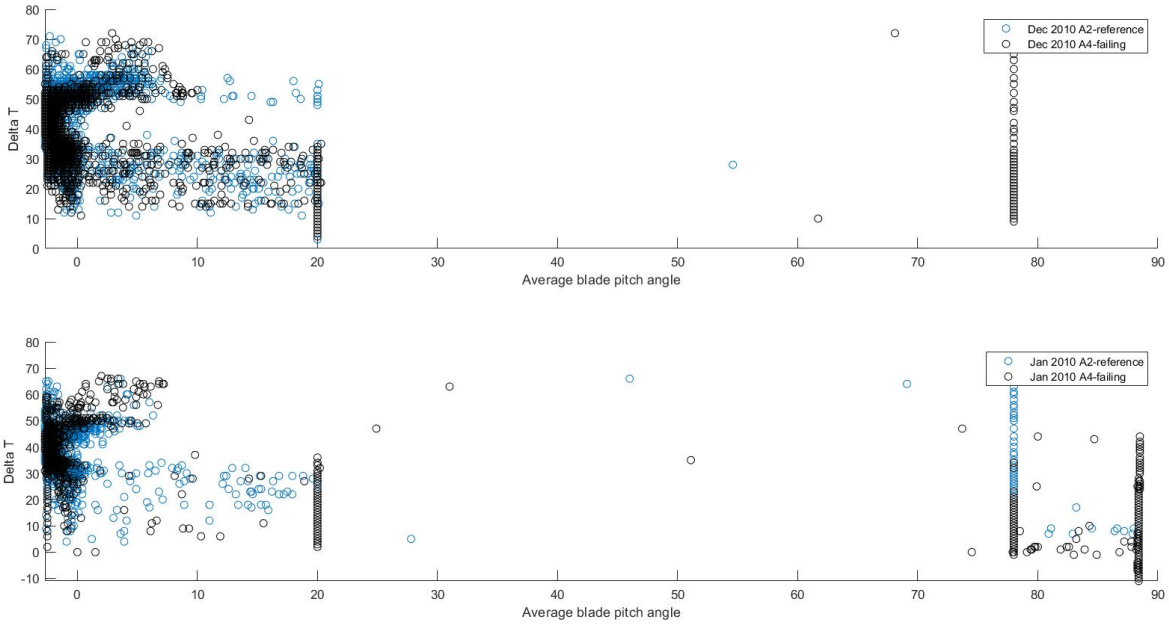

Figure C.24: Comparison of $T_{generator\ bearing\ 2\ temperature}$ - $T_{nacelle}$ v.s. power output data of WTA4 with the reference WT for the months December 2010 and January 2011.

Gen_Bear_Temp_Avg, Gen_Bear2_Temp_Avg v.s. Grd_Prod_Pwr_Avg
Figure C.25 - C.36 show the Gen_Bear_Temp_Avg v.s. Grd_Prod_Pwr_Avg and Gen_Bear2_Temp_Avg v.s. Grd_Prod_Pwr_Avg graphs for the complete study period. A discussion on these graphs is found in **section 4.5**.

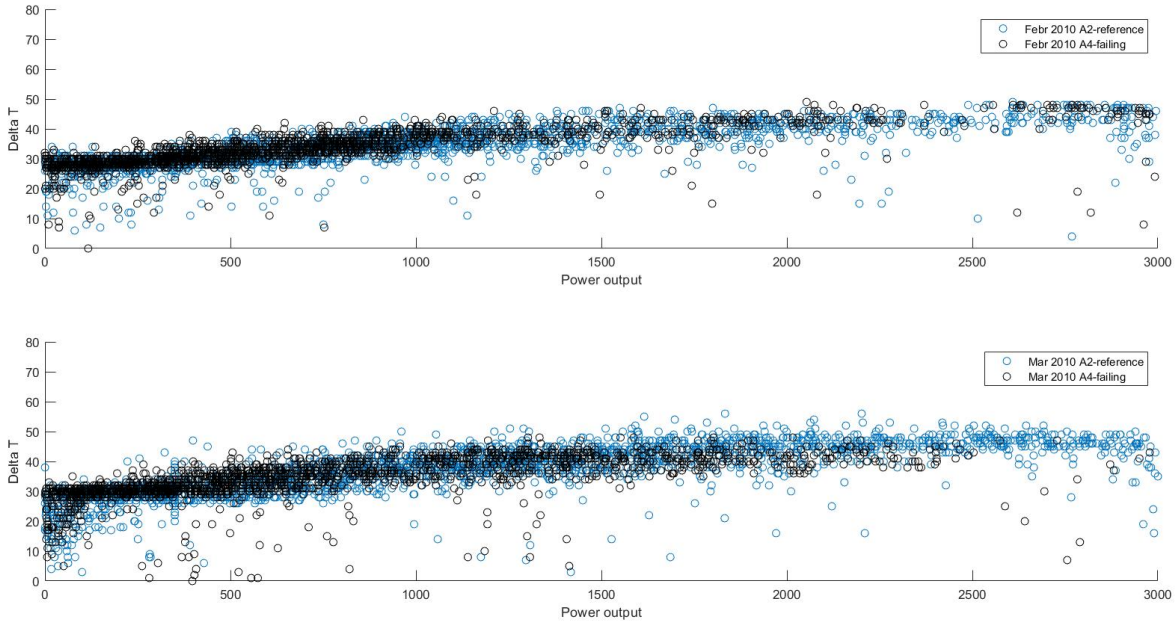

Figure C.25: Comparison of $T_{temperature\ generator\ bearing\ 1}$ - $T_{nacelle}$ v.s. power output data of WTA4 with the reference WT for the months February 2010 and March 2010.

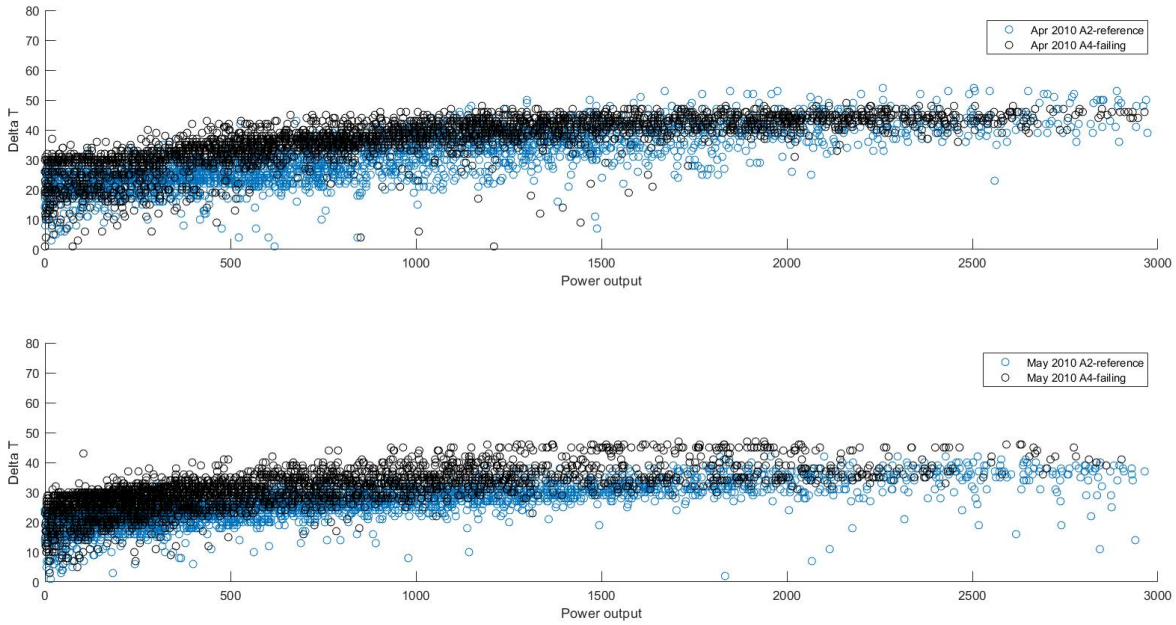

Figure C.26: Comparison of $T_{temperature\ generator\ bearing\ 1}$ - $T_{nacelle}$ v.s. power output data of WTA4 with the reference WT for the months April 2010 and May 2010.

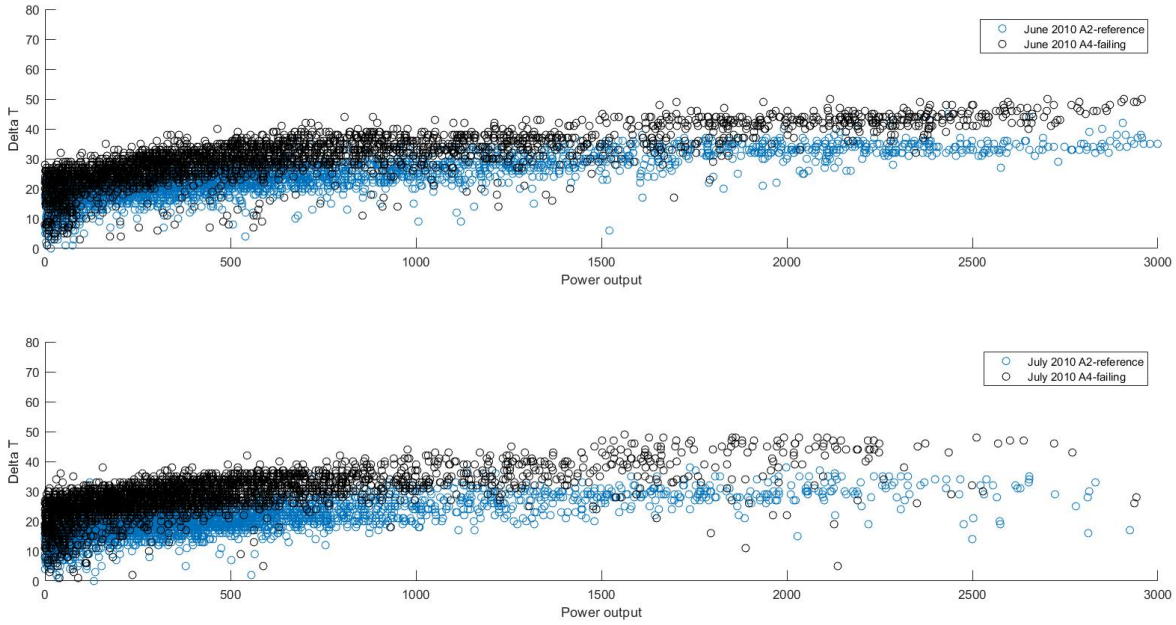

Figure C.27: Comparison of $T_{temperature\ generator\ bearing\ 1}$ - $T_{nacelle}$ v.s. power output data of WTA4 with the reference WT for the months June 2010 and July 2010.

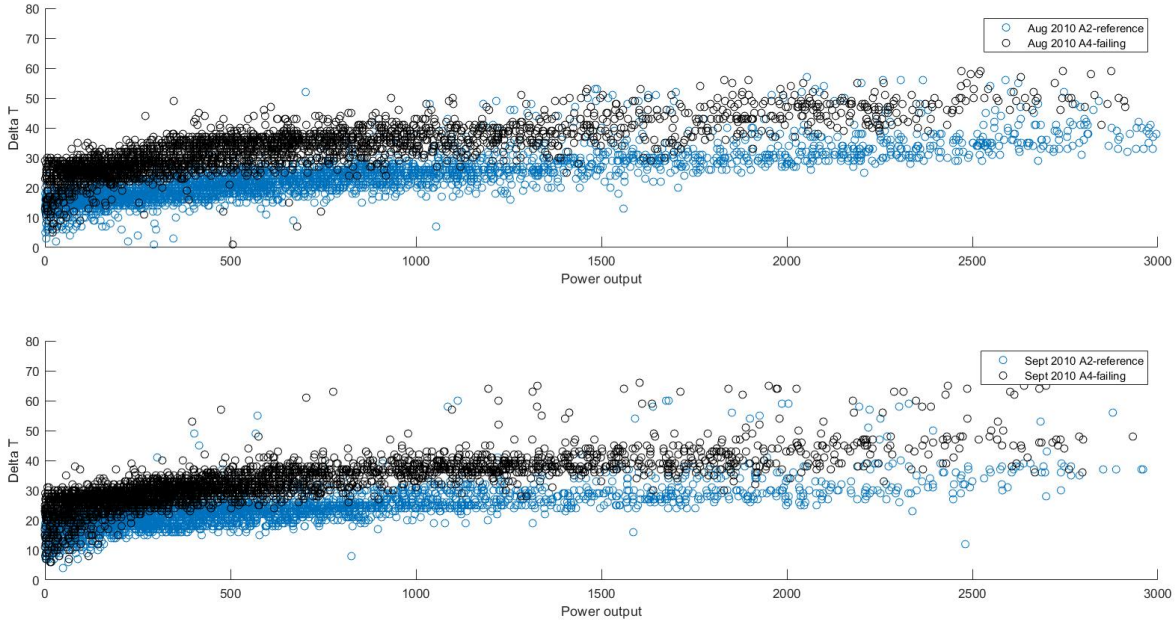

Figure C.28: Comparison of $T_{temperature\ generator\ bearing\ 1}$ - $T_{nacelle}$ v.s. power output data of WTA4 with the reference WT for the months August 2010 and September 2010.

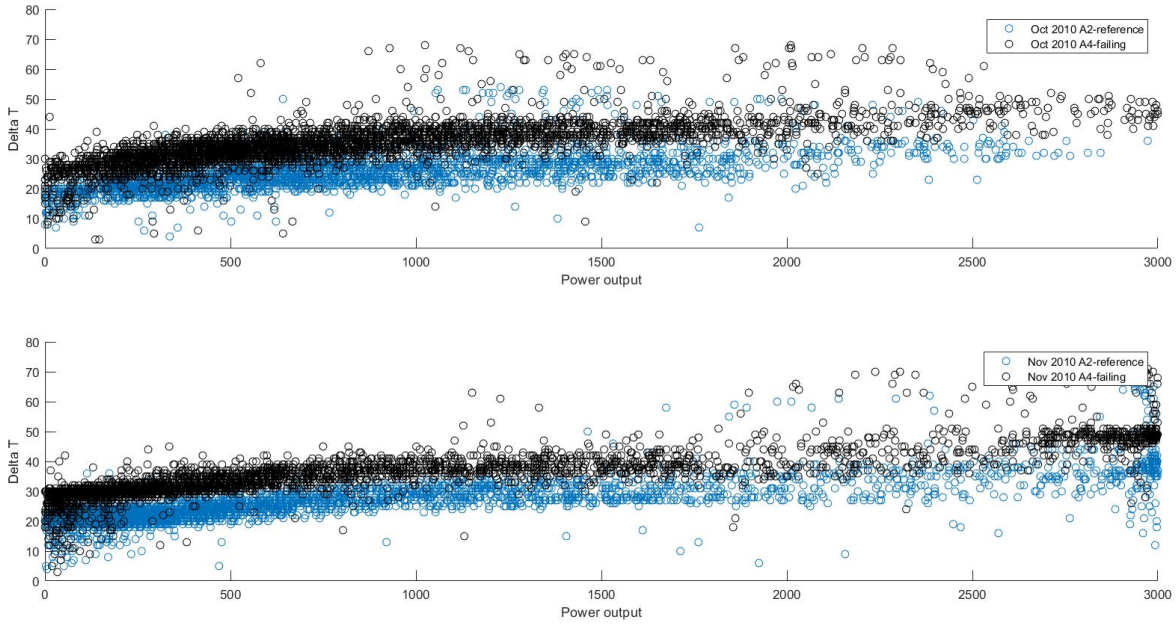

Figure C.29: Comparison of $T_{temperature\ generator\ bearing\ 1}$ - $T_{nacelle}$ v.s. power output data of WTA4 with the reference WT for the months October 2010 and November 2010.

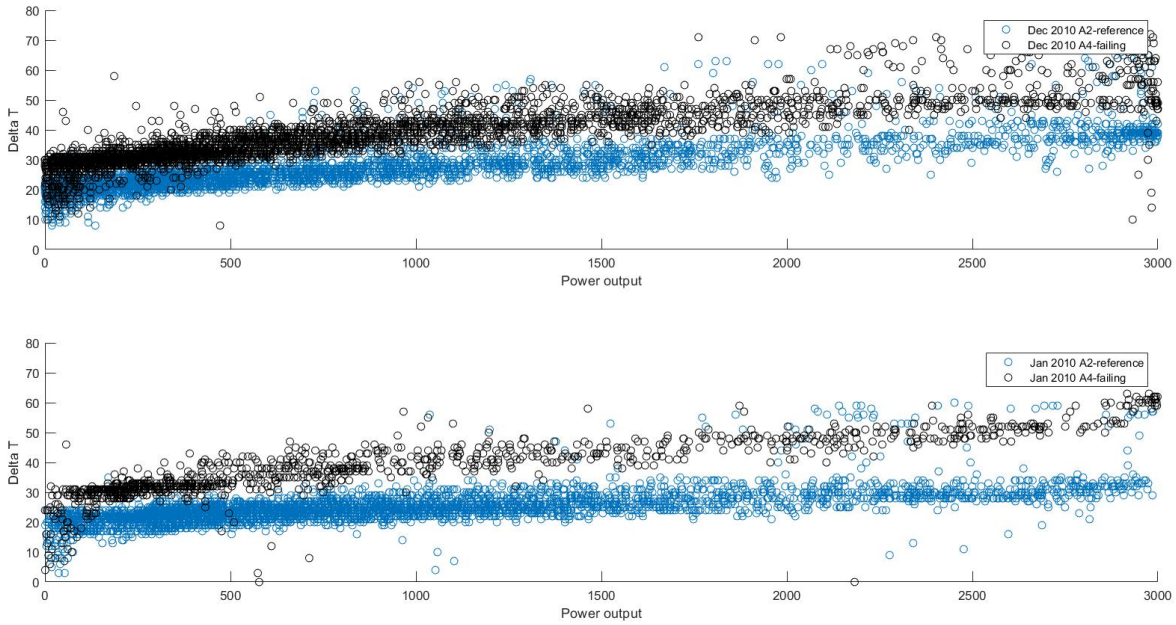

Figure C.30: Comparison of $T_{temperature\ generator\ bearing\ 1}$ - $T_{nacelle}$ v.s. power output data of WTA4 with the reference WT for the months December 2010 and January 2011.

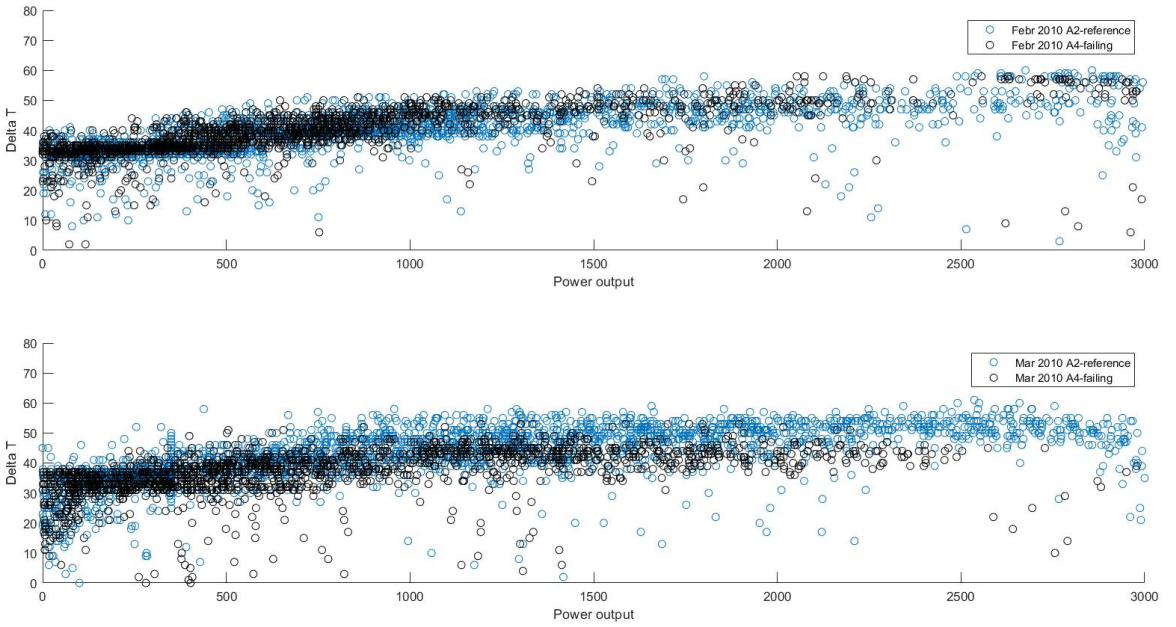

Figure C.31: Comparison of $T_{generator\ bearing\ 2\ temperature}$ - $T_{nacelle}$ v.s. power output data of WTA4 with the reference WT for the months February 2010 and March 2010.

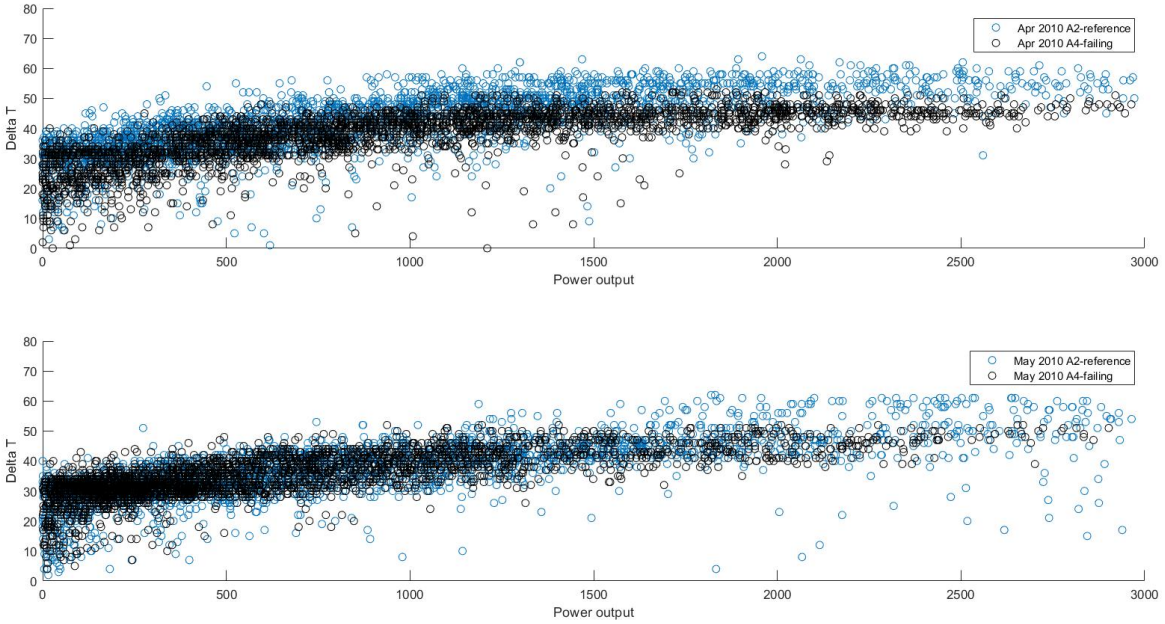

Figure C.32: Comparison of $T_{generator\ bearing\ 2\ temperature}$ - $T_{nacelle}$ v.s. power output data of WTA4 with the reference WT for the months April 2010 and May 2010.

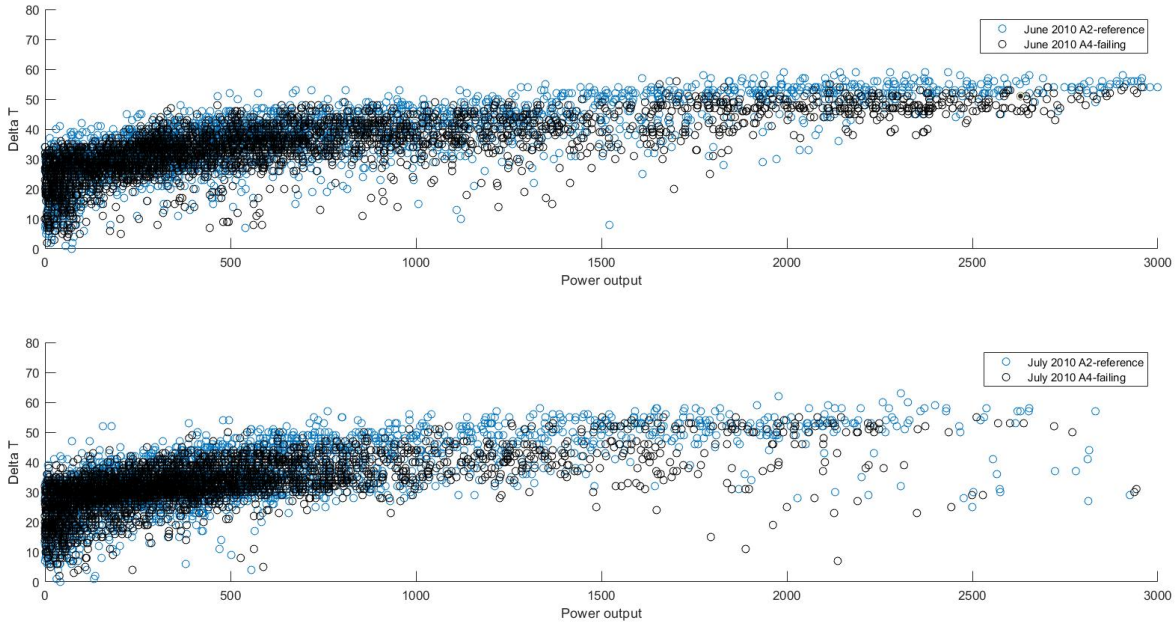

Figure C.33: Comparison of $T_{generator\ bearing\ 2\ temperature}$ - $T_{nacelle}$ v.s. power output data of WTA4 with the reference WT for the months June 2010 and July 2010.

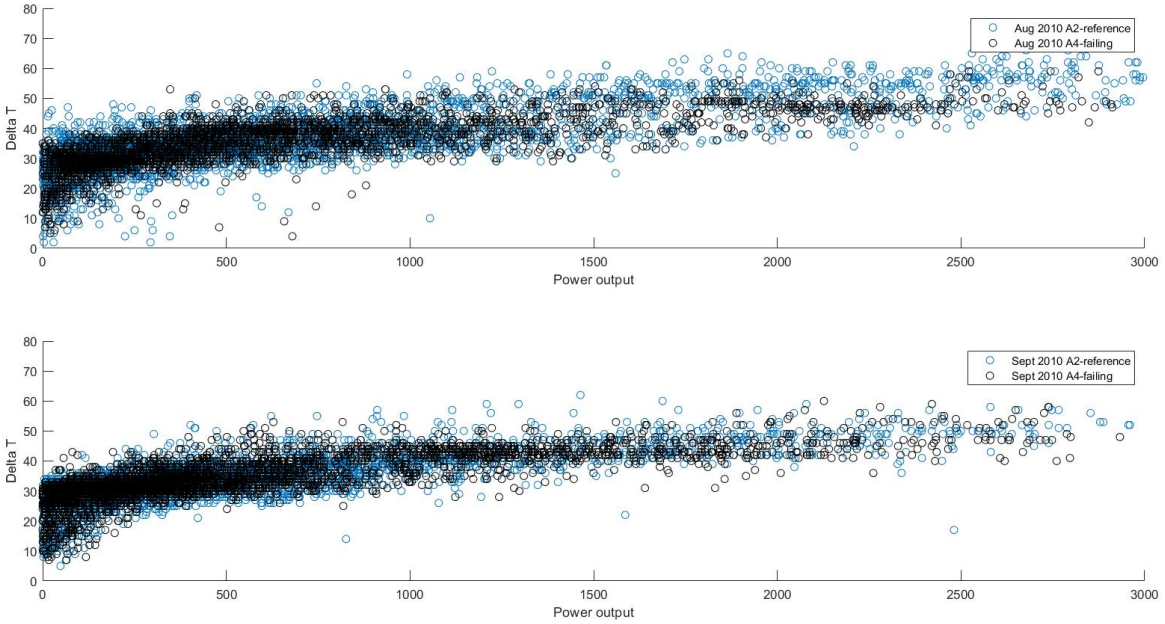

Figure C.34: Comparison of $T_{generator\ bearing\ 2\ temperature}$ - $T_{nacelle}$ v.s. power output data of WTA4 with the reference WT for the months Augustus 2010 and September 2010.

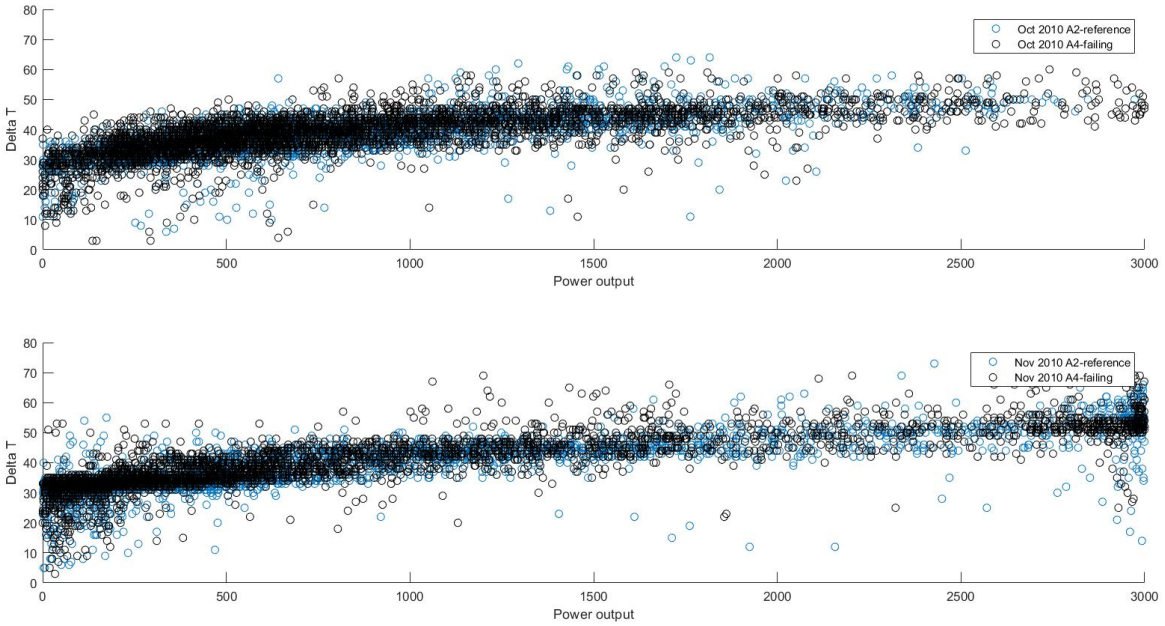

Figure C.35: Comparison of $T_{generator\ bearing\ 2\ temperature}$ - $T_{nacelle}$ v.s. power output data of WTA4 with the reference WT for the months October 2010 and November 2010.

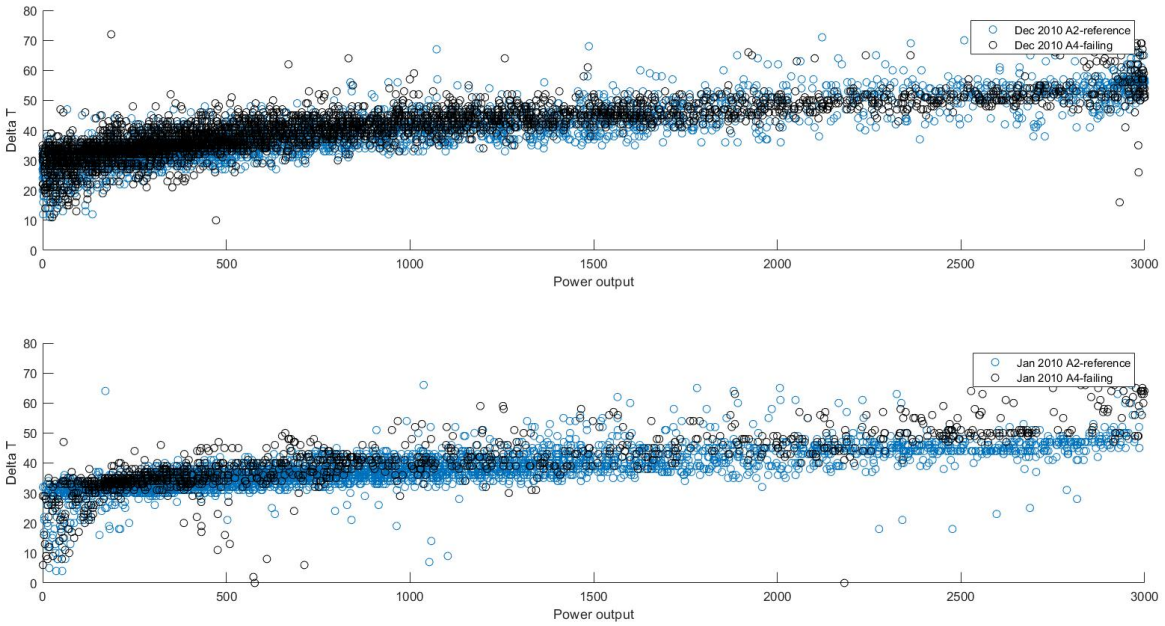

Figure C.36: Comparison of $T_{generator\ bearing\ 2\ temperature}$ - $T_{nacelle}$ v.s. power output data of WTA4 with the reference WT for the months December 2010 and January 2011.

Grd_Pwr_Avg v.s. Blds_PitchAngle_Avg

Figure C.37 - C.42 show the Grd_Prod_Pwr_Avg v.s. Blds_PitchAngle_Avg graphs for the complete study period. A discussion on these graphs is found in **section 4.5**.

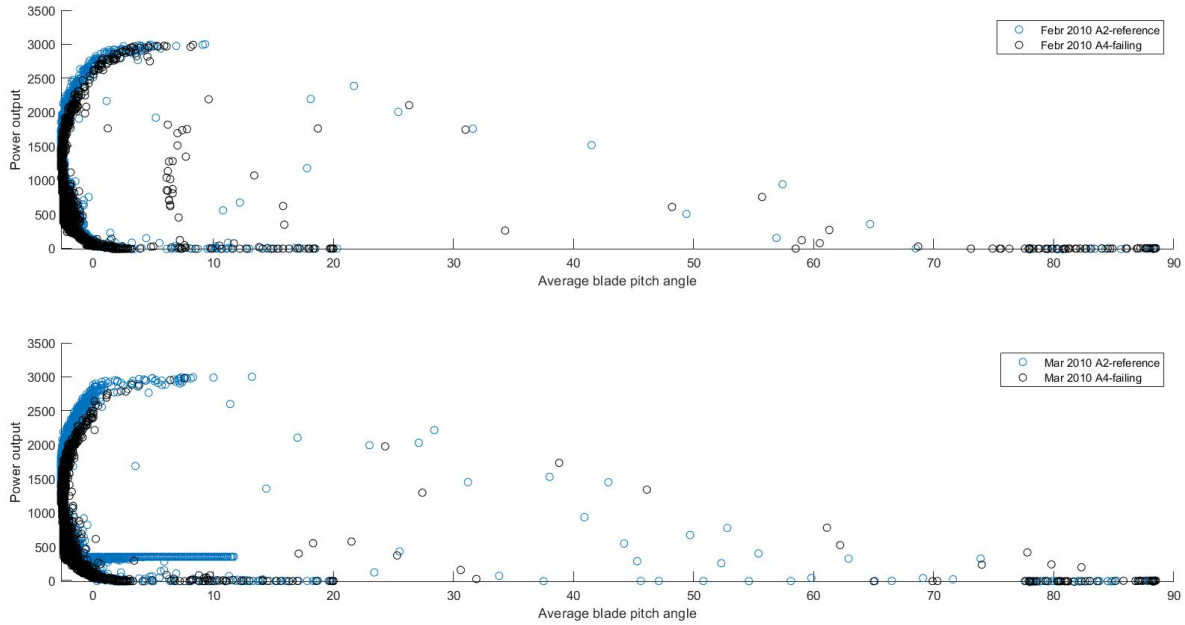

Figure C.37: Comparison of power output v.s. average blade pitch angle of WTA4 with the reference WT for the months February 2010 and March 2010.

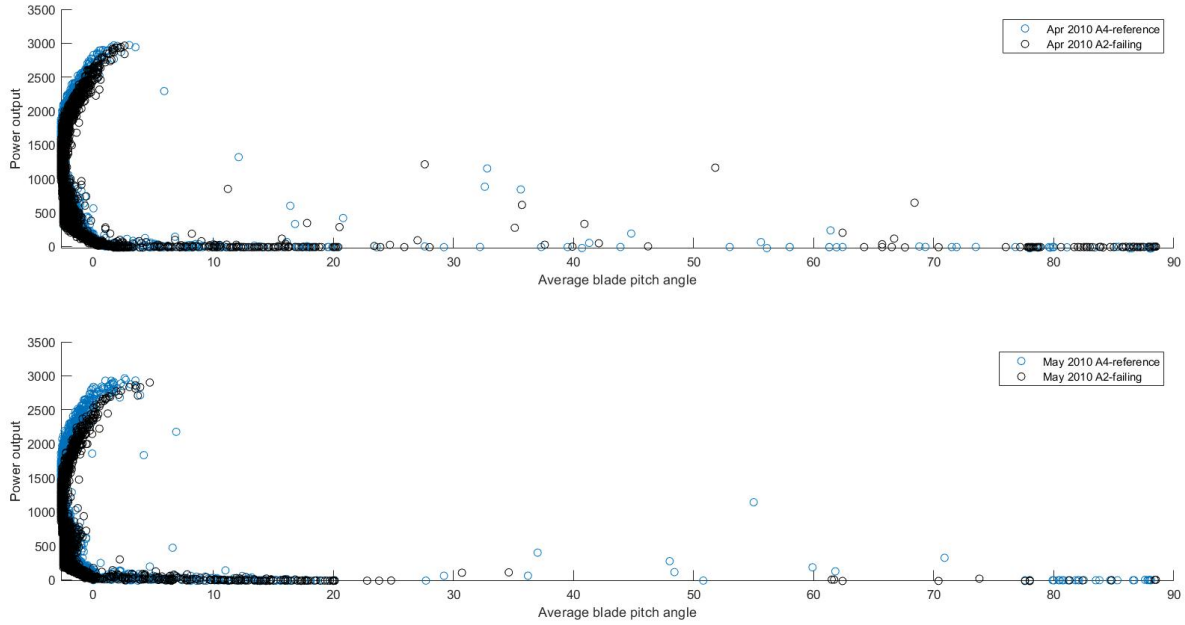

Figure C.38: Comparison of power output v.s. average blade pitch angle of WTA4 with the reference WT for the months April 2010 and May 2010.

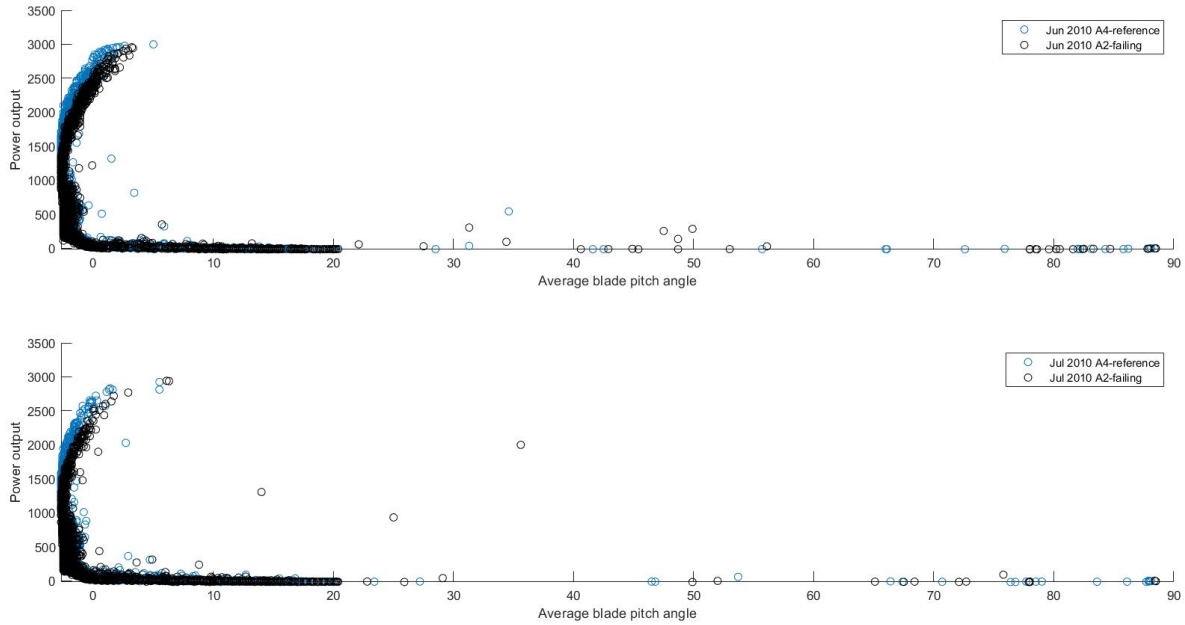

Figure C.39: Comparison of power output v.s. average blade pitch angle of WTA4 with the reference WT for the months June 2010 and July 2010.

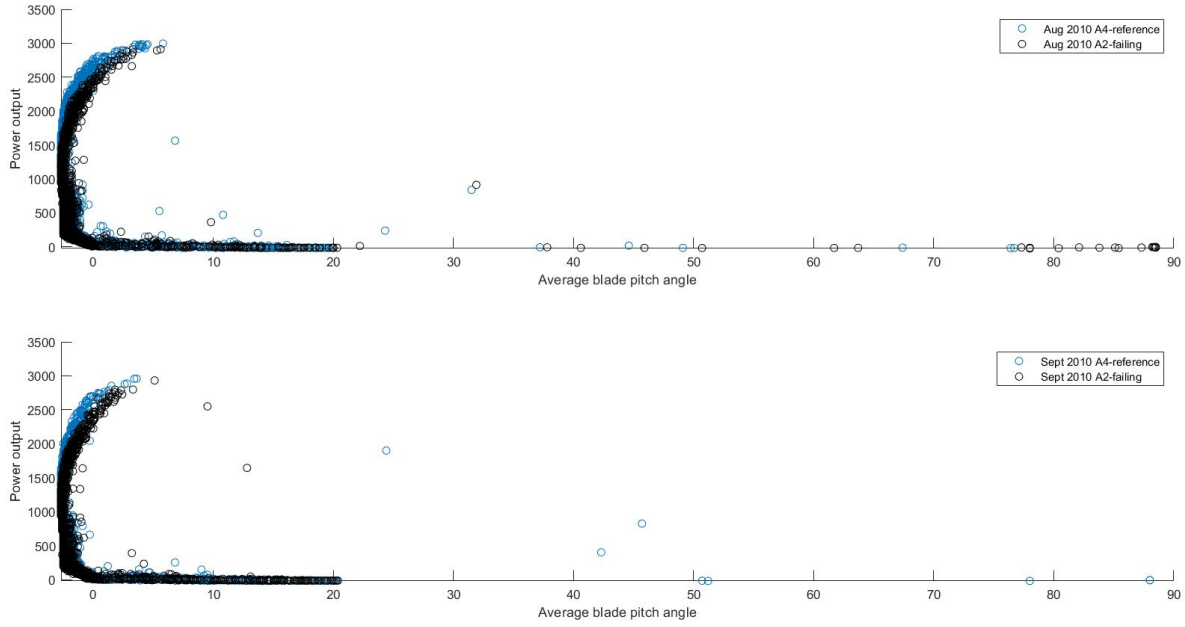

Figure C.40: Comparison of power output v.s. average blade pitch angle of WTA4 with the reference WT for the months August 2010 and September 2010.

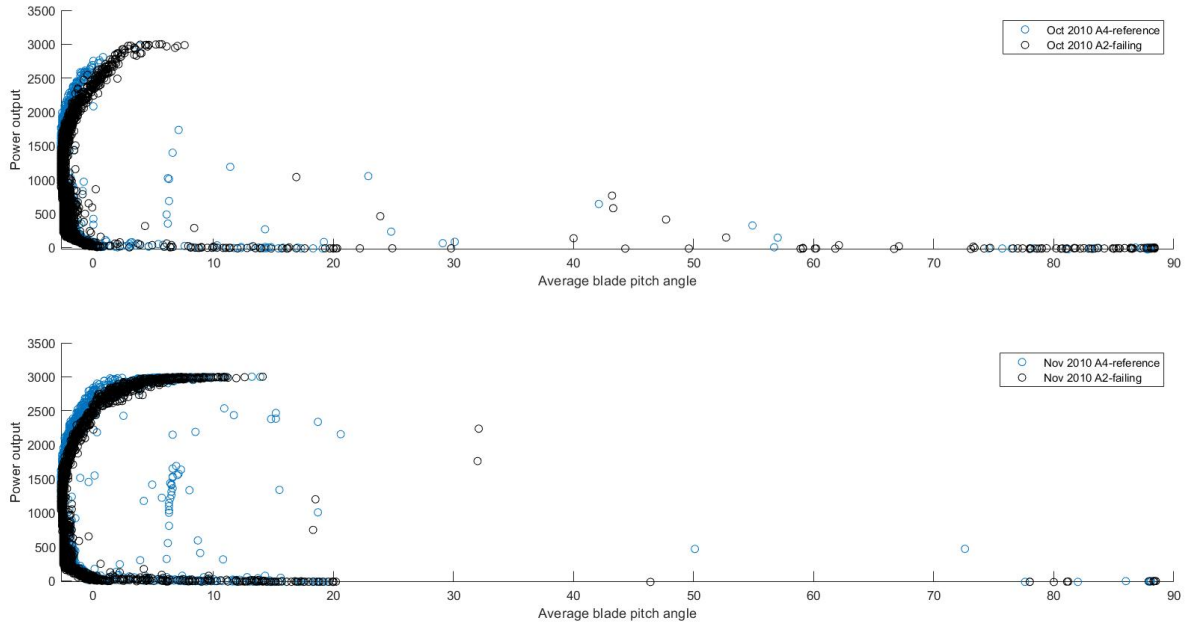

Figure C.41: Comparison of power output v.s. average blade pitch angle of WTA4 with the reference WT for the months October 2010 and November 2010.

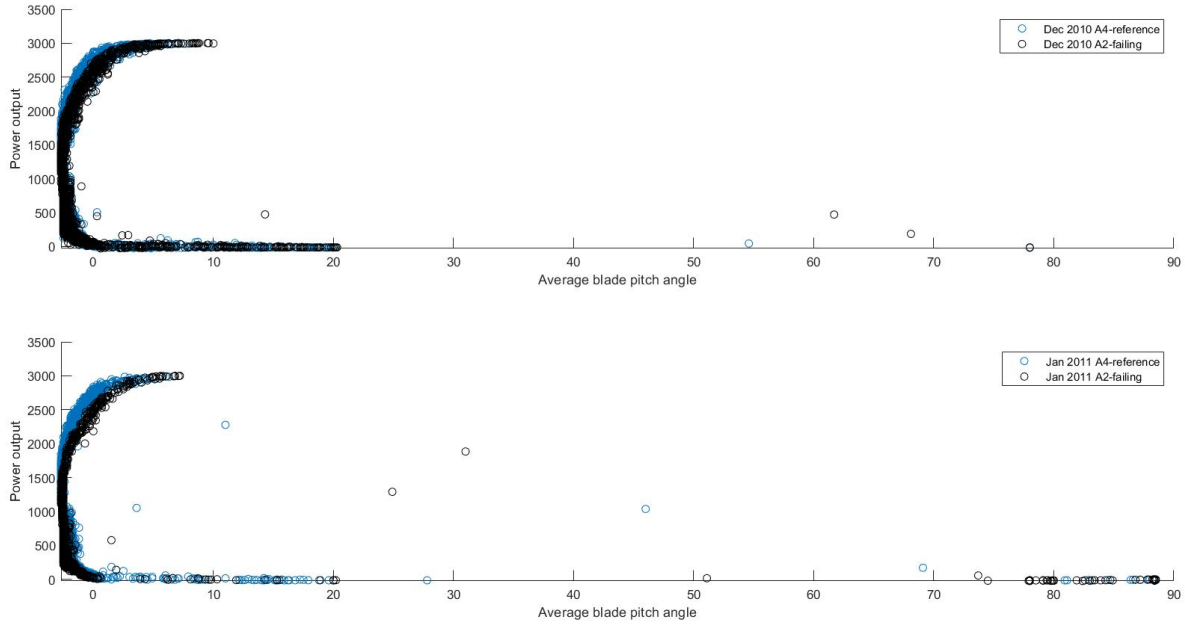

Figure C.42: Comparison of power output v.s. average blade pitch angle of WTA4 with the reference WT for the months December 2010 and January 2011.